

Copy 19  
Extra  
RM H56A06

6 Copy

NACA RM H56A06



# RESEARCH MEMORANDUM

AN ANALOG STUDY OF THE RELATIVE IMPORTANCE OF  
VARIOUS FACTORS AFFECTING ROLL COUPLING

By Joseph Weil and Richard E. Day

High-Speed Flight Station  
Edwards, Calif.

**NATIONAL ADVISORY COMMITTEE  
FOR AERONAUTICS  
WASHINGTON**

April 24, 1956  
Declassified January 20, 1958

## NATIONAL ADVISORY COMMITTEE FOR AERONAUTICS

## RESEARCH MEMORANDUM

AN ANALOG STUDY OF THE RELATIVE IMPORTANCE OF  
VARIOUS FACTORS AFFECTING ROLL COUPLING

By Joseph Weil and Richard E. Day

## SUMMARY

An analog study of the roll-coupling problem has been made for a representative swept-wing and tailless delta-wing configuration. The investigation, made primarily for subsonic flight conditions, included the determination of the effects of wide variations in many of the pertinent aerodynamic derivatives on the motions developed in rolling maneuvers. The influence of large changes in principal axis inclination and mass distribution is also considered.

The results indicated that as first predicted in NACA TN 1627 the relationship between the longitudinal and directional stability is of paramount importance. For most current designs an optimum condition exists when the natural frequencies in pitch and yaw are approximately equal. Increases in pitch damping had a pronounced favorable effect in reducing the amplitudes of the motions encountered and were, in general, considerably more effective than corresponding increases in yaw damping.

Practical redistribution of mass produced only relatively minor changes in the overall results.

It was found that the amplitude of the motions developed for a given aileron deflection depends to a large extent on the duration of the maneuver (change in bank angle). Limited studies indicated that 90° roll maneuvers would be considerably less critical than 360° rolls. The angle of attack of the principal axis has an important bearing on the behavior, particularly in the absence of other disturbing functions. If the initial angle of attack is maintained constant, a reduction in altitude will delay critical conditions to a higher roll rate but the maximum amplitudes may be only slightly affected.

Small inadvertent stabilizer inputs can greatly affect the magnitude of the motions developed.

It is difficult to generalize on the effects of Mach number variation because this variable affects many of the controlling parameters.

Utilizing simple concepts proved useful in assessing the qualitative effects of many of the aerodynamic and inertia parameters and changes in flight condition. The calculated lower resonant frequency generally corresponded to the average roll velocity at which the more serious motions could be expected.

It is indicated that rational design procedure can avoid the problem of serious roll coupling at supersonic speeds and minimize the problem in the subsonic speed range for the configurations of the type considered.

## INTRODUCTION

Until recently the motions of a rigid airplane with deflected ailerons could be adequately predicted in most instances from the classic three-degree-of-lateral freedom solutions (for example, ref. 1). That the longitudinal modes can exert a powerful effect on the overall motions of the rolling aircraft was first demonstrated theoretically in 1948 (refs. 2 and 3); however, not until 1954 were strong manifestations of coupled motions in rolling maneuvers experienced on a full-scale airplane (ref. 4).

Following the flight experiences described in reference 4, a five-degree-of-freedom analog study was initiated by staff members of the NACA Langley Laboratory and NACA High-Speed Flight Station to determine whether the actual flight motions could be calculated and also to determine the effects of variations in certain of the stability parameters. Some of the results of these preliminary studies were reported briefly in references 5 and 6.

An analog investigation of several generalized airplane configurations encompassing a considerably broader scope than the work of references 5 and 6 has recently been completed at the NACA High-Speed Flight Station. In this study wide variations in many of the pertinent aerodynamic derivatives were investigated at subsonic and supersonic speeds. The effects of large changes in principal axis inclination and mass distribution are also included.

The primary purpose of this paper is to summarize the information obtained from the analog calculations and to compare the results with the trends predicted from a slightly modified version of reference 2.

## SYMBOLS

b            wing span, ft

$C_L$	lift coefficient, $\frac{\text{Lift}}{\frac{1}{2}\rho V^2 S}$
$C_L$	rolling-moment coefficient, $\frac{\text{Rolling moment}}{\frac{1}{2}\rho V^2 S b}$
$C_m$	pitching-moment coefficient, $\frac{\text{Pitching moment}}{\frac{1}{2}\rho V^2 S \bar{c}}$
$C_n$	yawing-moment coefficient, $\frac{\text{Yawing moment}}{\frac{1}{2}\rho V^2 S b}$
$C_Y$	lateral-force coefficient, $\frac{\text{Lateral force}}{\frac{1}{2}\rho V^2 S}$
$\bar{c}$	wing mean aerodynamic chord, ft
$g$	acceleration due to gravity, ft/sec <sup>2</sup>
$h_p$	pressure altitude, ft
$i_t$	stabilizer deflection, deg
$I_X$	moment of inertia of airplane about X-axis, slug-ft <sup>2</sup>
$I_{X_e}$	moment of inertia of rotating engine parts about X-axis, slug-ft <sup>2</sup>
$I_{XZ}$	product of inertia referred to X- and Z-axes, slug-ft <sup>2</sup>
$I_Y$	moment of inertia of airplane about Y-axis, slug-ft <sup>2</sup>
$I_Z$	moment of inertia of airplane about Z-axis, slug-ft <sup>2</sup>
$M$	Mach number
$M$	pitching moment, ft-lb
$m$	airplane mass, $\frac{W}{g}$ , slugs
$N$	yawing moment, ft-lb
$p$	rolling velocity, radians/sec
$\bar{p}$	average rolling velocity, radians/sec
$p_0$	steady rolling velocity, radians/sec

q	pitching velocity, radians/sec
r	yawing velocity, radians/sec
S	wing area, sq ft
t	time, sec
V	true airspeed, ft/sec
W	airplane weight, lb
X, Y, Z	body axes of airplane
$\alpha$	angle of attack of airplane body axis, radians or deg
$\alpha_{T_0}$	angle of attack at zero lift, radians or deg
$\alpha_0$	initial angle of attack of airplane body axis, deg
$\alpha_p$	initial angle of attack of principal axis, deg
$\beta$	angle of sideslip, radians or deg
$\Delta\alpha, \Delta\beta$	increments from initial conditions, radians or deg
$\delta_{at}$	total aileron deflection (positive for right rolls), radians or deg
$\delta_r$	rudder deflection, radians or deg
$\epsilon$	angle between body axis and principal X-axis, positive when reference axis is above principal axis at the nose, deg
$\zeta_\theta$	fraction of critical damping in pitch of nonrolling aircraft, $\frac{-\bar{c}M_q}{4V\sqrt{-M_\alpha I_Y}}$
$\zeta_\psi$	fraction of critical damping in yaw of nonrolling aircraft, $\frac{-bN_r}{4V\sqrt{N_\beta I_Z}}$
$\rho$	mass density of air, slugs/cu ft

$\Delta\phi$  increment in angle of bank, deg  
 $\omega_e$  rotational velocity of engine rotor, radians/sec  
 $\omega_\theta$  nondimensional undamped natural frequency in pitch of non-rolling aircraft (ratio of pitching frequency to steady rolling velocity)  
 $\omega_\psi$  nondimensional undamped natural frequency in yaw of nonrolling aircraft

$C_{L\alpha}, C_{L_{it}}, C_{l\beta}, C_{l\delta_{at}},$   
 $C_{m\alpha}, C_{m\beta}, C_{m\delta_e}, C_{m_{it}},$   
 $C_{n\beta}, C_{n\delta_{at}}, C_{n\delta_r},$   
 $C_{Y\beta}, M_\alpha, N_\beta$

} indicates derivative with respect to subscript

$C_{l_p}, C_{l_r}, C_{n_p}, C_{n_r},$   
 $C_{Y_p}, C_{Y_r}, N_r$

} indicates derivative with respect to  $\frac{b}{2V} \times$  subscript

$C_{m\dot{\alpha}}, C_{m\dot{q}}, M_{\dot{q}}$  indicates derivative with respect to  $\frac{\bar{c}}{2V} \times$  subscript

Dot over a symbol indicates derivative with respect to time.

## CALCULATIONS

### Motion Studies

The basic time histories, upon which the analysis of this report is based, were calculated in real time using a five-degree-of-freedom approach (forward speed assumed constant). The fundamental equations used to calculate the motions are shown in table I. These equations were solved by

means of a Goodyear Electronic Differential Analyzer (GEDA).<sup>1</sup> The initial conditions used in the calculations simulated either trimmed level flight or constant  $g$  accelerated flight. Aileron deflection was generally the sole control input used in the calculations.

Several thousand time histories were run off in the course of the general study. The initial calculations were made with the simple aileron input of figure 1(a) (input A). A ramp-type input of  $50^\circ$  per second was used until the desired control angle was reached. At the nominal bank angle (usually  $360^\circ$ ) the control was returned to zero at  $50^\circ$  per second. It was found in a number of instances that this simple aileron input produced unrealistic results (for example, fig. 1(b)) because it failed to arrest the rolling motion after the aileron was returned to neutral. To obtain a more realistic evaluation in these instances it was necessary to use a control stick in conjunction with the analog, as shown in figure 2. A typical control input using the stick (input B) is shown in figure 1(c). It should be noted that the inputs A and B were similar until the point of corrective control. In the latter instance, the operator attempted to stop the rolling motion as rapidly as possible.

A number of approaches were tried in an effort to arrive at the most significant parameters for summary purposes. It was finally decided that the maximum positive and negative excursions in angle of attack and sideslip (fig. 1(c)) plotted against the average roll rate obtained in a given maneuver might provide the best overall representation. The average roll velocity is defined as the bank angle at control reversal divided by the time required to reach this angle. The bank angle was determined from the direction cosine  $m_z$  (table I).

#### Simplified Analysis

Throughout the analog program reference 2 served as a valuable guide notwithstanding the fact that the analysis of reference 2 assumed constant roll rate and made other simplifying assumptions. It was thought desirable, however, to account for engine gyroscopic effects and to use the actual value for the ratio  $\frac{I_z - I_x}{I_y}$  instead of assuming unity.

Another approach in considering the effects of engine momentum on rolling maneuvers is presented in reference 7.

It is shown in appendix A that inclusion of the previously mentioned modifications to the theory of reference 2 results in an increment to the

---

<sup>1</sup>The GEDA equipment was made available through the cooperation of the Air Force Flight Test Center.

parameters used to define the stability chart, and also lowers the horizontal boundary slightly (appendix A and fig. 3). The basic meaning of figure 3 is identical to that discussed in reference 2 in that the region between a boundary and axis indicates a divergent condition. The roll velocity at which the effective stability first becomes unstable for a condition of zero damping is referred to as the resonant frequency and is given by the following equations

$$\bar{p} = \pm \sqrt{\frac{C_{n\beta} \frac{1}{2} \rho V^2 S b}{I_Y - I_X}} + \frac{I_{X_e} \omega_e}{2(I_Y - I_X)} \quad (1)$$

applicable where the vertical boundary is first intersected as the roll velocity is progressively increased, and

$$\bar{p} = \pm \sqrt{\frac{-C_{m\alpha} \frac{1}{2} \rho V^2 S \bar{c}}{I_Z - I_X}} + \frac{I_{X_e} \omega_e}{2(I_Z - I_X)} \quad (2)$$

applicable where the horizontal boundary is first intersected.

Note that equations (1) and (2) are identical to equations 10 and 11 of appendix A; however, the notation  $p_0$  of reference 2 was retained in the appendix whereas the average roll velocity is used in the remainder of this paper.

#### SCOPE

Two basic fighter airplane configurations are included in this study. One configuration had the mass and aerodynamic characteristics representative of current swept-wing airplane types, while the other used parameters estimated for a tailless delta-wing type. All the rolling maneuvers for the swept-wing airplane included in this paper were calculated for a Mach number of 0.7, whereas the delta configuration is presented for  $M = 0.8$  and  $M = 1.2$ . Unless otherwise indicated, the basic aerodynamic and mass parameters shown in table II were used in the calculations. The aerodynamic derivatives were based on wind-tunnel results, flight tests, and theory. The derivatives used (with the exception of  $C_{l\beta}$ ) were assumed invariant with angle of attack. Table II presents the variation of  $C_{l\beta}$  with  $\alpha$  used for the several basic flight conditions.

For each configuration a series of calculations were made with successive increments in aileron deflection using the basic derivatives of

table II. Additional series were obtained by varying the stability derivatives  $C_{m_\alpha}$  and  $C_{n_\beta}$  and the damping derivatives  $C_{m_q}$  and  $C_{n_r}$  over a rather wide range. The effects of roll direction and duration and initial angle of attack were also considered for each basic condition.

To obtain a better insight into the mechanism of roll coupling, additional information was obtained for the swept-wing configuration with arbitrary variations in yawing moment due to rolling  $C_{n_p}$ , dihedral effect  $C_{l_\beta}$ , principal axis inclination, altitude, and mass distribution. The importance of relatively small inadvertent stabilizer inputs was also determined.

## PRESENTATION OF RESULTS

A summary of the figures presenting the results of this investigation are:

	Figures
Effects of:	
$C_{m_\alpha}$ at various levels of $C_{n_\beta}$ . . . . .	4 to 16
Roll direction . . . . .	17 and 18
Roll duration . . . . .	19 to 21
Damping in yaw . . . . .	22 to 25
Damping in pitch . . . . .	26 to 33
Inadvertent stabilizer input . . . . .	34 and 35
Initial angle of attack and principal axis inclination . . . . .	36 to 40
Altitude . . . . .	41
Yaw due to roll . . . . .	42 and 43
Dihedral effect . . . . .	44
Mass distribution . . . . .	45 to 47
Analysis of coupling problem on specific design . . . . .	48

## DISCUSSION

### Individual Effects

Importance of  $C_{m_\alpha}$ ,  $C_{n_\beta}$  relationship.- Figures 4 to 6 present a summary of the effects of variations in  $C_{m_\alpha}$  at three levels of  $C_{n_\beta}$  for the swept-wing configuration. The data of figures 4 to 6 present

the envelopes of the maximum angle of sideslip and angle of attack excursions from trim (fig. 1(c)) as a function of average roll velocity in nominal  $360^\circ$  left rolling maneuvers. The results indicate that the value of  $C_{m\alpha}$  has a profound effect on the calculated amplitudes at all levels of directional stability. Moreover, the value of  $C_{m\alpha}$  at which the smallest angles are obtained appears to increase as  $C_{n\beta}$  is increased.

The average roll velocity at which the peak amplitudes occur would appear to vary in a somewhat erratic fashion. To analyze the trends shown, the simple theory of reference 2 (modified as indicated in appendix A) was utilized. In figure 7 the nondimensional frequency parameters in pitch and yaw are plotted with suitable terms added to account for engine gyroscopic effects. For any given flight condition, variation in the roll velocity will trace out a curve which for the values of the aerodynamics and engine momentum considered is very close to a straight line. For conditions falling between the coordinate axes and the vertical neutral stability boundary (region A) the simple theory predicts primarily a directional divergence, whereas conditions between the coordinate axis and the horizontal neutral stability boundary (region B) are primarily indicative of a pitch divergence. It should be noted that, inasmuch as the physical and inertia characteristics were assumed constant, the slopes of the lines shown in figure 7 are for all practical purposes dependent on the ratio of  $C_{m\alpha}$  to  $C_{n\beta}$ . Each condition in figures 4 to 6 is numbered and represented in figure 7 by a line. The several instances of identical  $C_{m\alpha}/C_{n\beta}$  ratios are indicated by a common reference number.

It can now be seen that the farther from the origin the representative line intersects the boundaries of figure 7, the worse the coupled motions. Thus, conditions 1 and 5 which represent the most extreme ratios of natural frequency in yaw and pitch also are characterized by the least desirable motions. The average roll velocity at which the lower undamped resonant frequency for the nonrolling airplane occurs (equation 1 or 2) is shown ticked on the curves in figures 4 to 6. It seems that this frequency in general occurs fairly close to the roll velocity at which maximum excursions occur. For a given ratio of  $C_{m\alpha}$  to  $C_{n\beta}$  the higher the roll velocity for resonance, the greater the maximum amplitude of the motions for the more extreme conditions 2 and 4. Condition 3, which has a more desirable proportioning of stability, does not show this trend to any degree.

The effect of increasing  $C_{n\beta}$  at constant  $C_{m\alpha}$  is also evident in figures 4 to 6 and the results follow the foregoing analysis.

Representative time histories for aileron deflections at which near peak amplitudes were obtained are shown for each combination of  $C_{m\alpha}$

and  $C_{n\beta}$  in figures 8 to 10. In nearly all instances the maximum excursions occur during the recovery phase of the maneuver. Although the recovery is perhaps not mathematically definable, the results of figures 4 to 6 were not particularly sensitive to the exact control manipulations used during recovery, and repeat runs produced very little scatter on the summary plots. For conditions 1 and 2 which produced an intersection in the upper portion of the diagram of figure 7 the predominant angle-of-attack change during the constant aileron portion of the maneuver was negative, whereas for conditions 4 and 5 the predominant angle-of-attack change was positive. The initial sideslip motion was always negative, although the yawing velocity histories varied markedly.

A series of runs was made in which individual terms were eliminated singly from the equations of table I. The results are shown in figures 11 and 12 for the two most extreme conditions, 1 and 5 (figs. 4 and 6).

For condition 1, which represents a condition having a  $C_{n\beta}$  value which is much too low in relation to  $C_{m\alpha}$ , it is evident that elimination of the  $pq$  term in the  $\dot{r}$  equation effectively de-couples the motion (fig. 11(c)). When the  $pr$  term in the  $\dot{q}$  equation is removed, however, little effect is shown. The elimination of the  $p\beta$  term in the  $\dot{\alpha}$  equation shows an effect similar to omission of the  $pq$  term.

For condition 5, which represents a condition having a  $C_{n\beta}$  value much too high relative to  $C_{m\alpha}$ , removal of the  $pr$  term has the primary de-coupling effect (fig. 12). It is seen, moreover, that the removal of the  $pq$  or  $p\beta$  terms produces an unfavorable effect for condition 5.

The importance of the  $C_{m\alpha}$ ,  $C_{n\beta}$  relationship for the delta-wing configuration at  $M = 0.8$  and  $M = 1.2$  is illustrated in figures 13 and 14. Stability diagrams for these conditions are presented as figures 15 and 16. From a close inspection of figures 13 to 16 it is seen that the major points brought out in the discussion of the swept-wing configuration are substantiated for the delta-wing configuration.

For the  $M = 0.8$  condition (figs. 13 and 15) the expected favorable effect of reducing  $C_{m\alpha}$  from  $-0.36$  to  $-0.18$  (condition 1 to condition 3) is evident, although the magnitude of the motions is still quite large for the latter case. When the value of  $C_{m\alpha}$  is further reduced to  $-0.09$ , a considerable reduction in the peak amplitudes is obtained probably because of the decrease in lower resonant frequency.

At  $M = 1.2$ , doubling the basic value of  $C_{n\beta}$  resulted in an appreciable improvement because of a more desirable proportioning of stability (conditions 1 and 3, fig. 16) and because of the increased stability level.

Detailed comparisons of the several configurations discussed should be made only in the light of the different initial conditions present (table II). The effects of some of these variables will be treated in later sections of this paper.

Effect of roll direction.- The effect of roll direction is summarized in figure 17 for the swept-wing configuration at  $C_{n\beta}$  levels of 0.057 and 0.114 per radian. The data indicate that in left rolls with the lower  $C_{n\beta}$ , the peak motions occur at a somewhat lower average roll rate and are 30 percent larger than corresponding right rolls. For  $C_{n\beta}$  of 0.114 a similar trend is indicated but is less marked.

The simple theory of reference 2 modified to include the engine terms has been applied to the conditions of figure 17. The stability chart (fig. 18) shows that for the lower  $C_{n\beta}$  the representative line for the left roll intersects in a slightly less desirable location than the corresponding line for the right roll. For the higher  $C_{n\beta}$  the two lines are coincident. The lower resonant frequencies for the undamped conditions are indicated by the ticks (fig. 17) and it is apparent that the increase in resonant frequency calculated for the right rolls correlates fairly well with the motion studies.

It should be mentioned that although the left rolls of figure 17 are seen to be somewhat more critical than the corresponding right rolls, a number of factors could cause the reverse to be true. Among these factors would be direction of engine rotation, and the values of  $C_{n\delta_{at}}$ ,  $C_{np}$ , and perhaps initial angle of attack. For all conditions considered in this paper however, the left roll is the more critical and all of the remaining results are presented for left rolls.

Effect of roll duration.- A summary of the effects of roll duration is shown for the swept-wing configuration in figure 19. It is seen that the maximum amplitudes calculated for the 90° and 180° maneuvers are much lower than for the 360° rolls. This is not surprising if the motions are considered to be the manifestation of an effective reduction in stability or actual instability, thus the time duration (change in bank angle) would be expected to be a determining factor in the motion build up. Representative time histories are shown in figure 20 for 90°, 180°, 360°, and 1440° maneuvers. The possible effects of roll duration are clearly evident particularly for the 1440° maneuver in which angles of attack and angles of sideslip of very large magnitude are obtained. In most instances, however, the amplitudes attained in the 360° rolls were comparable with those calculated for 1440° rolls, particularly when the recovery phase is included.

According to simple theory (appendix B) it can be shown that the rate of divergence for an unstable condition will be directly proportioned

to the roll velocity and also be adversely affected when the intersection of the determining line with the stability boundary occurs at large distances from the "neck" of the diagram. Thus the magnitude of the motions might be expected to build up quite rapidly for the delta-wing configuration (condition 1, fig. 16) at supersonic speeds. Time histories showing the effect of bank angle are presented in figure 21 for the delta-wing configuration at  $M = 1.2$ . A  $360^\circ$  roll is seen to produce a violent maneuver with sideslip angles greater than  $20^\circ$  and large  $\alpha$  excursions. The  $180^\circ$  maneuver still develops  $17.5^\circ$  of sideslip and  $\pm 6^\circ$  in  $\Delta\alpha$  ( $\pm 2g$ ). Even the  $90^\circ$  maneuver, for this condition, is accompanied by  $12^\circ$  of sideslip but the  $\alpha$  amplitudes are considerably reduced.

Effect of damping in yaw.- The influence of changes in  $C_{n_r}$  is summarized in figure 22 for the swept-wing configuration for a  $C_{n_\beta}$  level of 0.057. A tenfold increase in  $C_{n_r}$  reduces the peak  $\beta$  motions appreciably but has very little effect on the maximum angle-of-attack amplitudes. A value of  $C_{n_r}$  100 times the basic value produced no significant additional decrease in the maximum  $\beta$  amplitudes although a reduction in the  $\alpha$  motion is evident. Moreover, particularly for the highest damping ratio, the peak amplitudes were materially increased at the lower roll rates. A stability diagram of the type used previously is shown as figure 23. From the simple theory it might be expected that a more significant improvement would exist for the two conditions of increased damping in yaw. Note also that the peak amplitudes of figure 22 occur near the same average roll rate, whereas the results of figure 23 might lead one to believe the maximum excursions with increased damping would occur at appreciably higher roll rates.

Recalling the results of figure 11(b), the elimination of the  $rp$  term in the  $\dot{q}$  equation did not alter the basic level of the motion for conditions intersecting the vertical divergence boundary. For conditions intersecting the horizontal divergence boundary (fig. 12(b)) elimination of the  $rp$  term was very effective.

Figures 24 and 25 show the effects of increasing  $C_{n_r}$  by factors of 10 and 100 for the extreme conditions 1 and 5 (figs. 4 and 6). The results indicate that the increases in  $C_{n_r}$  have a more significant effect in reducing the motions for condition 5 than for condition 1.

Effect of damping in pitch.- The effects of increasing the basic damping in pitch for the swept-wing configuration are summarized in figure 26 for two levels of  $C_{n_\beta}$ . It is seen that a threefold increase in

pitch damping<sup>2</sup> ( $\zeta_\theta = 0.27$ ) results in an appreciable reduction in the  $\beta$  motions and some reduction in the  $\alpha$  amplitudes. A tenfold increase in  $C_{mq}$  ( $\zeta_\theta = 0.92$ ) produces a marked improvement at each stability level. The stability charts of figure 27 show the effect on the divergence boundaries of increasing the pitch damping. These results correlate fairly well with the trends presented in figure 26. The results of the time histories of figures 28 and 29 show the favorable effects of increases in  $C_{mq}$  of 10 and 100 times the basic value on the motions for the two extreme basic conditions examined in the preceding paragraph.

In figure 30 the effects of variations in pitch damping are presented for the delta-wing configuration at a Mach number of 0.8. At this Mach number increasing the level of  $C_{mq}$  showed a considerable improvement but was not quite as effective as for the swept-wing configuration. The stability diagram is presented in figure 31 for this flight condition.

At a Mach number of 1.2 the results shown in figure 32 indicate a relatively small effect of increasing  $C_{mq}$  until an extremely large level is assumed. It is believed this condition is caused by the intersection of the basic determinant line with the divergence boundary at a relatively large value of the ordinate. It is seen (fig. 33) that for this condition moderate increases in  $C_{mq}$  would be expected to have only a slight favorable effect.

Effect of stabilizer input.- In the previous section the important effects of pitch damping were discussed. Inasmuch as these changes are attributable to reductions in the pitching velocity, it might be reasoned that even small stabilizer inputs during the rolls could likewise have an important effect on the results. Figure 34 presents a summary of results for simultaneous stabilizer and aileron inputs for  $C_{n\beta} = 0.114$ . The type of stabilizer input used is illustrated in the representative time histories of figure 35. It is evident that 1° of airplane nose-up stabilizer results in a 50-percent increase in the amplitudes of the  $\beta$  motions and also produces large increases in the  $\alpha$  excursions, whereas a stabilizer input of the opposite sense has a large alleviating

---

<sup>2</sup>The damping ratio considering only  $C_{mq}$  is shown in the figures because this value was used in calculating the boundaries shown. Of course, the total angle of attack damping ratio is also dependent on  $C_{m\dot{\alpha}}$  and the lift-curve slope. Thus, for the swept wing airplane (figs. 26 and 27) the total damping ratio will be about 0.16 higher than  $\zeta_\theta$ , whereas for the delta wing configuration (figs. 30 and 33) the total damping ratio will be about 0.17 higher at  $M = 0.8$  and 0.07 higher at  $M = 1.2$ .

effect (fig. 34). The reason for these trends is, of course, that the negative stabilizer increases the pitching velocity (fig. 35) while the positive input appreciably reduces the pitching rate. Reference 8 presents flight data showing similar effects of stabilizer inputs. When the basic pitch damping is increased about sixfold, much less critical motions are experienced for the unfavorable stabilizer input (symbols, fig. 34).

Data not presented indicated that somewhat more positive stabilizer inputs than shown in figure 34 were undesirable. This was attributed to the fact that large negative pitching rates were produced.

It should be noted that, whereas negative stabilizer input aggravated the motions in this instance, conditions in which the basic pitching velocity were negative or instances in which "complementary" sideslip were present might be made more critical with positive stabilizer inputs (table I).

It should also be pointed out that large changes in pitching moment due to sideslip could also have a decided effect on the characteristics.

Effect of initial angle of attack.- The effects of initial angle of attack for the swept-wing configuration are presented in figure 36 for a principal axis inclination of  $1^\circ$  at two levels of directional stability. Data are presented at  $\alpha = 5^\circ, 1^\circ, \text{ and } -3^\circ$  or at angles of attack of the principal axis of  $\pm 4^\circ$  and  $0^\circ$ . The results shown in figure 36 indicate that the peak excursions occur at about the same roll rate for negative and positive conditions of angle of attack with the amplitudes appearing as nearly mirror images of each other. This is even more evident in the representative time history plots of figures 37(a) and 37(b), which illustrate the expected diametric opposite nature of the motions. For this flight condition the major disturbing function is produced by the angle of attack of the principal axis through the  $\alpha_p$  term and the  $I_{XZ}$  terms in the equations of table I ( $C_{n_p} = C_{n_{\delta_{at}}} = 0$ ). Thus, when the principal axis is lined up with the relative wind, essentially no motion is produced. If, however, a small yawing moment is introduced by assuming  $C_{n_p} = -0.05$ , then relatively large peak<sup>3</sup> amplitudes are obtained, particularly in regard to sideslip motions (symbols, fig. 36). This is not too surprising if it is considered that near  $\bar{p} = 1.6$  radians/sec an effective instability is present for the  $C_{n_p} = 0.057$  condition. Thus a relatively small out-of-trim movement could be expected to produce a sizable effect.

---

<sup>3</sup>The yawing moment introduced would have produced about  $\Delta\beta = 2^\circ$  for a roll rate of 1.6 radians if a three-degree-of-freedom uncoupled motion is assumed.

Similar trends on a somewhat reduced scale are indicated for  $C_{n\beta} = 0.114$  (fig. 36).

A summary plot is presented in figure 38 for a principal axis inclination of  $5^\circ$ . The overall effects are, as might be expected, with the greatest amplitudes recorded for conditions having the largest initial angle of the principal axis. In figure 39 the results of figures 36 and 38 are compared by plotting the maximum values shown for any conditions as functions of the initial angle of attack of the principal axis. The importance of the latter parameter in correlating the results is at once evident upon inspection of figure 39. The amplitudes were in each case a minimum when  $\alpha_p \approx 0^\circ$ .

It should be mentioned that if rolling performance at initial  $g$  levels of 1 or greater is considered to be of primary importance, then a moderately large nose-down inclination of the principal axis (positive  $\epsilon$ ) would be beneficial because it would reduce  $\alpha_p$ .

It is believed that if an appreciable value of  $C_{n\beta}$  or  $C_{n\delta_{at}}$  is present, the angle of attack (fig. 39) at which minimum motions occur would be shifted, depending on the sign and magnitude of the additional disturbing functions.

The sensitivity to change in the initial angle of attack is illustrated for the delta-wing configuration at a Mach number of 1.2 (fig. 40). Data are presented for initial angles of attack of  $2.0^\circ$  and  $3.9^\circ$  ( $\alpha_p = 0^\circ$  and  $1.9^\circ$ ). On first inspection it might seem surprising that such a large motion would be obtained for the case of  $\alpha_p = 0^\circ$  at high roll rate. However, a small value of  $C_{n\delta_{at}}$  was used (table II) which provided the necessary disturbing function. When  $C_{n\delta_{at}}$  was assumed zero (symbols, fig. 40), essentially no  $\alpha$  or  $\beta$  motions were obtained.

Effect of altitude.- The influence of a large altitude change on the motions developed in rolls is shown in figure 41. Data are presented for the swept-wing airplane ( $C_{n\beta} = 0.057$ ) at initial angles of attack of  $2^\circ$  and  $5^\circ$  and altitudes of 10,000 feet and 32,000 feet. It should be noted that the initial angles of attack of  $2^\circ$  and  $5^\circ$  correspond to level flight conditions at 10,000 feet and 32,000 feet, respectively. It is evident from the results that the major effect of decreasing altitude (at constant initial  $\alpha$ ) is to delay the buildup of large motions to a higher average roll velocity. From the loads standpoint, of course, much more critical conditions could be obtained at the lower altitude because of the two- and one-half-fold increase in dynamic pressure. The lower resonant frequency calculated from equation (1) is noted by ticks

for each altitude and it is apparent that the increase in average roll velocity at which largest coupling effects occur is predicted rather well from the simple theory. It might be mentioned that the decrease in maximum amplitude at the lower altitude is possibly attributable to the 60 percent increase in damping ratio in pitch ( $C_{mq}$  assumed invariant with altitude).

Effect of yawing moment due to roll.- For most of the calculations a value of  $C_{np} = 0$  was assumed for the swept-wing configuration. Figure 42 shows the effects of large arbitrary increases in  $C_{np}$  for  $C_{n\beta} = 0.057$  and  $0.114$ . For the lower value of  $C_{n\beta}$  an increase in  $C_{np}$  to  $0.10$  is seen to reduce appreciably the size of the motions obtained. A further increase to  $0.20$  produces rather violent motions at a relatively low roll rate. For a value of  $C_{n\beta} = 0.114$  an increase in  $C_{np}$  to either value has a deleterious effect on the maximum amplitudes.

It was mentioned in the discussion of initial angle-of-attack effects that changes in  $C_{np}$  or  $C_{n\delta_{at}}$  which might alleviate the motions for certain  $\alpha_0$  could aggravate the coupling problem for other initial angles of attack. Figure 43 shows the effects of introducing a value of  $C_{np} = 0.10$  ( $C_{n\beta} = 0.057$ ) in rolling maneuvers performed at  $\alpha_0 = 5^\circ$  and  $-3^\circ$ . For  $\alpha_0 = 5^\circ$  the favorable effect of increasing  $C_{np}$  is clearly shown (figs. 43(a) and (b)) and probably results from the large change in the yawing velocity buildup. When the roll is made at  $\alpha_0 = -3^\circ$ , however, the positive  $C_{np}$  is seen to aggravate the motion appreciably.

Effect of  $C_{l\beta}$ .- A number of  $C_{l\beta}$  variations were investigated for the basic swept-wing configurations ( $C_{n\beta} = 0.057$ ). Figure 44(a) illustrates the effect of doubling the ordinates of the  $C_{l\beta}$  variation with  $\alpha$  (table II). No appreciable change in the amplitude of the motions is indicated.

Unswept-wing configurations are generally characterized by much smaller variation in  $C_{l\beta}$  with  $\alpha$  than are swept-wing configurations. It was decided, therefore, to study the effects on the roll coupling problem for three constant levels of  $C_{l\beta}$ . Figure 44(b) presents the results for  $C_{l\beta}$  values of  $0$ ,  $-0.063$ , and  $-0.126$  per radian. The data indicate that as the level of  $C_{l\beta}$  is increased the peak motions occur at a slightly higher roll rate, but the peak amplitudes are not much reduced. Another aspect of the problem results from the combination of

high dihedral effect and adverse sideslip which reduces the average roll velocity attainable for a given aileron deflection (fig. 44). Thus, for the highest  $C_{l\beta}$  level if maximum aileron deflection is limited to  $30^\circ$  (although  $-14^\circ$  of sideslip would be obtained), the angle-of-attack excursions would be greatly reduced at the maximum obtainable roll rate of  $-1.60$  radians per second (fig. 44(b)).

Effect of mass distribution.- The importance of the mass distribution parameter  $\frac{I_Y - I_X}{I_Z}$  is treated in this section. In figure 45 data are presented illustrating the effects obtained in changing from a configuration with its mass concentrated along the fuselage  $\frac{I_Y - I_X}{I_Z} = 0.9$  to a condition of more equitable distribution  $\frac{I_Y - I_X}{I_Z} = 0.2$ . In this study the inertia in yaw  $I_Z$  was held constant (table III).

For a  $C_{n\beta}$  level of 0.057 it would appear that reducing the mass concentration along the fuselage, such that  $\frac{I_Y - I_X}{I_Z}$  is reduced from 0.90 to 0.50, results in a slight decrease in the peak amplitude of the motions and an increase in the roll velocity at which these peak values occur. A further reduction in the inertia ratio to 0.20 appears to improve the situation appreciably. To compare these trends with simple theory, a stability plot has been prepared (fig. 46). The lower resonant frequency is indicated by the ticks on figure 45. As has been demonstrated previously in this paper, the simple theory adequately predicts the trends. As the mass distribution factor  $\frac{I_Y - I_X}{I_Z}$  is reduced, the resonant frequency is of course raised and the intersection of the stability line is changed from one indicating an appreciable  $\beta$  divergence to an intersection tangent to the  $\alpha$  divergence side of the boundary. A series of representative time histories showing the basic character of the motions for near peak coupling conditions is presented as figure 47. Note that the large value of  $I_X$  associated with the lowest inertia ratio reduces the rolling acceleration to such a degree that a much higher aileron deflection is required to obtain a given average roll rate in the  $360^\circ$  maneuvers. Otherwise, the general character of the motions developed is quite similar.

For the  $C_{n\beta}$  level of 0.114 per radian, the summary plot (fig. 45) indicates very little difference in the inertia range from 0.5 to 0.9. Moreover, for the condition of most equal mass distribution,  $\frac{I_Y - I_X}{I_Z} = 0.2$ ,

the results are seen to be slightly worse than for the other conditions. The reason for this condition can be explained with the aid of the stability chart of figure 46. For this stability level, as the mass is progressively more evenly distributed, the characteristic stability line intersects further in the  $\alpha$  divergence side of the boundary.

### General Design Considerations

In the foregoing analysis various individual effects have been examined relative to the roll coupling problem at several flight conditions. A contemporary swept-wing airplane designed for Mach numbers near 1.7 is now examined briefly to assess the roll coupling problem and also to determine how the results of the previous sections apply to the airplane.

It should be noted in the airplane design under consideration (tail C of ref. 8) the vertical tail size was primarily dictated by static stability considerations at design supersonic Mach number. The longitudinal stability corresponded to a static margin of about 10 percent at subcritical speeds with the usual large increase in stability occurring at transonic speeds.

First, a roll stability diagram is constructed (fig. 48(a)), to illustrate the effect of Mach number on the stability proportioning. The derivatives used were taken from unpublished data (table IV). The stability diagram indicates that at  $M = 0.73$  the proportioning of longitudinal to directional stability is near optimum, whereas at  $M = 0.93$  and  $M = 1.26$  the normal rearward aerodynamic-center shift produces a less desirable intersection. The flight envelope of the airplane is presented as figure 48(b). The solid lines represent lines of constant lower resonant frequency (calculated from data of table IV) and the dashed line indicates the maximum capabilities of the ailerons in relation to the average roll velocity obtainable in  $360^\circ$  rolls from initial lg flight.

For this airplane, in almost the entire supersonic flight range, the average roll rates available are considerably lower than the roll velocity at which the most violent maneuvers might be expected. At moderate subsonic speeds the ailerons are capable of producing roll rates in which serious roll coupling could be obtained; however, the desirable proportioning of longitudinal and directional stabilities would be expected to have an alleviating effect on the amplitudes of the motions.

The use of figure 48 for a quick assessment of the roll coupling problem is obvious. It should be realized, however, that conditions falling slightly to the right of the available aileron power line can also produce large motions as indicated in previous sections of this paper. This condition is particularly important when the increase in dynamic pressure is considered. Preparation of a figure similar to figure 48 at

a number of g levels supplemented by a knowledge of principal axis inclination would appear to be a logical first step in arriving at critical conditions for detailed analog calculations.

As indicated in reference 8, a comprehensive roll investigation of the airplane (full aileron  $360^\circ$  rolls) has been made particularly at the flight conditions shown by the symbols in figure 48. At supersonic speeds, no serious coupling problem has been encountered in flight. At  $M = 0.73$ , although no violent maneuvers were experienced, the motions obtained were fairly large and were sensitive to inadvertent longitudinal control motions. At  $M = 0.93$  fairly large motions were also obtained and calculations indicated that, had slightly higher aileron deflections been available, a rather serious maneuver might have been encountered.

It would appear that the airplane of reference 8 is acceptable from the overall roll coupling standpoint. Based on the results of figures 26 and 34, however, a substantial increase in pitch damping would materially improve the situation at subsonic speeds both for rolls made with and without inadvertent stabilizer inputs. At supersonic speeds the aileron power was considered more than adequate by the pilot, although the average roll rates were slightly lower than at subsonic speeds.

To summarize, then, it would appear that present design practice (adequate static directional stability at design high-speed Mach number and moderate longitudinal stability at subcritical speeds) would probably furnish a good starting point in obtaining acceptable motions in rolling maneuvers. It might be desirable, however, to insure the presence of an adequate margin between the lower resonant frequency and the average roll velocity obtainable from the ailerons at supersonic speeds. In this connection it should be stated that the ailerons should be designed so that excessive roll rates are not attainable particularly at supersonic speeds. Finally, if a pitch damper producing a total damping ratio on the order of 0.7 to 1.0 at subcritical speeds is used, the tendency for serious roll coupling effects in this speed range will be minimized.

## CONCLUSIONS

A fairly comprehensive five-degree-of-freedom analog study of the roll coupling problem for a generalized swept-wing and for a tailless delta-wing airplane configuration has been completed and the following conclusions are in order:

1. The various aerodynamic and inertia parameters considered indicated:

- (a) The relationship of the longitudinal and directional stabilities is of paramount importance. An optimum condition exists when the resonant frequencies in pitch and yaw are approximately equal.

(b) Increases in pitch damping had a pronounced favorable effect in reducing the amplitudes of the motions encountered and were, in general, considerably more effective than corresponding changes in yaw damping.

(c) Changes in mass distribution in the practical range produced only relatively small effects.

(d) Alterations in the yawing moment due to rolling  $C_{n_p}$  although sometimes producing favorable effects would not be useful in alleviating the coupling problem throughout the angle-of-attack range.

(e) Changes in the rolling moment due to sideslip parameter  $C_{l_\beta}$  could produce significant improvements under certain conditions.

2. A study of the effects of flight condition revealed that:

(a) The amplitude of the motions developed depends to a large extent on the duration of the maneuver. Limited studies indicated that  $90^\circ$  roll maneuvers would be considerably less critical than  $360^\circ$  rolls.

(b) Small inadvertent stabilizer inputs can greatly affect the motions that would otherwise be obtained.

(c) The engine gyroscopic terms can cause rolls in one direction to be somewhat more critical than corresponding rolls in the opposite direction.

(d) The initial angle of attack of the principal axis has an important bearing on the amplitude of the motions, particularly in the absence of other disturbing functions.

(e) For a given initial angle of attack a reduction in altitude will delay critical conditions to a higher roll rate, but the maximum amplitudes may be affected only slightly.

(f) The effects of variations in Mach number cannot easily be generalized since there are likely to be changes in most of the controlling parameters.

3. Utilizing simple concepts proved useful in assessing the qualitative effects of many of the aerodynamic and inertia parameters and changes in flight condition. The calculated lower resonant frequency generally corresponded to the average roll velocity at which the more serious motions could be expected.

4. It is reasoned that rational design procedure can avoid the problem of serious roll coupling at supersonic speeds and minimize the problem at subsonic speeds for the configurations of the type considered.

High-Speed Flight Station,  
National Advisory Committee for Aeronautics,  
Edwards, Calif., December 20, 1955.

## APPENDIX A

If the equations at the top of page 9 of NACA TN 1627 (ref. 2) are written to include the engine inertia terms and actual value of  $\frac{I_Z - I_X}{I_Y}$ , the equations become in the notation of reference 2

$$\begin{aligned} \ddot{\theta} - p_0 \dot{\psi} - (p_0 \dot{\psi} + p_0^2 \theta) F' + 2\zeta_{\theta} \omega_{\theta} p_0 (\dot{\theta} - p_0 \psi) + \\ (\dot{\psi} + p_0 \theta) K + \omega_{\theta}^2 p_0^2 \theta = 0 \end{aligned} \quad (1)$$

$$\begin{aligned} \ddot{\psi} + p_0 \dot{\theta} + (p_0^2 \psi - p_0 \dot{\theta}) F + 2\zeta_{\psi} \omega_{\psi} p_0 (\dot{\psi} + p_0 \theta) - \\ (\dot{\theta} - p_0 \psi) K_1 + \omega_{\psi}^2 p_0^2 \psi = 0 \end{aligned} \quad (2)$$

where

$$\begin{aligned} \frac{I_X - I_Y}{I_Z} = F & \qquad \frac{I_X \omega_e}{I_Y} = K \\ \frac{I_Z - I_X}{I_Y} = F' & \qquad \frac{I_X \omega_e}{I_Z} = K_1 \end{aligned}$$

$\theta$  angle of pitch relative to flight-path direction, radians

$\psi$  angle of yaw relative to flight-path direction, radians

$p_0$  steady rolling velocity, radians/sec

Then, as in NACA TN 1627, assuming

$$t' = p_0 t \quad \text{and} \quad D = \frac{d}{dt'} = \frac{1}{p_0} \frac{d}{dt}$$

equations (1) and (2) become

$$D^2 \theta - D \psi - D \psi F' - \theta F' + \frac{K D \psi}{p_0} + \frac{K \theta}{p_0} + 2\zeta_{\theta} \omega_{\theta} D \theta - 2\zeta_{\theta} \omega_{\theta} \psi + \omega_{\theta}^2 \theta = 0 \quad (3)$$

$$D^2 \psi + D \theta + \psi F - D \theta F - \frac{K_1 D \theta}{p_0} + \frac{K_1 \psi}{p_0} + 2\zeta_{\psi} \omega_{\psi} D \psi + 2\zeta_{\psi} \omega_{\psi} \theta + \omega_{\psi}^2 \psi = 0 \quad (4)$$

The determinant of equations (3) and (4) is

$$\begin{vmatrix} D^2 - F' + 2\zeta_\theta\omega_\theta D + \omega_\theta^2 + \frac{K}{P_0} & -D - DF' + \frac{KD}{P_0} - 2\zeta_\theta\omega_\theta \\ D - DF + 2\zeta_\psi\omega_\psi - \frac{K_1 D}{P_0} & D^2 + F + 2\zeta_\psi\omega_\psi D + \omega_\psi^2 + \frac{K_1}{P_0} \end{vmatrix} = 0$$

The determinant may be expanded to give the quartic

$$aD^4 + bD^3 + cD^2 + dD + e = 0$$

The divergence boundary is obtained by setting the coefficient  $e = 0$

$$\begin{aligned} e = & -FF' + \omega_\theta^2\omega_\psi^2 - F'\omega_\psi^2 + \omega_\theta^2F + 4\zeta_\psi\omega_\psi\zeta_\theta\omega_\theta + \\ & \frac{KF}{P_0} + \frac{K\omega_\psi^2}{P_0} + \frac{K_1K}{P_0^2} - \frac{F'K_1}{P_0} + \frac{K_1\omega_\theta^2}{P_0} = 0 \end{aligned} \quad (5)$$

if  $\zeta_\theta = \zeta_\psi = 0$  then equation (5) becomes

$$\begin{aligned} e = & -FF' + \omega_\theta^2\omega_\psi^2 - F'\omega_\psi^2 + \omega_\theta^2F + \frac{KF}{P_0} + \frac{K\omega_\psi^2}{P_0} + \\ & \frac{K_1K}{P_0^2} - \frac{F'K_1}{P_0} + \frac{K_1\omega_\theta^2}{P_0} = 0 \end{aligned}$$

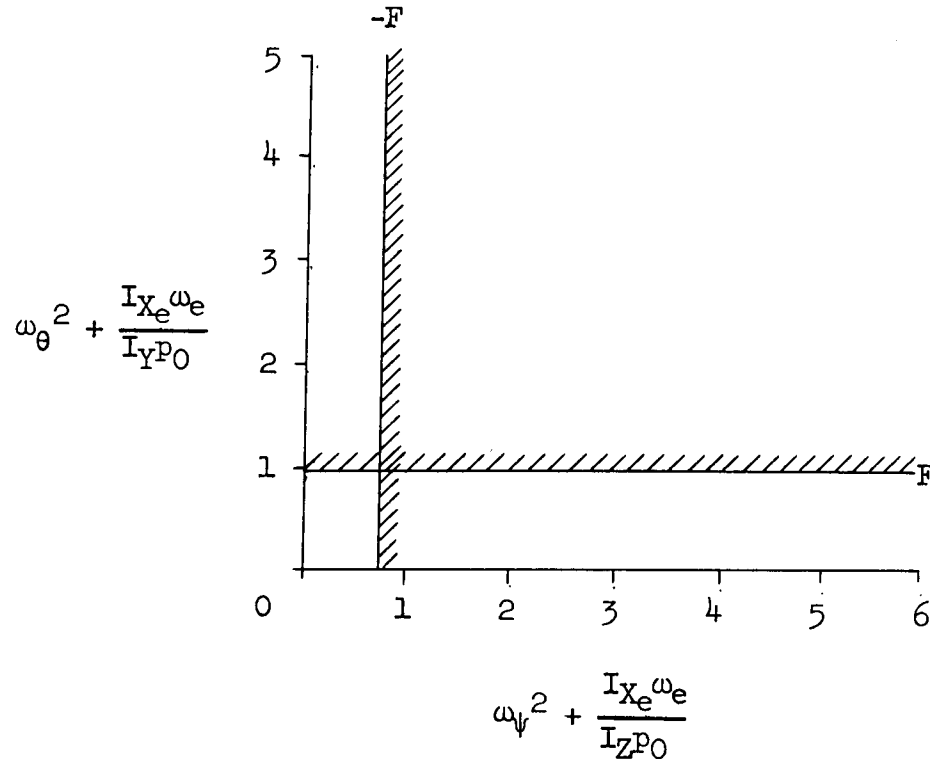
from which it can be shown

$$\omega_\theta^2 = F' - \frac{K}{P_0} = F' - \left( \frac{I_{X_e}\omega_e}{I_Y P_0} \right) \quad (6)$$

$$\omega_\psi^2 = -F - \frac{K_1}{P_0} = -F - \left( \frac{I_{X_e}\omega_e}{I_Z P_0} \right) \quad (7)$$

if  $\omega_\theta^2 + \frac{I_{X_e}\omega_e}{I_Y P_0}$  is plotted as ordinate and  $\omega_\psi^2 + \frac{I_{X_e}\omega_e}{I_Z P_0}$  as abscissa,

it is seen that a stability plot can be obtained similar to those in NACA TN 1627



It will be of interest to determine the roll velocity at which resonance occurs. The square of the undamped natural frequency in yaw can be written

$$\omega_{\psi}^2 P_0^2 = \frac{C_{n\beta} \frac{1}{2} \rho V^2 S b}{I_Z} \quad (8)$$

then, substituting equation (8) into equation (7), enables calculation of the steady roll velocity at which instability first occurs

$$P_0^2 + \left( \frac{I_{X_e} \omega_e}{I_X - I_Y} \right) P_0 + \frac{C_{n\beta} \frac{1}{2} \rho V^2 S b}{I_X - I_Y} = 0$$

$$P_0 = - \frac{I_{X_e} \omega_e}{2(I_X - I_Y)} \pm \sqrt{\frac{1}{4} \left( \frac{I_{X_e} \omega_e}{I_X - I_Y} \right)^2 - \left( \frac{C_{n\beta} \frac{1}{2} \rho V^2 S b}{I_X - I_Y} \right)} \quad (9)$$

Inasmuch as the engine term inside the radical is usually small relative to the directional stability term, equation (9) can be simplified to

$$p_0 = \pm \sqrt{\frac{C_{n\beta} \frac{1}{2} \rho V^2 S b}{I_Y - I_X}} + \frac{I_{X_e} \omega_e}{2(I_Y - I_X)} \quad (10)$$

applicable when the directional divergence boundary is intersected first as roll velocity is progressively increased. Similarly it can be shown

$$p_0 = \pm \sqrt{\frac{-C_{m\alpha} \frac{1}{2} \rho V^2 S \bar{c}}{I_Z - I_X}} + \frac{I_{X_e} \omega_e}{2(I_Z - I_X)} \quad (11)$$

applicable when the pitch divergence boundary is first crossed.

These equations indicate that left rolls will have a somewhat lower resonant frequency than right rolls for right-hand engine rotation.

For the practical condition of finite damping in pitch and yaw, it appears the boundaries can be calculated as if engine terms were neglected (ref. 2) and then used with the modified parameters to account for the engine inertia effects.

## APPENDIX B

The effects of roll rate and the basic proportioning of longitudinal to directional stability on divergence rate can be examined by treating a simple condition of zero damping and by neglecting the engine terms of equations 1 and 2 of appendix A. If these assumptions are made, the determinant of equations 3 and 4 of appendix A can be expanded to give

$$aD^4 + cD^2 + e = 0$$

where

$$a = 1$$

$$c = 1 - FF' + \omega_\psi^2 + \omega_\theta^2$$

$$e = -FF' + \omega_\theta^2 \omega_\psi^2 - \omega_\psi^2 F' + \omega_\theta^2 F$$

This equation can be solved as a quadratic in  $D^2$  as follows:

$$D^2 = \frac{-(\omega_\psi^2 + \omega_\theta^2 + 1 - FF')}{2} \pm$$

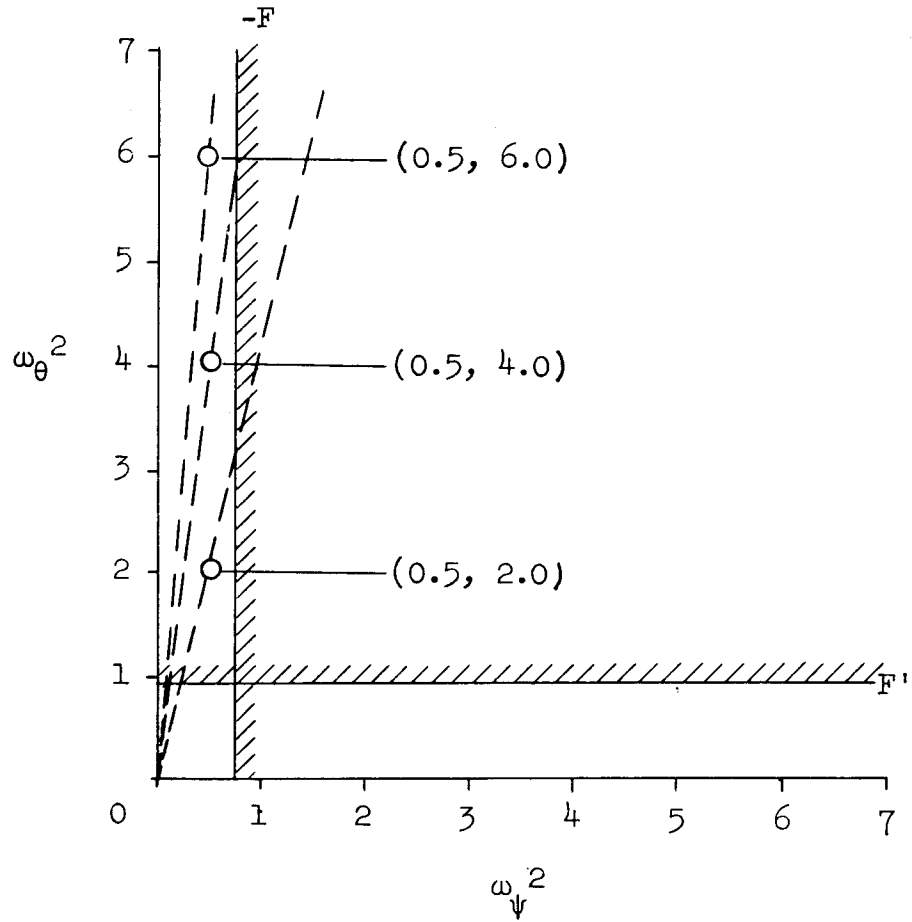
$$\sqrt{\left(\frac{\omega_\psi^2 + \omega_\theta^2 + 1 - FF'}{2}\right)^2 - \omega_\theta^2 \omega_\psi^2 + \omega_\psi^2 F' - \omega_\theta^2 F + FF'}$$

The value of the positive real root  $D$  of the preceding equation will determine the nondimensional time to double amplitude in accordance with the formula

$$t'_2 = \frac{0.693}{\text{Positive real root}}$$

where  $t'_2$  is the nondimensional time to double amplitude.

Consider the specified points in the unstable portion of the following stability chart



If  $-F = 0.71$  and  $F' = 0.95$  then the positive real root for the points considered will be as follows:

$\omega_{\psi}^2$	$\omega_{\theta}^2$	Positive real root	$t'_2$
0.5	2.0	0.228	3.03
.5	4.0	.319	2.17
.5	6.0	.357	1.94

Thus it would be expected that if the vertical displacement of the three points considered is caused, for example, by  $C_{m\alpha}$  variation (the rate of roll therefore being identical) the higher the location of the point in the unstable region the greater the rate of divergence.

If on the other hand the stability level of both  $C_{m\alpha}$  and  $C_{n\beta}$  are altered such that a given point in the unstable region is attained at a different roll rate, it would appear that the rate of divergence would be proportioned to roll rate inasmuch as

$$t'_2 = p_0 t_2 \qquad t_2 = \frac{t'_2}{p_0}$$

where  $t_2$  is the time to double amplitude measured in seconds.

## REFERENCES

1. Bird, John D., and Jaquet, Byron M.: A Study of the Use of Experimental Stability Derivatives in the Calculation of the Lateral Disturbed Motions of a Swept-Wing Airplane and Comparison With Flight Results. NACA Rep. 1031, 1951. (Supersedes NACA TN 2013.)
2. Phillips, William H.: Effect of Steady Rolling on Longitudinal and Directional Stability. NACA TN 1627, 1948.
3. White, R. J., Uddenberg, R. C., Murray, D., and Graham, F. D.: The Dynamic Stability and Control Equations of a Pivoted-Wing Supersonic Pilotless Aircraft, With Downwash, Wake and Interference Effects Included. Doc. No. D-8510, Boeing Aircraft Co., Jan. 9, 1948.
4. NACA High-Speed Flight Station: Flight Experience With Two High-Speed Airplanes Having Violent Lateral-Longitudinal Coupling in Aileron Rolls. NACA RM H55A13, 1955.
5. Weil, Joseph, Gates, Ordway B., Jr., Banner, Richard D., and Kuhl, Albert E.: Flight Experience of Inertia Coupling in Rolling Maneuvers. NACA RM H55E17b, 1955.
6. Gates, Ordway B., Jr., Weil, Joseph, and Woodling, C. H.: Effect of Automatic Stabilization on the Sideslip and Angle-of-Attack Disturbances in Rolling Maneuvers. NACA RM L55E25b, 1955.
7. Gates, Ordway B., Jr., and Woodling, C. H.: A Theoretical Analysis of the Effect of Engine Angular Momentum on Longitudinal and Directional Stability in Steady Rolling Maneuvers. NACA RM L55G05, 1955.
8. Finch, Thomas W., Peele, James R., and Day, Richard E.: Flight Investigation of the Effect of Vertical-Tail Size on the Rolling Behavior of a Swept-Wing Airplane Having Lateral-Longitudinal Coupling. NACA RM H55L28a, 1956.

TABLE I

EQUATIONS OF MOTION (REFERENCED TO BODY AXIS)

$$\dot{p} = \left( \frac{I_Y - I_Z}{I_X} \right) qr + \frac{IXZ}{I_X} \dot{r} + \frac{IXZ}{I_X} pq + \frac{Ab}{I_X} C_{l\delta_{at}} \delta_{at} + \frac{Ab}{I_X} C_{l\delta_r} \delta_r + \frac{Ab^2}{2VI_X} C_{l_p} p + \frac{Ab^2}{2VI_X} C_{l_r} r + \frac{Ab}{I_X} C_{l\beta} \beta + \frac{Ab^2}{2VI_X} C_{l\dot{\beta}} \dot{\beta}$$

$$\dot{q} = \left( \frac{I_Z - I_X}{I_Y} \right) pr + \frac{IXZ}{I_Y} r^2 - \frac{IXZ}{I_Y} p^2 - \frac{I_{Xe}\omega_e}{I_Y} r + \frac{A\bar{C}}{I_Y} C_{m_{i_t}} i_t + \frac{A\bar{C}^2}{2VI_Y} C_{m_q} q + \frac{A\bar{C}^2}{2VI_Y} C_{m_{\dot{\alpha}}} \dot{\alpha} + \frac{A\bar{C}}{I_Y} C_{m_{\Delta\alpha}} \Delta\alpha + \frac{A\bar{C}}{I_Y} C_{m\beta} \beta$$

$$\dot{r} = \left( \frac{I_X - I_Y}{I_Z} \right) pq + \frac{IXZ}{I_Z} \dot{p} - \frac{IXZ}{I_Z} qr + \frac{I_{Xe}\omega_e}{I_Z} q + \frac{Ab}{I_Z} C_{n_{\delta_r}} \delta_r + \frac{Ab^2}{2VI_Z} C_{n_r} r + \frac{Ab^2}{2VI_Z} C_{n_p} p + \frac{Ab}{I_Z} C_{n\beta} \beta + \frac{Ab}{I_Z} C_{n\delta_{at}} \delta_{at}$$

$$\dot{\beta} = \frac{g}{V} m_\beta - r + \alpha p + \frac{A}{mV} C_{Y\beta} \beta + \frac{Ab}{2mV^2} C_{Y_p} p + \frac{Ab}{2mV^2} C_{Y_r} r + \frac{Ab}{2mV^2} C_{Y\dot{\beta}} \dot{\beta}$$

$$\dot{\alpha} = q + \frac{g}{V} n_\beta - p\beta - \frac{A}{mV} C_{I_\alpha} \alpha + \frac{A}{mV} C_{I_\alpha} L_0 - \frac{A}{mV} C_{L_{i_t}} i_t$$

$$\dot{l}_\beta = m_\beta r - n_\beta q \quad l_\beta = -\sin \theta_e$$

$$\dot{m}_\beta = n_\beta p - l_\beta r \quad m_\beta = \sin \varphi_e \cos \theta_e$$

$$\dot{n}_\beta = l_\beta q - m_\beta p \quad n_\beta = \cos \varphi_e \cos \theta_e$$

where

$$A = \frac{\rho V^2 S}{2}$$

 $\varphi_e, \theta_e$  angles between the body axis and earth gravity axis

TABLE II

DERIVATIVES AND CONSTANTS REQUIRED FOR BASIC CALCULATIONS

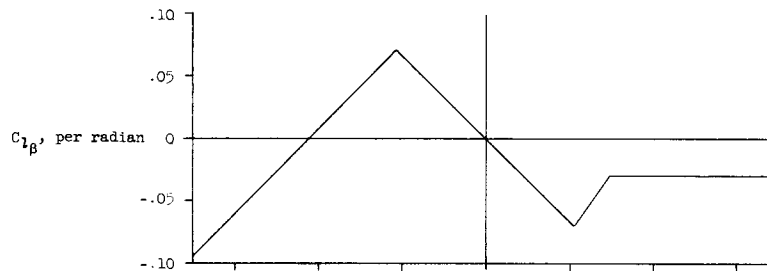
	Swept-wing airplane	Delta-wing airplane	
	M = 0.7	M = 0.8	M = 1.2
Basic flight condition			
$h_p$ , ft . . . . .	32,000	40,000	40,000
$\frac{1}{2} \rho V^2$ , lb/sq ft . .	197	175	395
V, ft/sec . . . . .	690	777	1,165
$\alpha_0$ , deg . . . . .	5.0	8.0	3.9
$n_0$ , g . . . . .	1.0	1.33	1.0
$\phi_0$ , deg . . . . .	0	0	0
$\alpha_{L_0}$ , deg . . . . .	0	0.8	1.0
Physical characteristics			
$\bar{c}$ , ft . . . . .	11.3	23.13	
b, ft . . . . .	36.6	37.8	
S, sq ft . . . . .	377	661.5	
m, slugs . . . . .	745	745	
$I_x$ , slug-ft <sup>2</sup> . . . .	10,976	13,200	
$I_y$ , slug-ft <sup>2</sup> . . . .	57,100	106,000	
$I_z$ , slug-ft <sup>2</sup> . . . .	64,975	114,600	
$I_{xz}$ , slug-ft <sup>2</sup> . . . .	942	3,540	
$\epsilon$ , deg . . . . .	1.0	2.0	
$I_{x_e} \omega_e$ , slug-ft <sup>2</sup> . .	17,554	17,554	

TABLE II.- Concluded

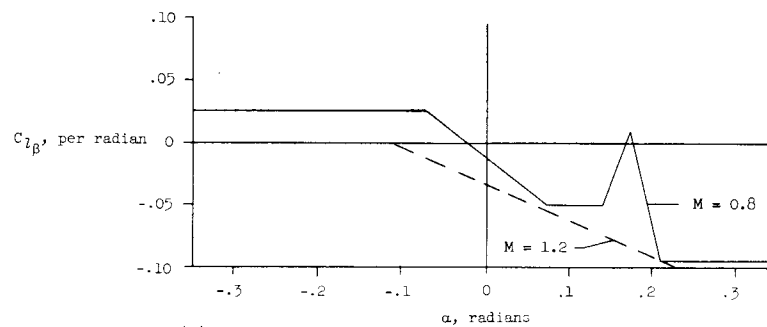
DERIVATIVES AND CONSTANTS REQUIRED FOR BASIC CALCULATIONS

	Swept-wing airplane		Delta-wing airplane	
	M = 0.7		M = 0.8	M = 1.2
Aerodynamic derivatives for basic flight conditions				
$C_{L_{\dot{\alpha}}}$ , per radian . . . . .	0		0	0
$C_{L_{\dot{\alpha}}}$ , per radian . . . . .	3.88		2.78	1.83
$C_{m_{\dot{\alpha}}}$ , per radian . . . . .	-1.0		*	*
$C_{m_{\dot{q}}}$ , per radian . . . . .	-3.5		-1.5	-0.7
$C_{m_{\dot{\omega}}}$ , per radian . . . . .	-0.36		-0.18	-0.54
$C_{m_{\dot{\alpha}}}$ , per radian . . . . .	-1.5		-0.5	-0.3
$C_{m_{\dot{\beta}}}$ , per radian . . . . .	0		0	0
$C_{n_{\dot{\beta}}}$ , per radian . . . . .	0		0	0
$C_{n_{\dot{r}}}$ , per radian . . . . .	-0.095		-0.140	-0.150
$C_{n_{\dot{\beta}}}$ , per radian . . . . .	0.057		0.070	0.051
$C_{n_{\dot{\beta}}}$ , per radian . . . . .	0		0	0
$C_{n_{\dot{\alpha}}}$ , per radian . . . . .	0		-0.014	-0.011
$C_{n_{\dot{r}}}$ , per radian . . . . .	*		*	*
$C_{Y_{\dot{p}}}$ , per radian . . . . .	0		0	0
$C_{Y_{\dot{r}}}$ , per radian . . . . .	0		0	0
$C_{Y_{\dot{\beta}}}$ , per radian . . . . .	-0.28		-0.57	-0.70
$C_{Y_{\dot{\beta}}}$ , per radian . . . . .	0		0	0
$C_{l_{\dot{p}}}$ , per radian . . . . .	-0.255		-0.195	-0.232
$C_{l_{\dot{r}}}$ , per radian . . . . .	0.042		0.070	0.080
$C_{l_{\dot{\alpha}}}$ , per radian . . . . .	0.054		0.0715	0.050
$C_{l_{\dot{r}}}$ , per radian . . . . .	*		*	*
$C_{l_{\dot{\beta}}}$ , per radian . . . . .	0		0	0
$C_{l_{\dot{\beta}}}$ , per radian . . . . .	(See curve)		(See curve)	(See curve)

\*Not applicable



(a) Swept-wing airplane.



(b) Delta-wing airplane.

TABLE III

## MOMENTS OF INERTIA USED IN MASS DISTRIBUTION STUDY

$\frac{I_Y - I_X}{I_Z}$	$I_X$ , slug-ft <sup>2</sup>	$I_Y$ , slug-ft <sup>2</sup>	$I_Z$ , slug-ft <sup>2</sup>
0.20	27,000	40,000	64,975
.50	18,200	51,000	64,975
.71	10,976	57,100	64,975
.90	4,430	63,000	64,975

TABLE IV

VALUES OF  $C_{n\beta}$  AND  $C_{m\alpha}$  USED IN COMPUTATIONS

M	$C_{n\beta}$	$C_{m\alpha}$
0.6	0.100	-0.39
.7	.100	-.39
.8	.100	-.43
.9	.110	-.80
1.0	.114	-1.14
1.2	.103	-1.14
1.4	.063	-1.00

Note: The physical and mass characteristics used to calculate figure 48 were the characteristics of the swept-wing airplane of table II.

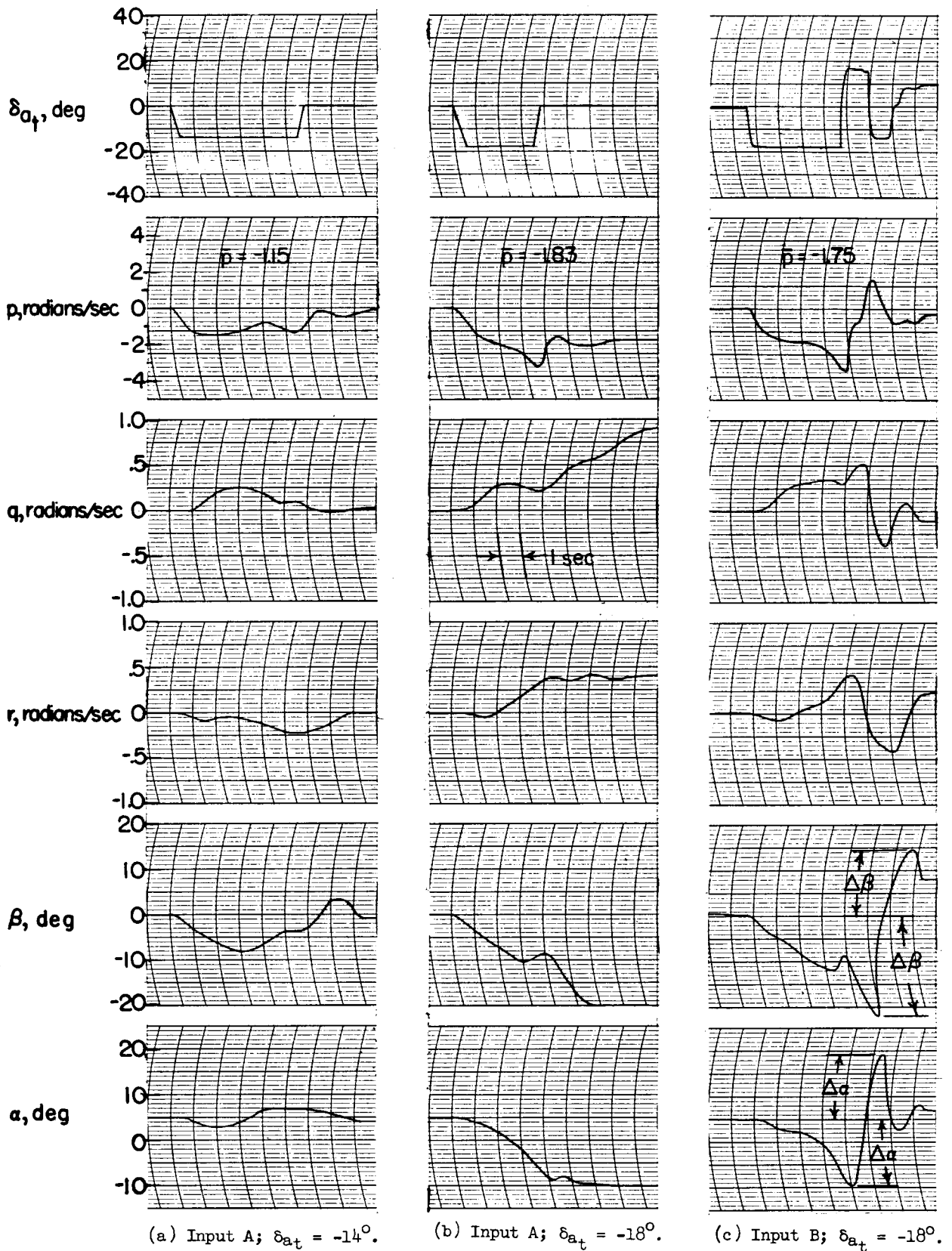
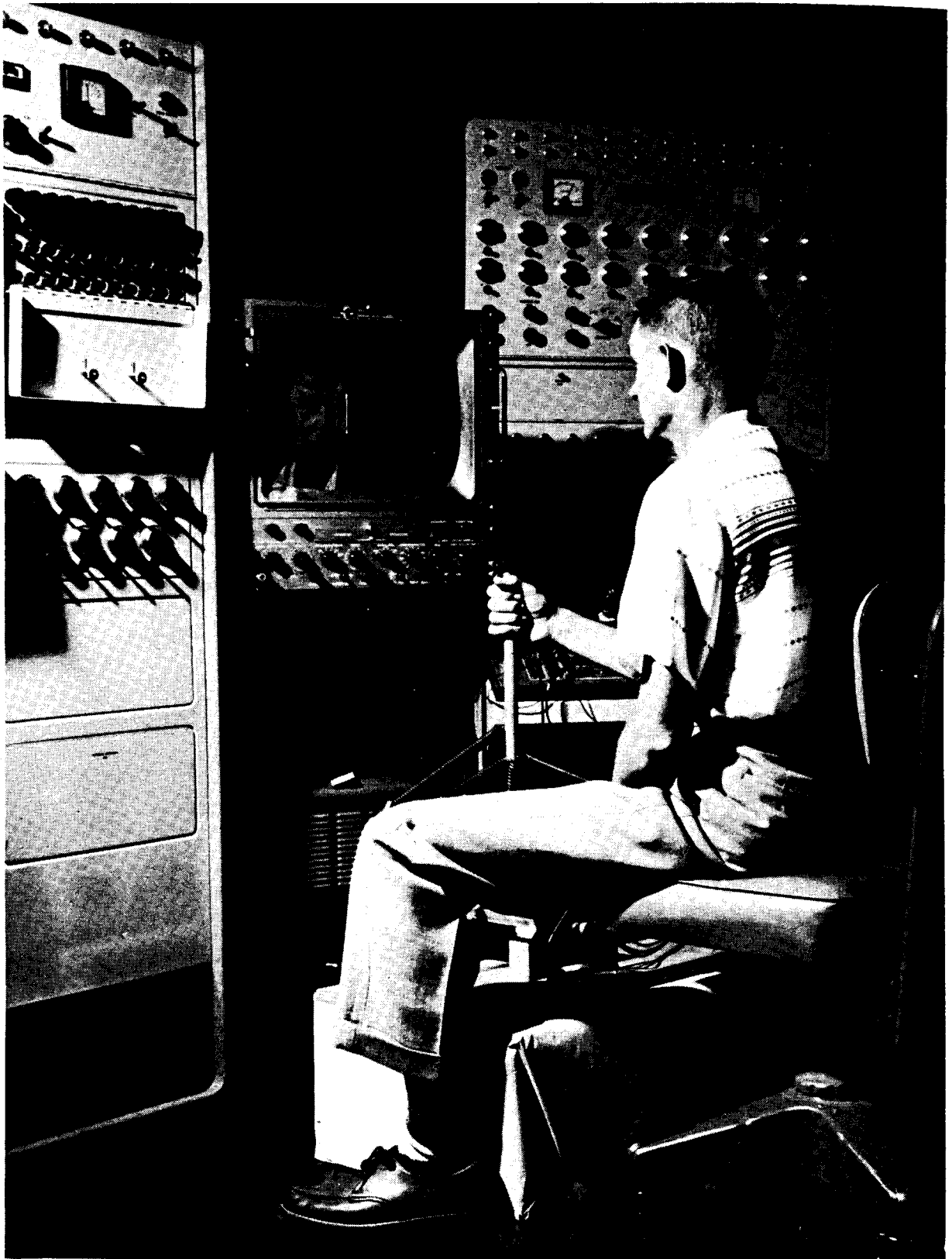


Figure 1.- Representative time histories.



E-1841  
Figure 2.- Photograph showing control stick and oscilloscope presentation.

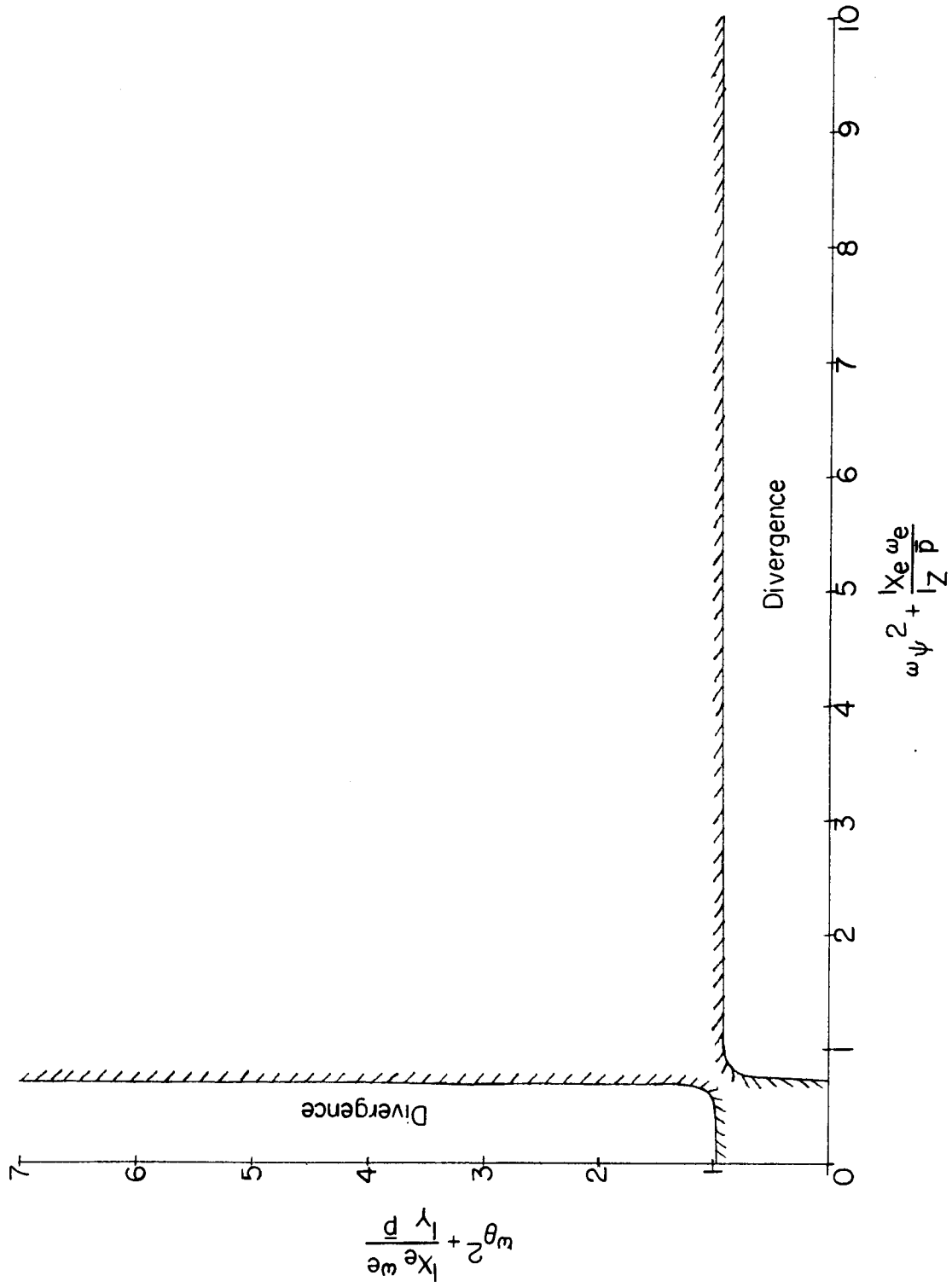


Figure 3.- Representative chart defining stability boundaries.

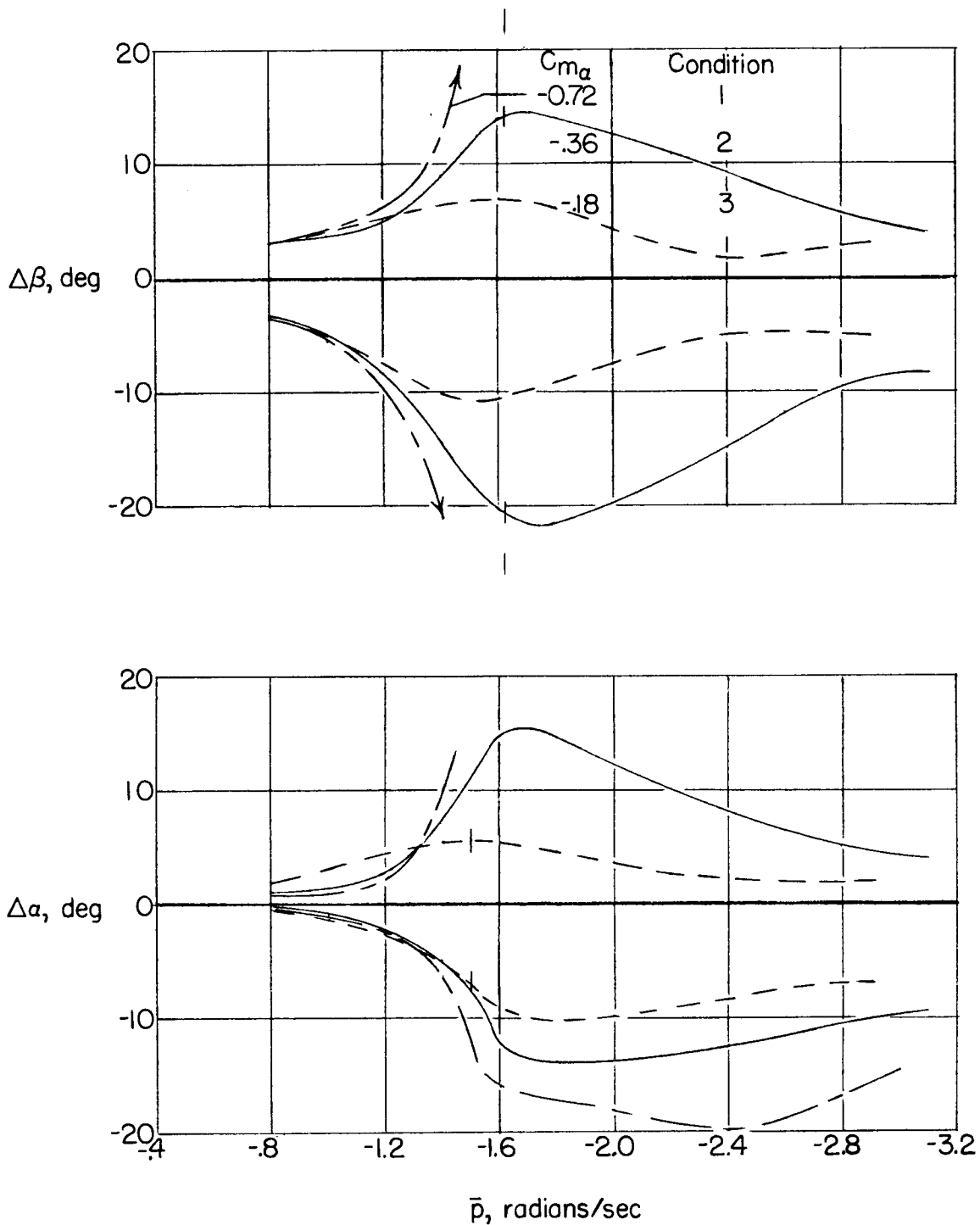


Figure 4.- Effect of  $C_{m\alpha}$  variation. Swept-wing configuration;  
 $C_{n\beta} = 0.057$ ; input B.

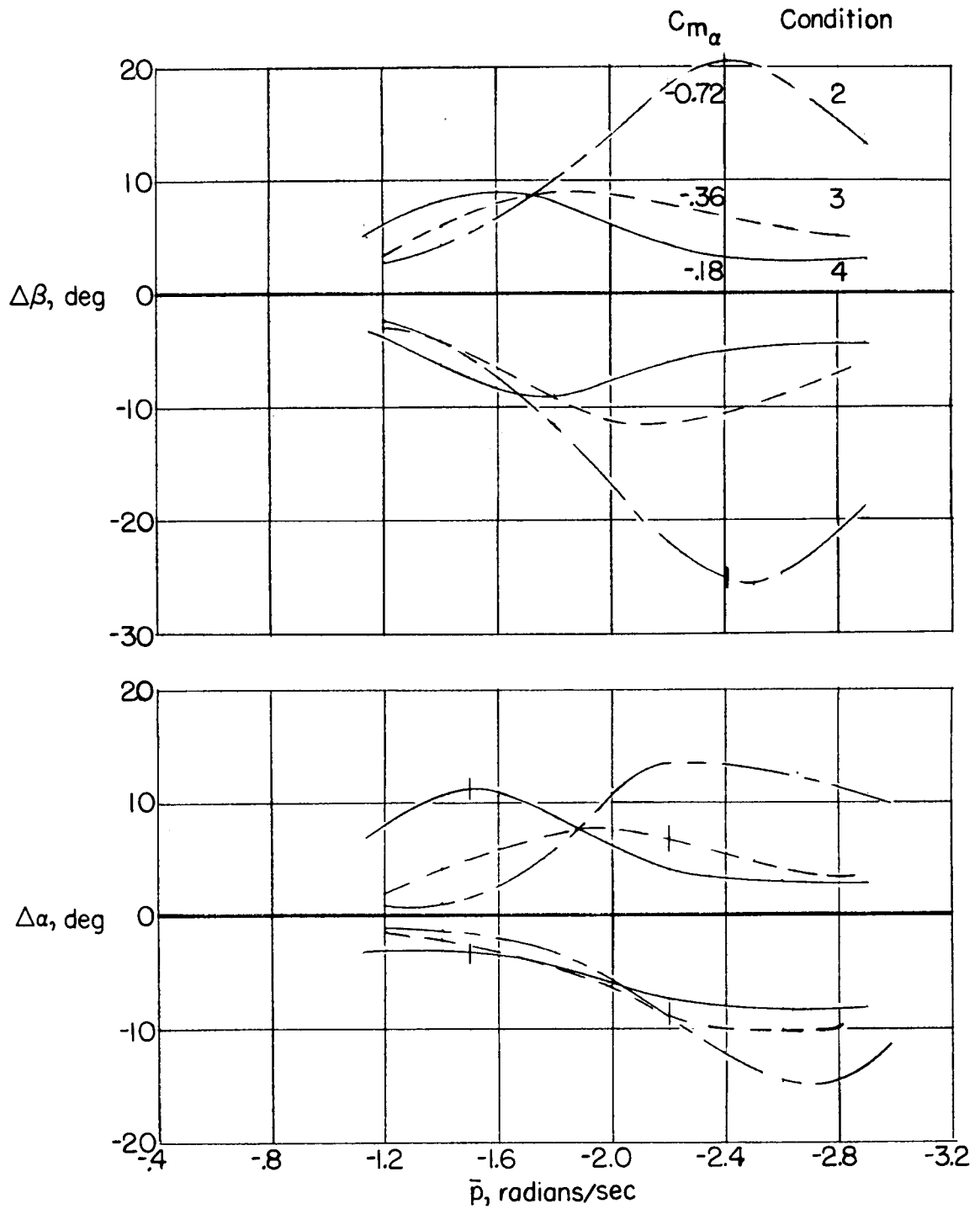


Figure 5.- Effect of  $C_{m_\alpha}$  variation. Swept-wing configuration;  
 $C_{n_\beta} = 0.114$ ; input B.

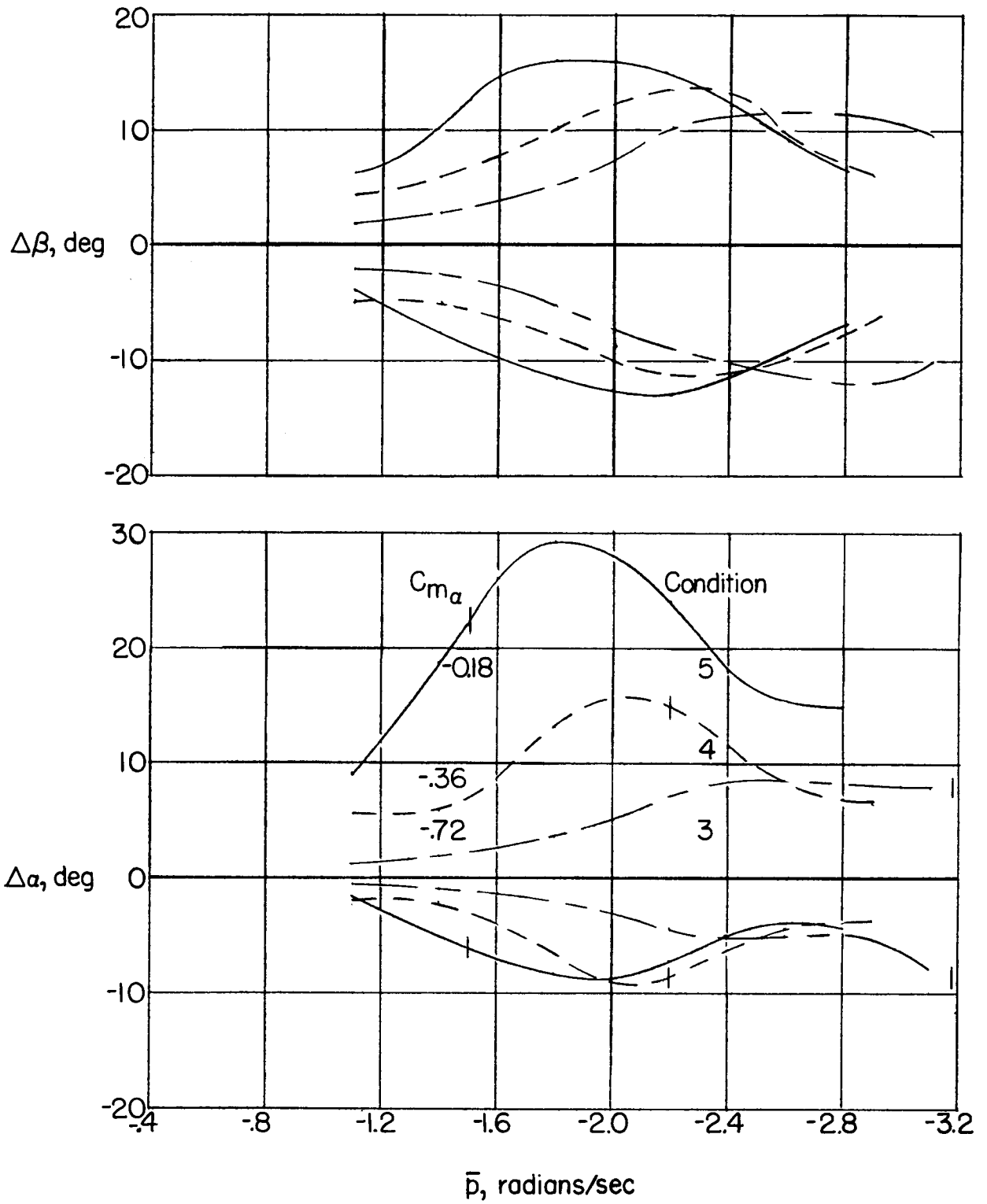


Figure 6.- Effect of  $C_{m\alpha}$  variation. Swept-wing configuration;  
 $C_{n\beta} = 0.228$ ; input B.

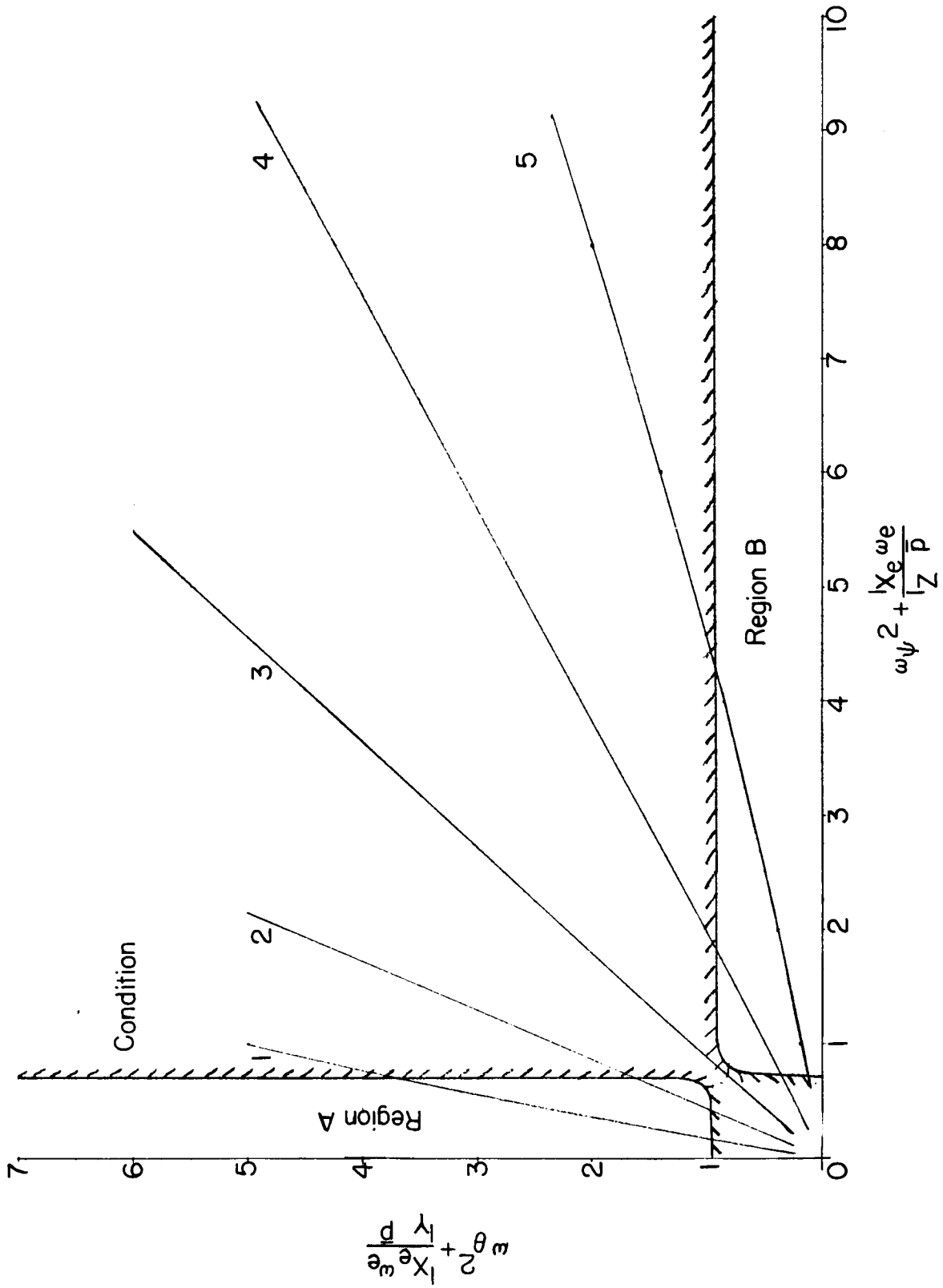
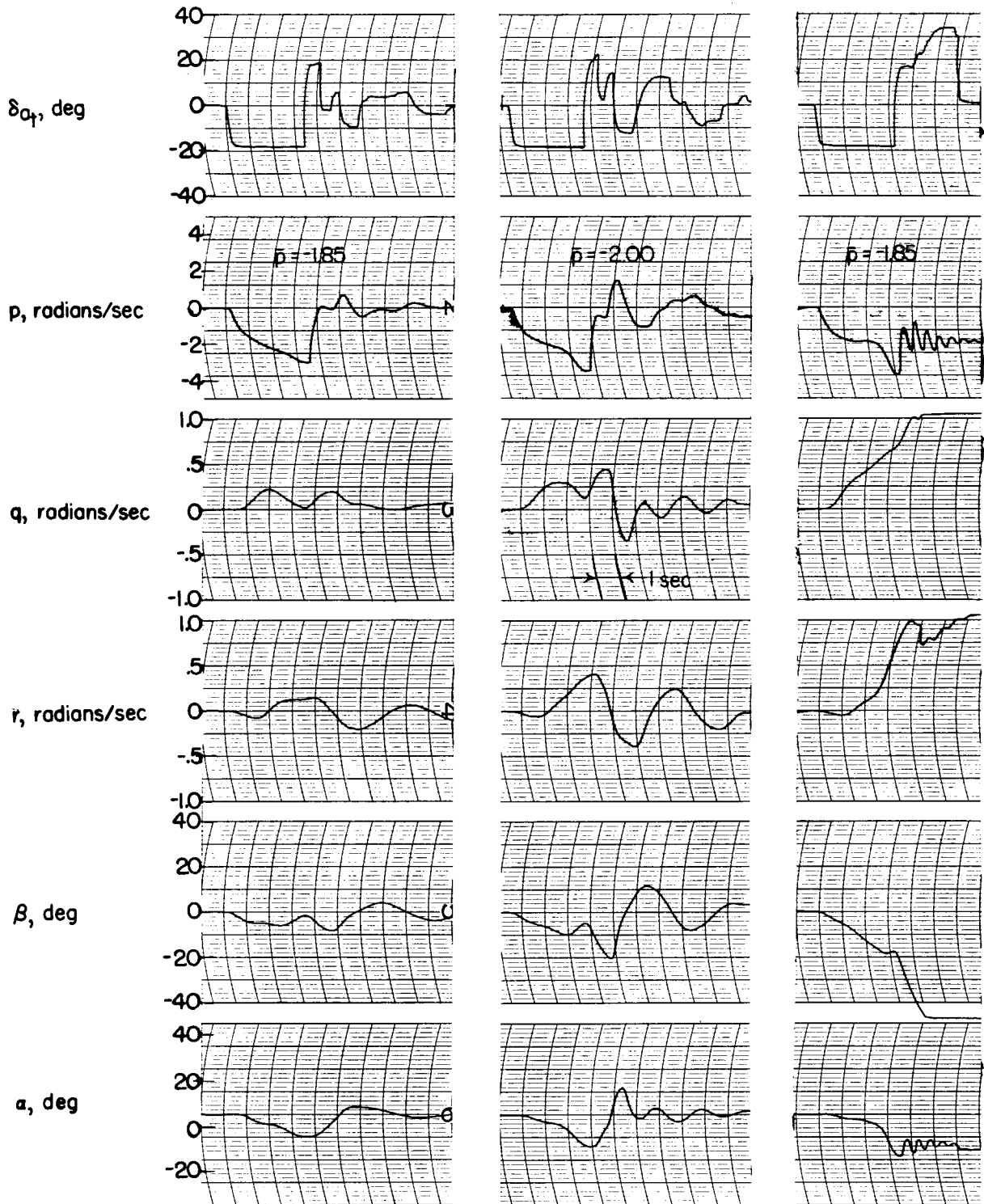


Figure 7.- Stability boundaries for swept-wing configuration. Left rolls.



(a) Condition 3;  
 $C_{m\alpha} = -0.18.$

(b) Condition 2;  
 $C_{m\alpha} = -0.36.$

(c) Condition 1;  
 $C_{m\alpha} = -0.72.$

Figure 8.- Representative time histories for swept-wing configuration.  
Input B;  $C_{N\beta} = 0.057.$

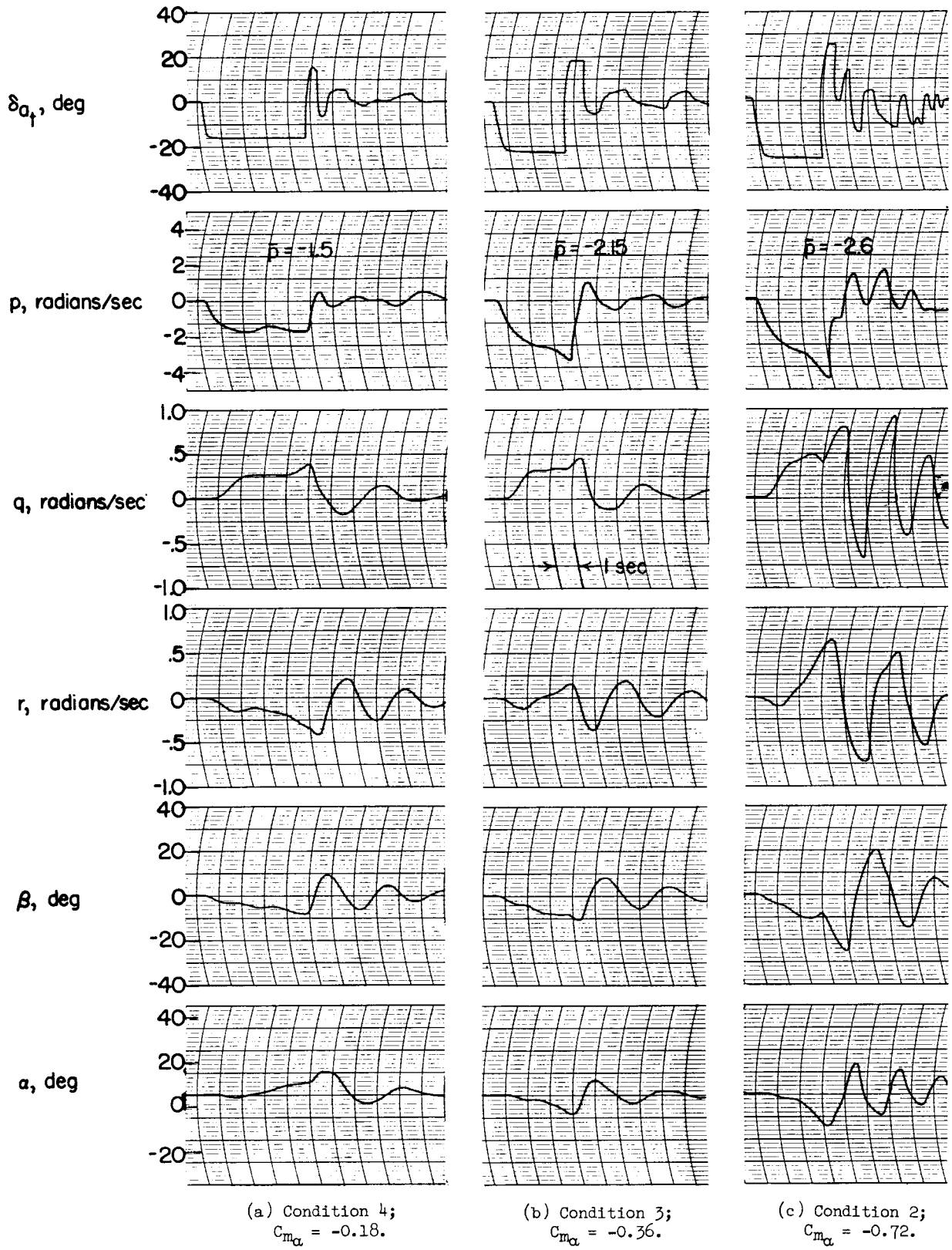


Figure 9.- Representative time histories for swept-wing configuration.  
 Input B;  $C_{n_\beta} = 0.114$ .

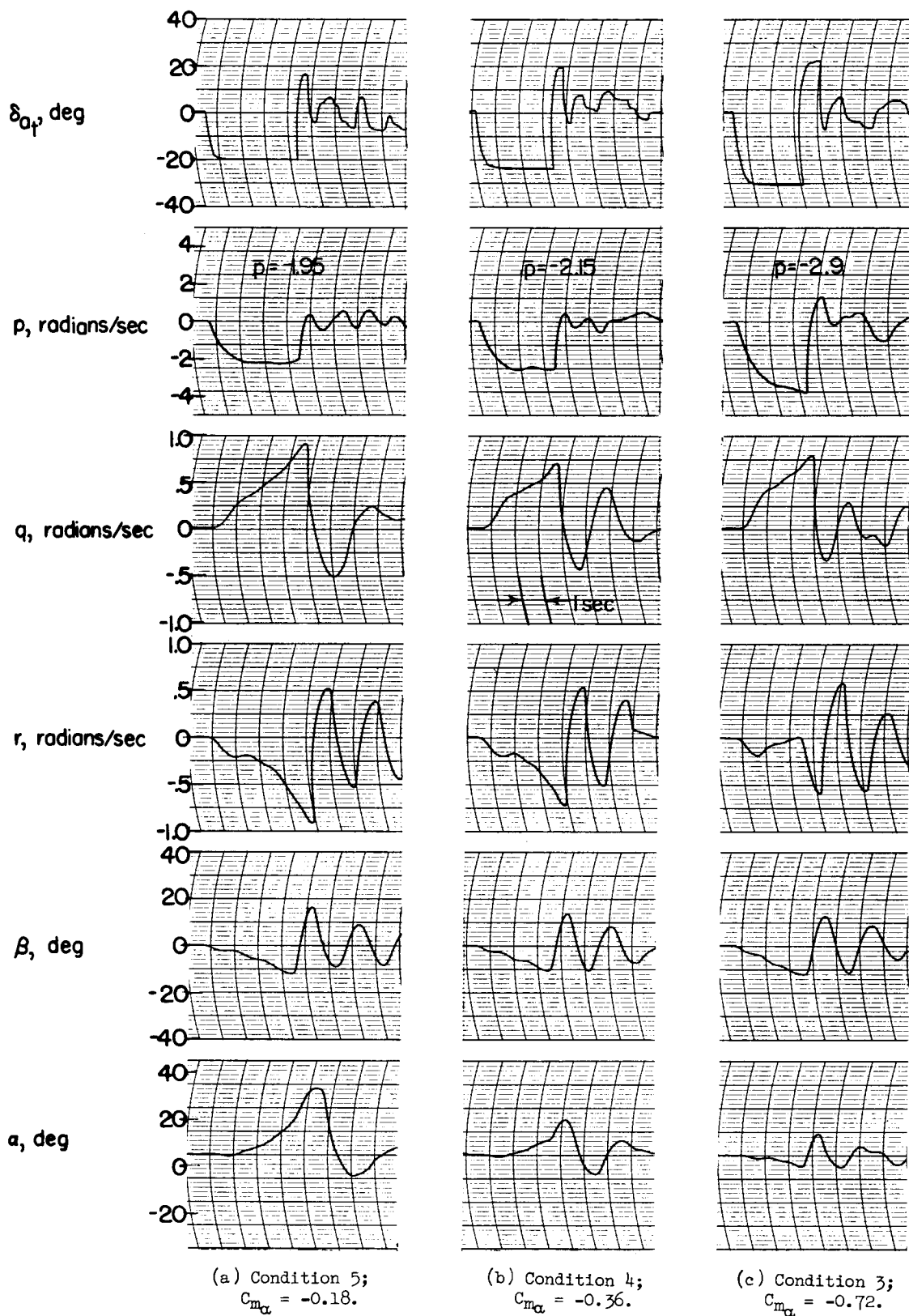


Figure 10.- Representative time histories for swept-wing configuration.  
 Input B;  $C_{n_{\beta}} = 0.228.$

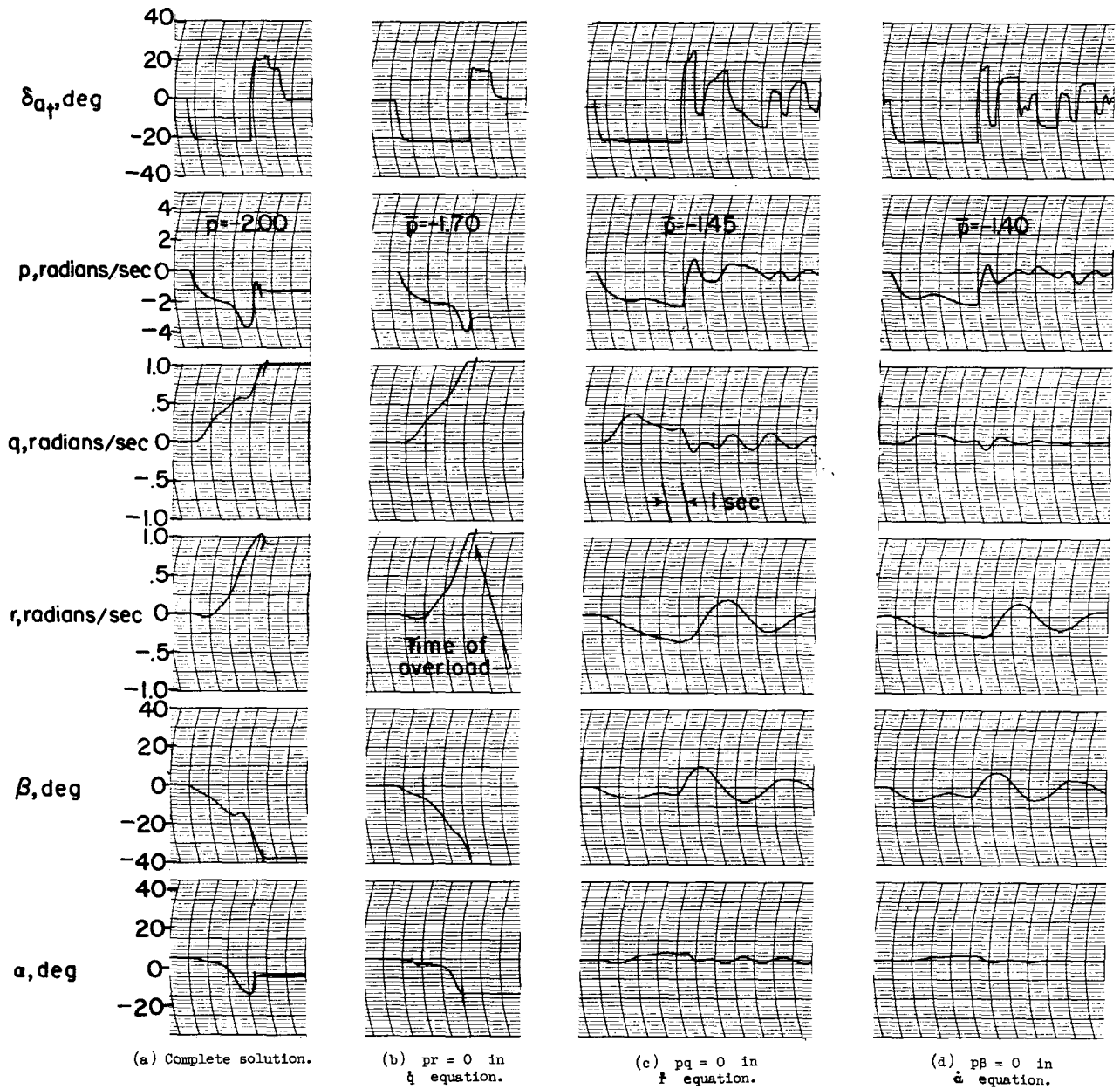


Figure 11.- Relative importance of various terms in equations of motions. Swept-wing configuration. Input B;  $C_{m\alpha} = -0.72$ ;  $C_{n\beta} = 0.057$ .

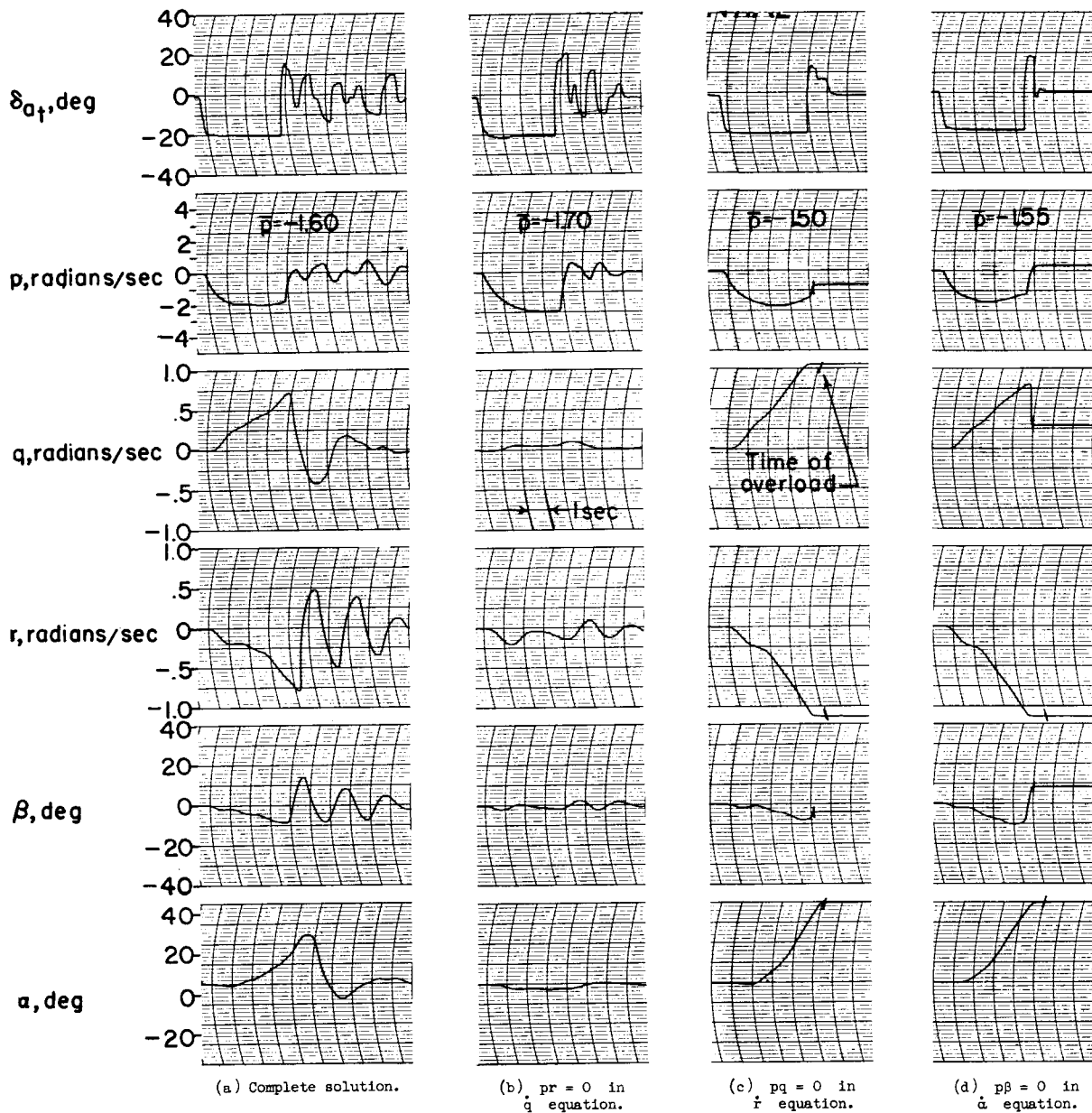


Figure 12.- Relative importance of various terms in equations of motions. Swept-wing configurations. Input B;  $C_{m\alpha} = -0.18$ ;  $C_{n\beta} = 0.228$ .

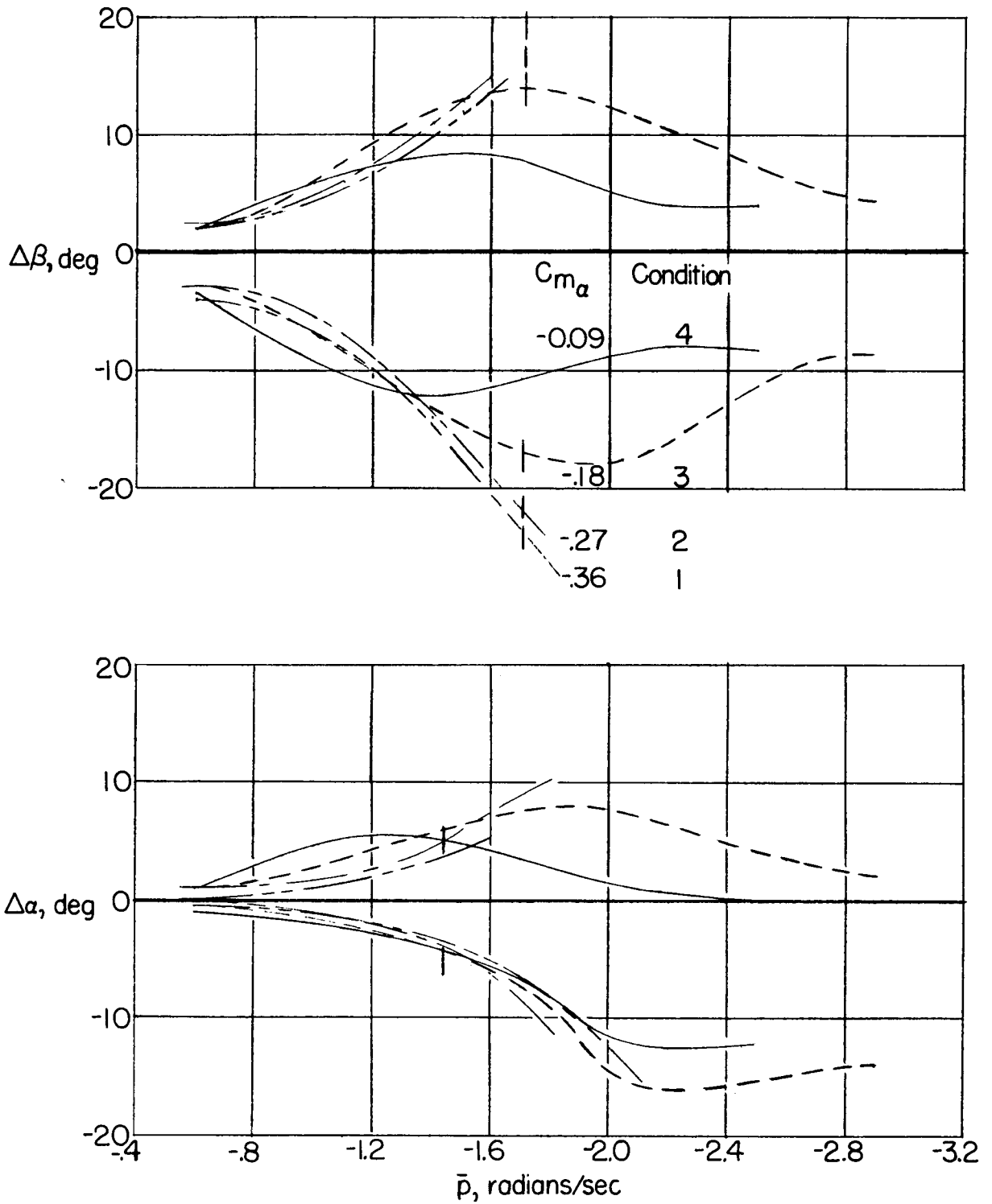


Figure 13.- Effect of  $C_{m_\alpha}$  variation. Delta-wing configuration;  $M = 0.8$ ; input A.

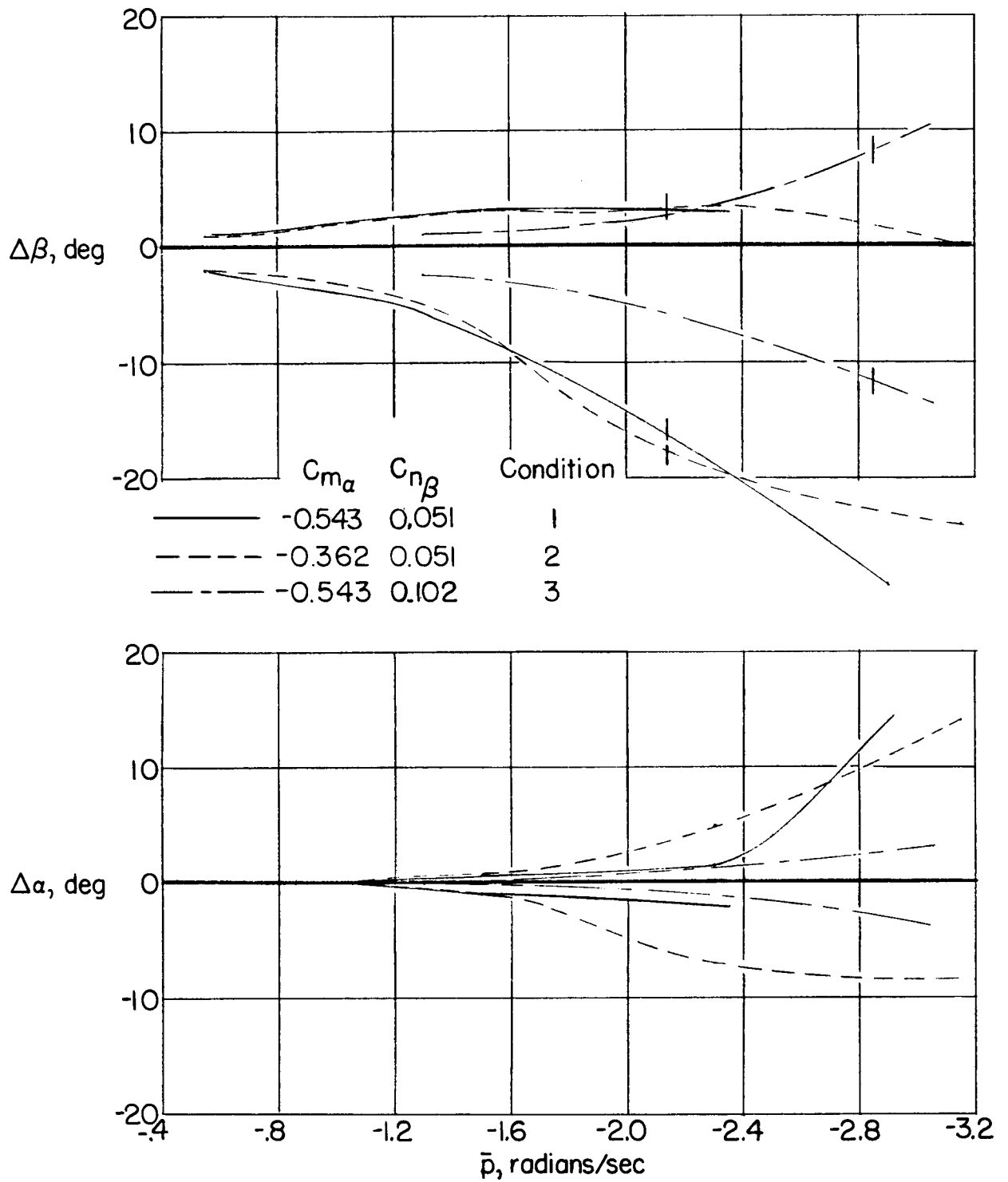


Figure 14.- Effect of  $C_{m_\alpha}$  and  $C_{n_\beta}$  combinations. Delta-wing configuration  $M = 1.2$ ; input A.

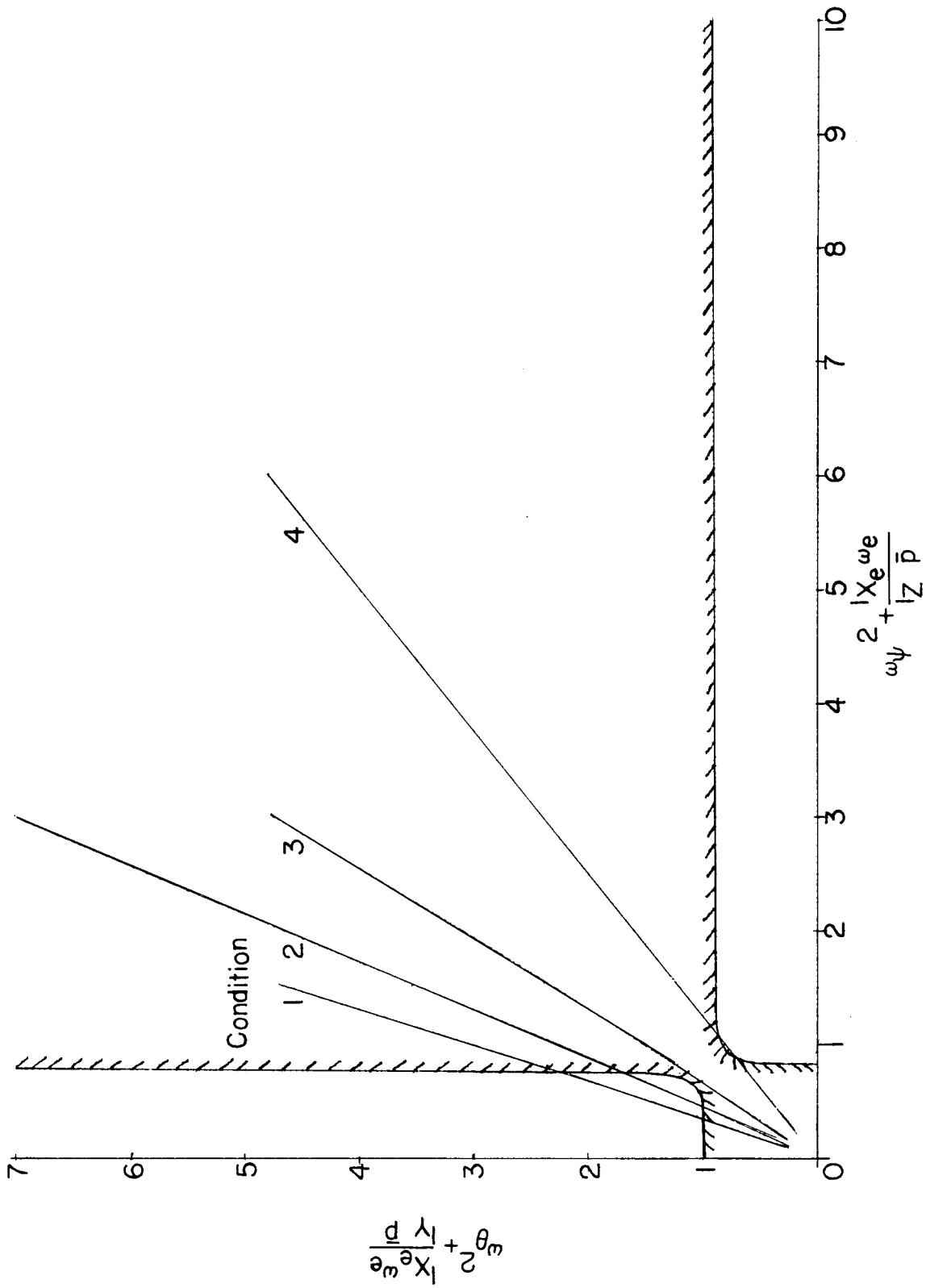


Figure 15.- Stability boundaries for delta-wing configurations.  $M = 0.80$ .  
Left rolls.

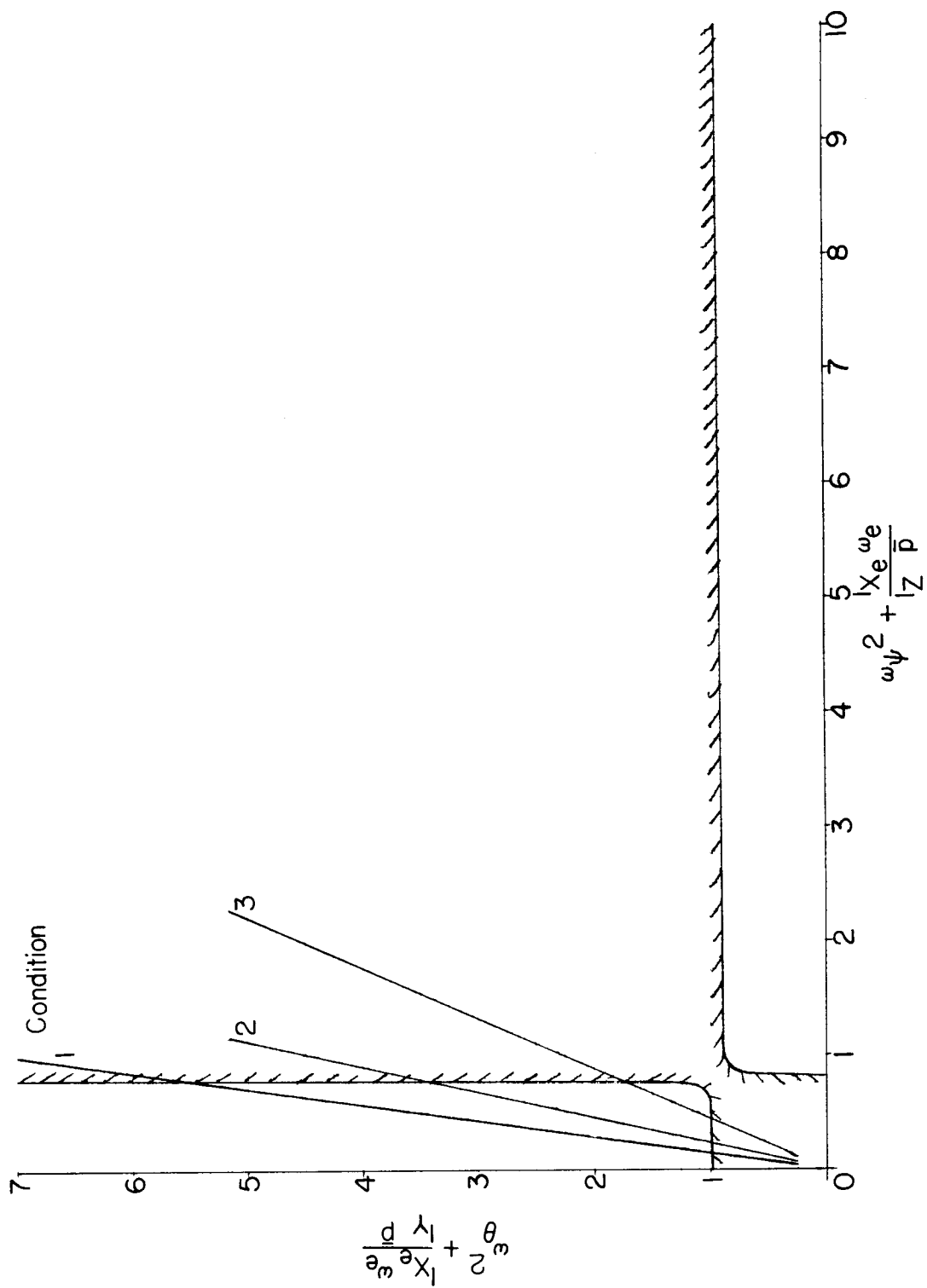
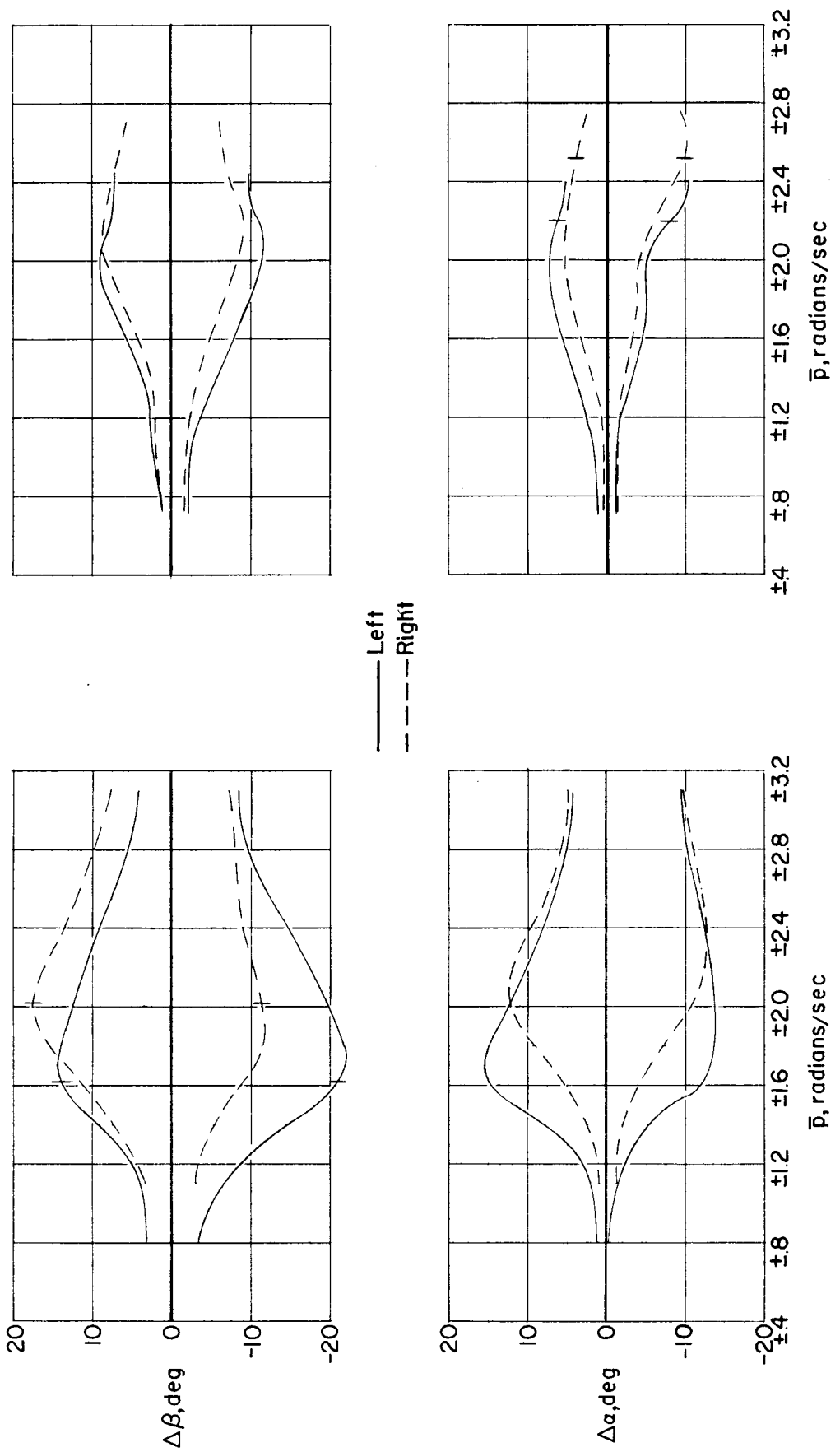


Figure 16.- Stability boundary for delta-wing configuration.  $M = 1.2$ .  
Left rolls.



(a) Input B;  $C_{n\beta} = 0.057$ .

(b) Input A;  $C_{n\beta} = 0.114$ .

Figure 17.- Effect of roll direction. Swept-wing configuration.

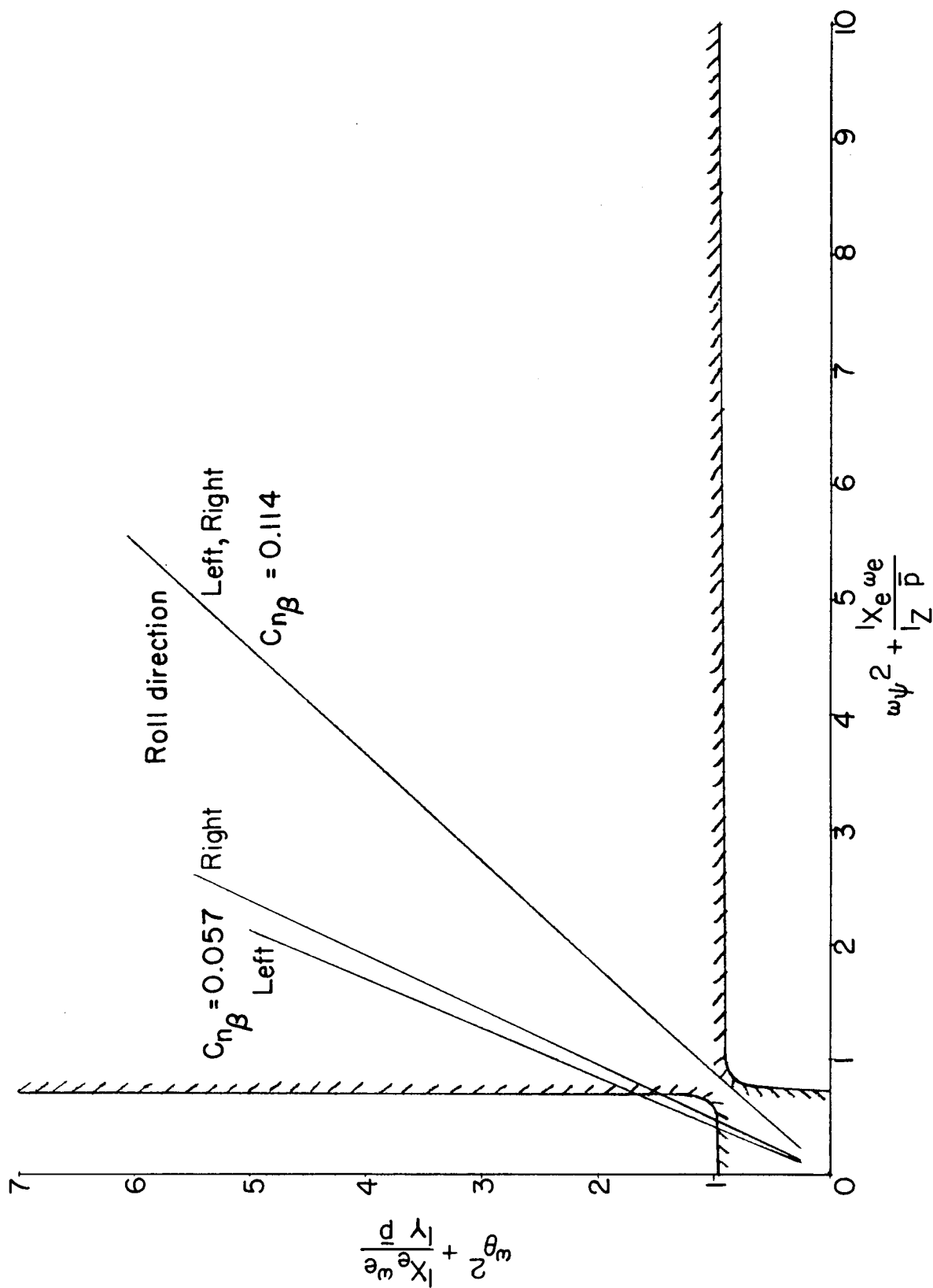
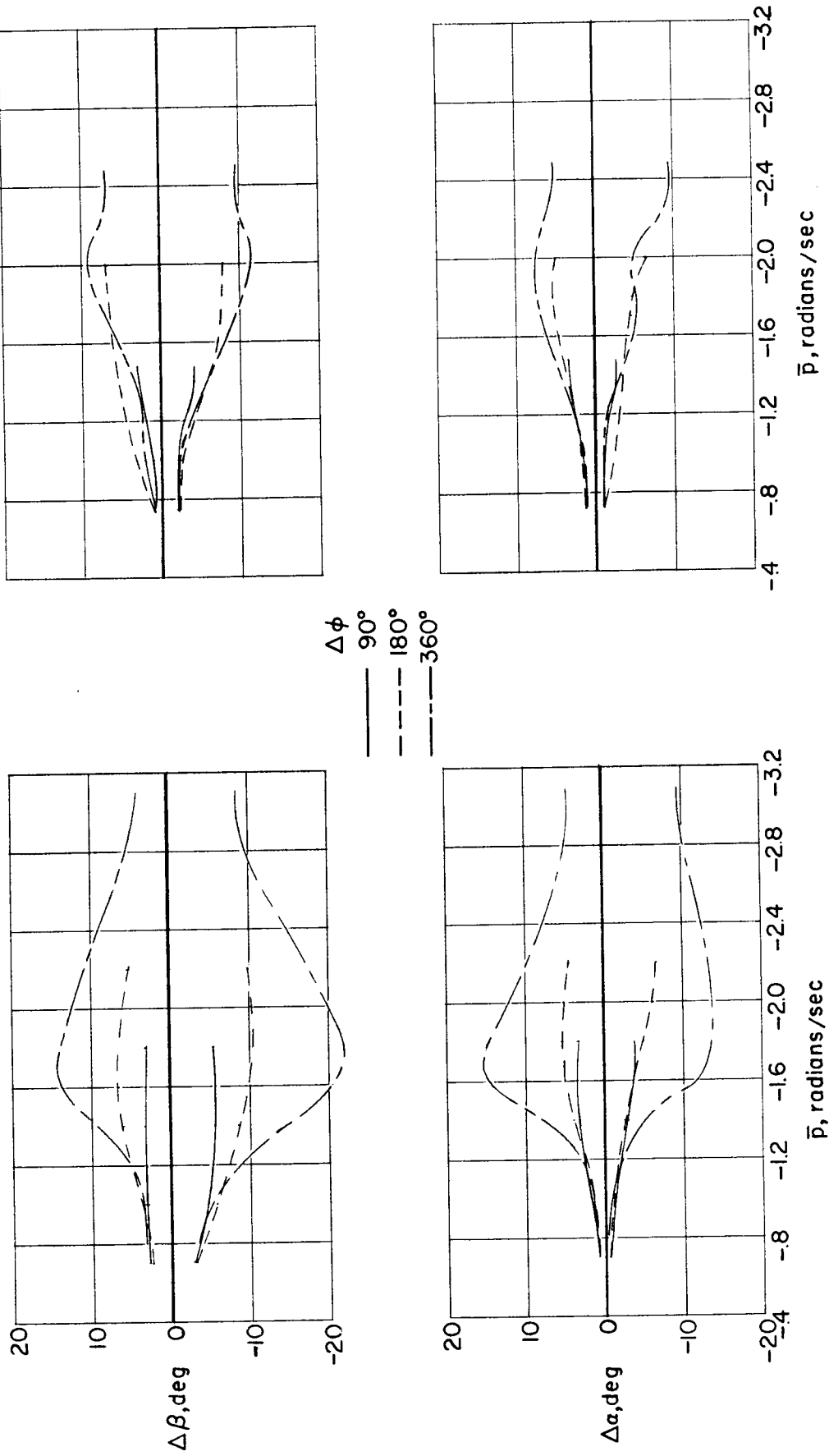


Figure 18.- Stability chart illustrating roll direction effects. Swept-wing configuration.



(b) Input A;  $C_{n\beta} = 0.114$ .

(a) Input B;  $C_{n\beta} = 0.057$ .

Figure 19.- Effect of roll duration. Swept-wing configuration.

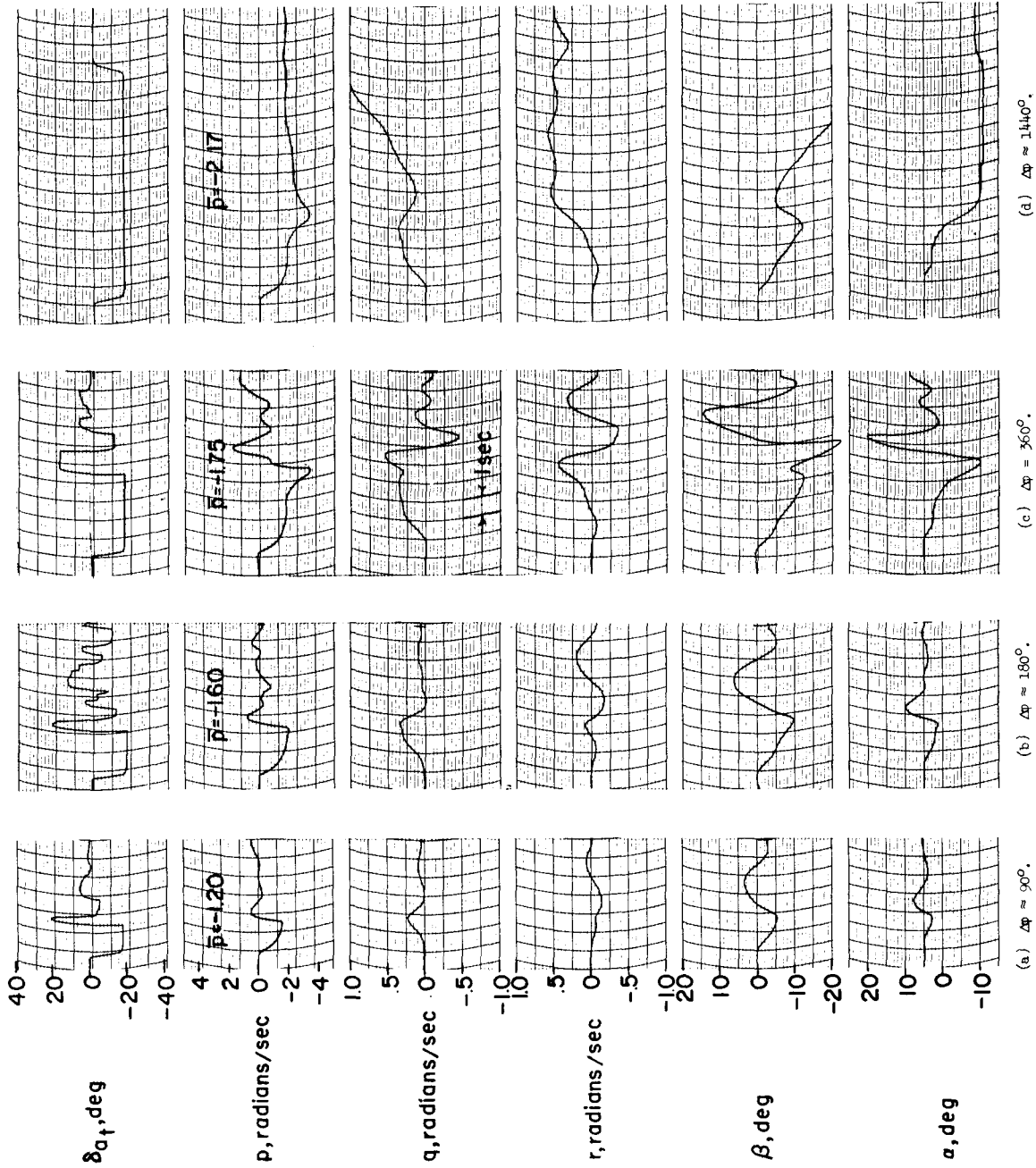


Figure 20.- Representative time histories showing effects of roll duration. Input B;  $C_{n\beta} = 0.057$ .

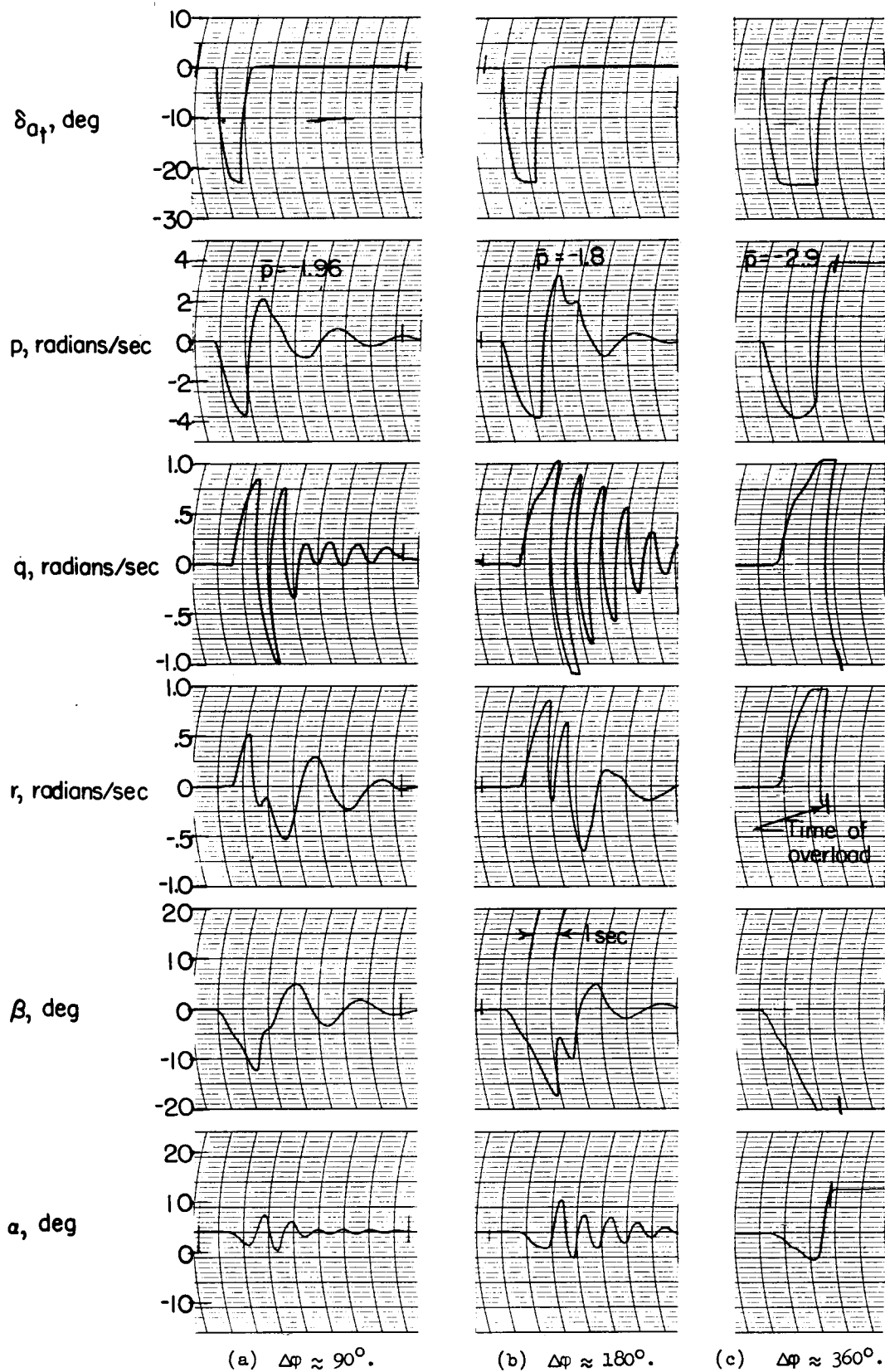


Figure 21.- Representative time histories showing roll duration effects. Delta-wing configuration. Input A;  $M = 1.2$ .

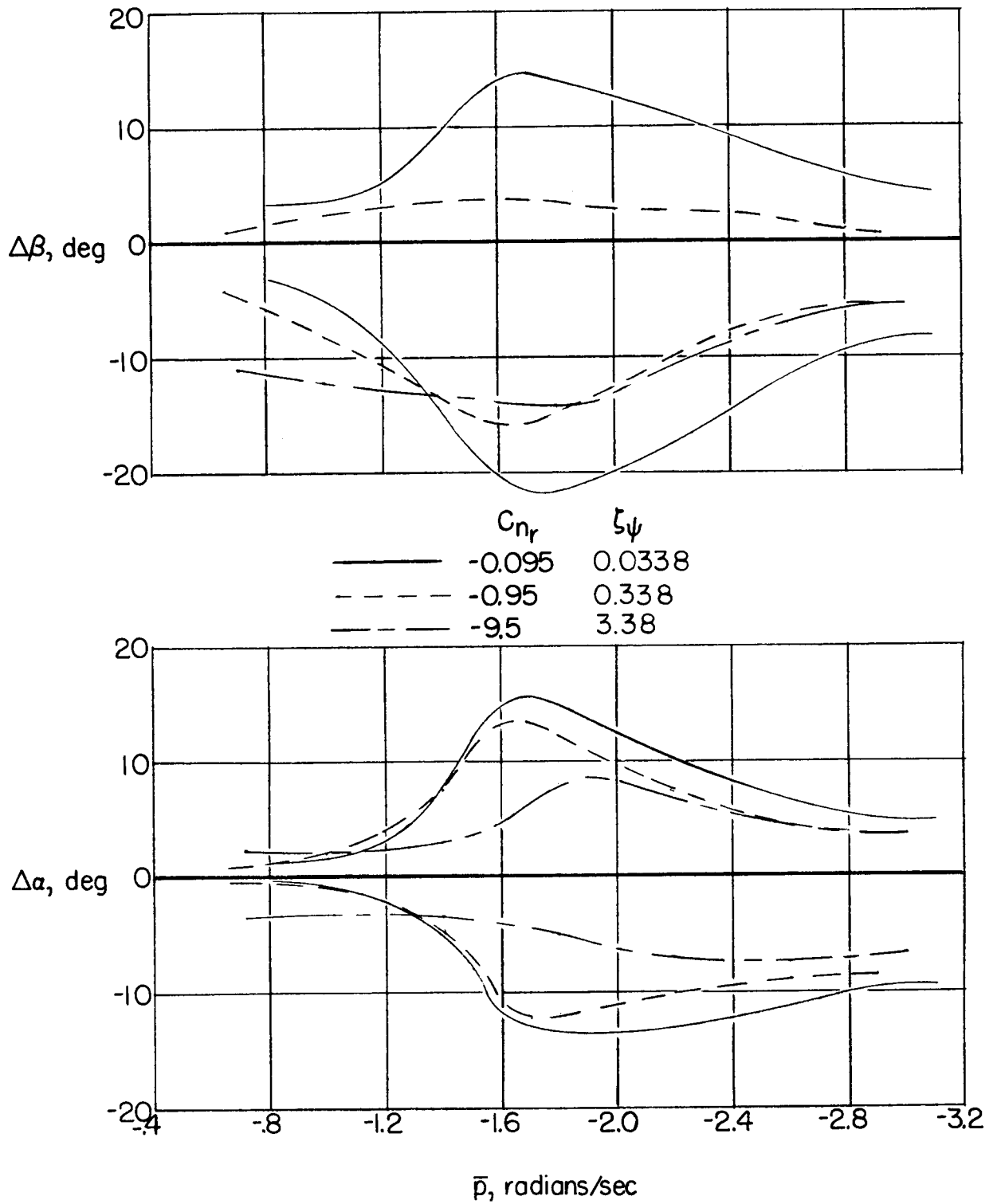


Figure 22.- Effect of increasing  $C_{nr}$ . Swept-wing configuration.  
 Input B;  $C_{n\beta} = 0.057$ .

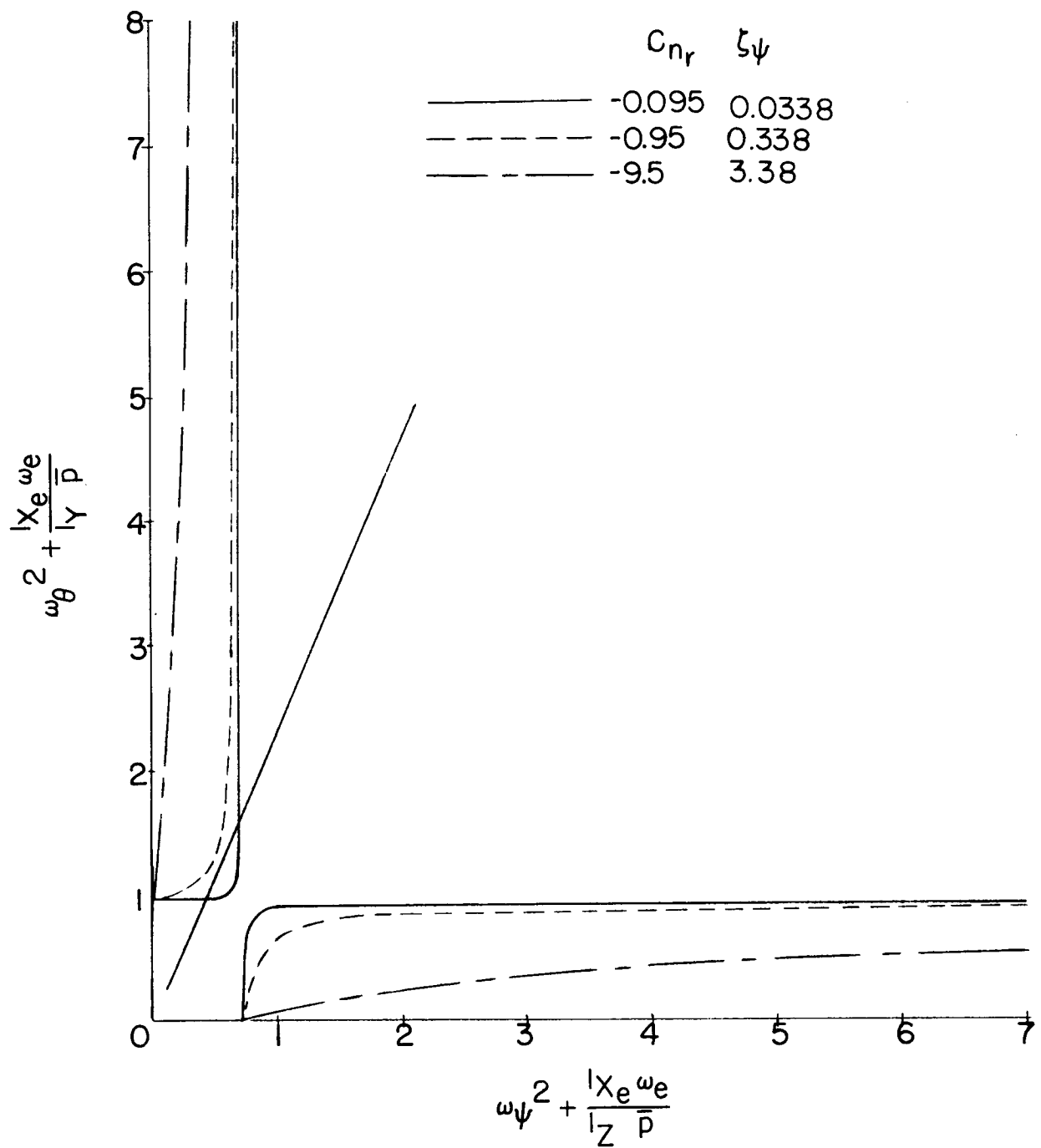


Figure 23.- Stability chart illustrating effects of increasing  $C_{nr}$ . Swept-wing configuration. Left rolls.

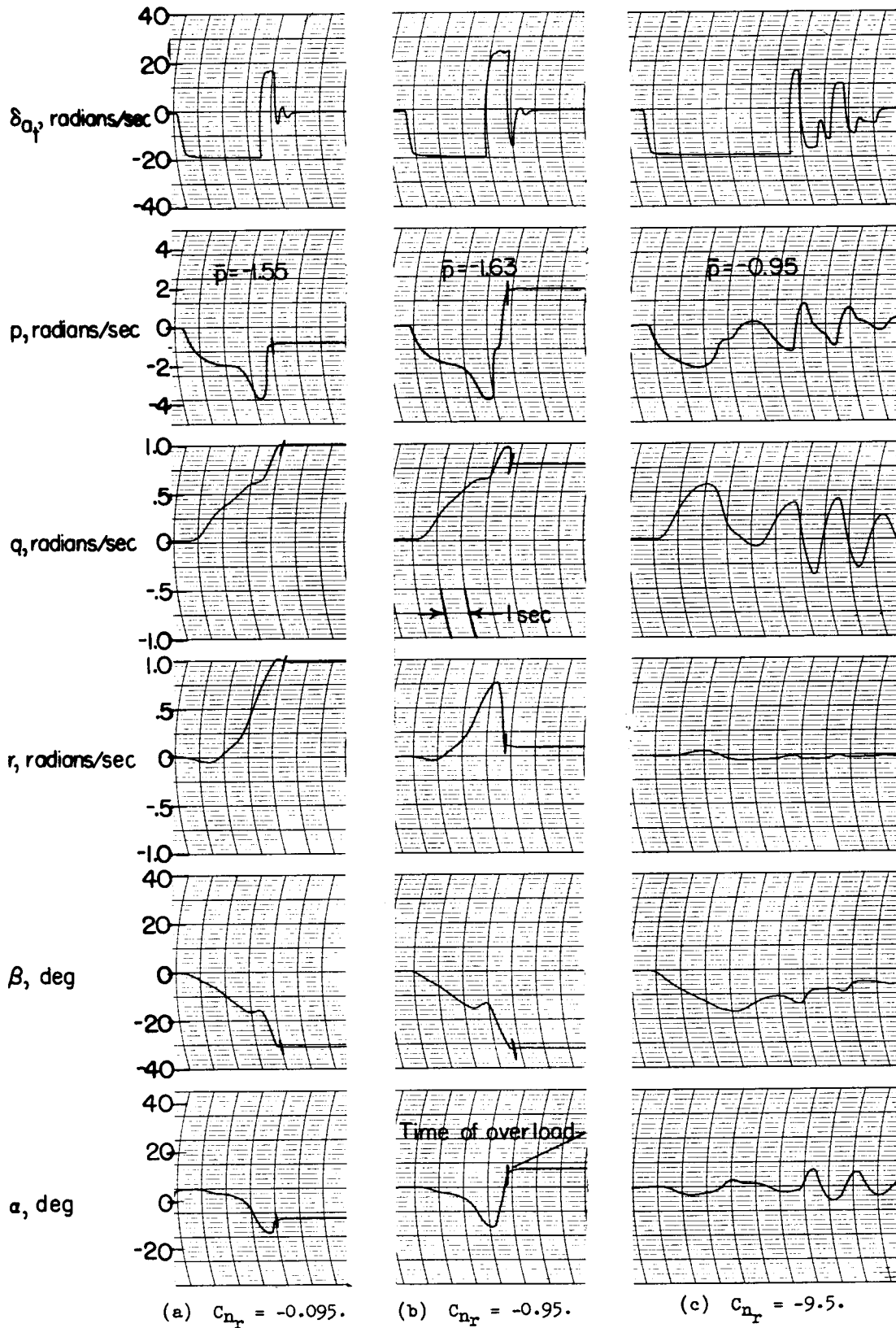


Figure 24.- Time histories showing effect of increasing  $C_{n_r}$ . Swept-wing configuration. Input B;  $C_{m_\alpha} = -0.72$ ;  $C_{n_\beta} = 0.057$ .

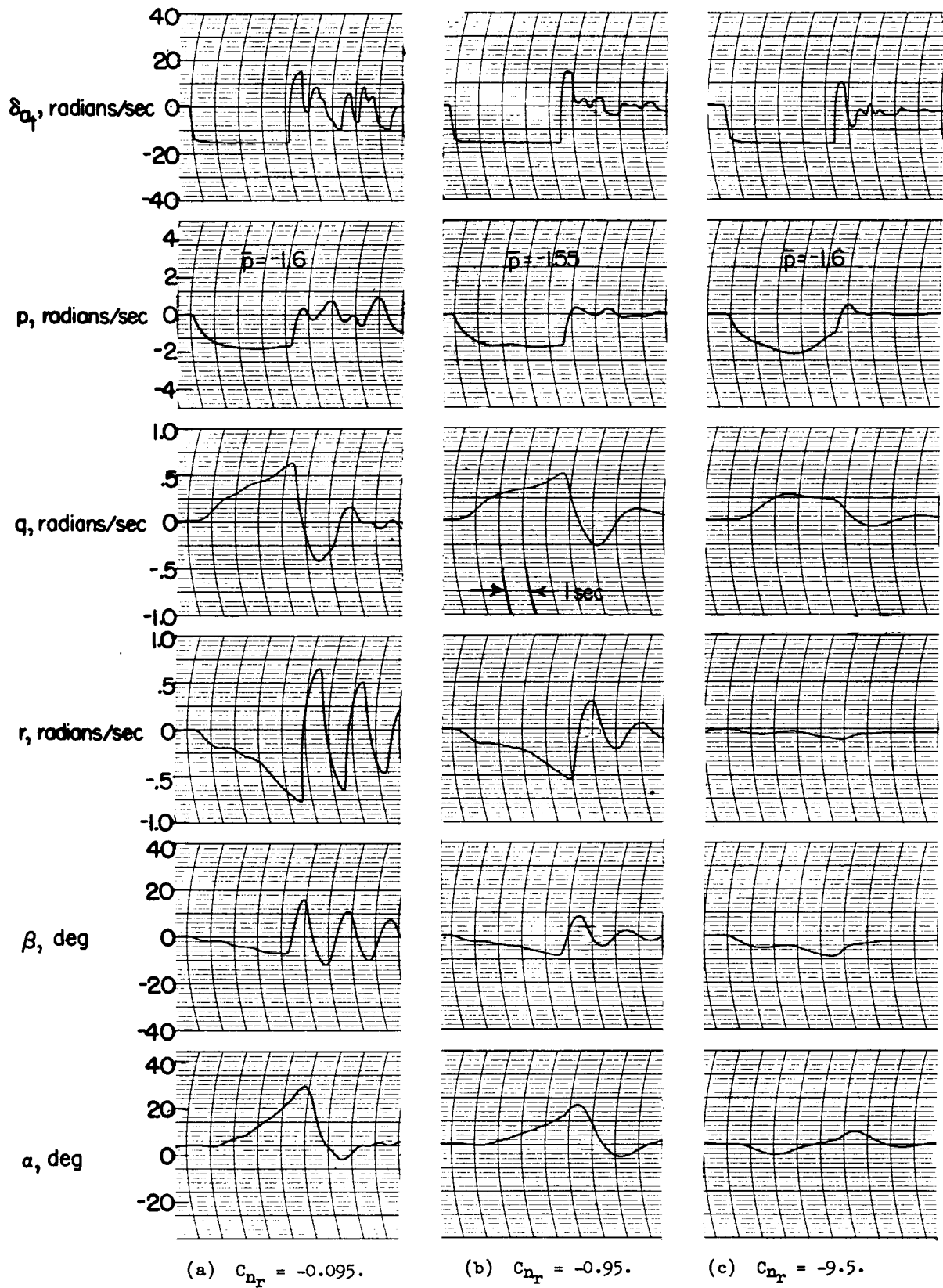
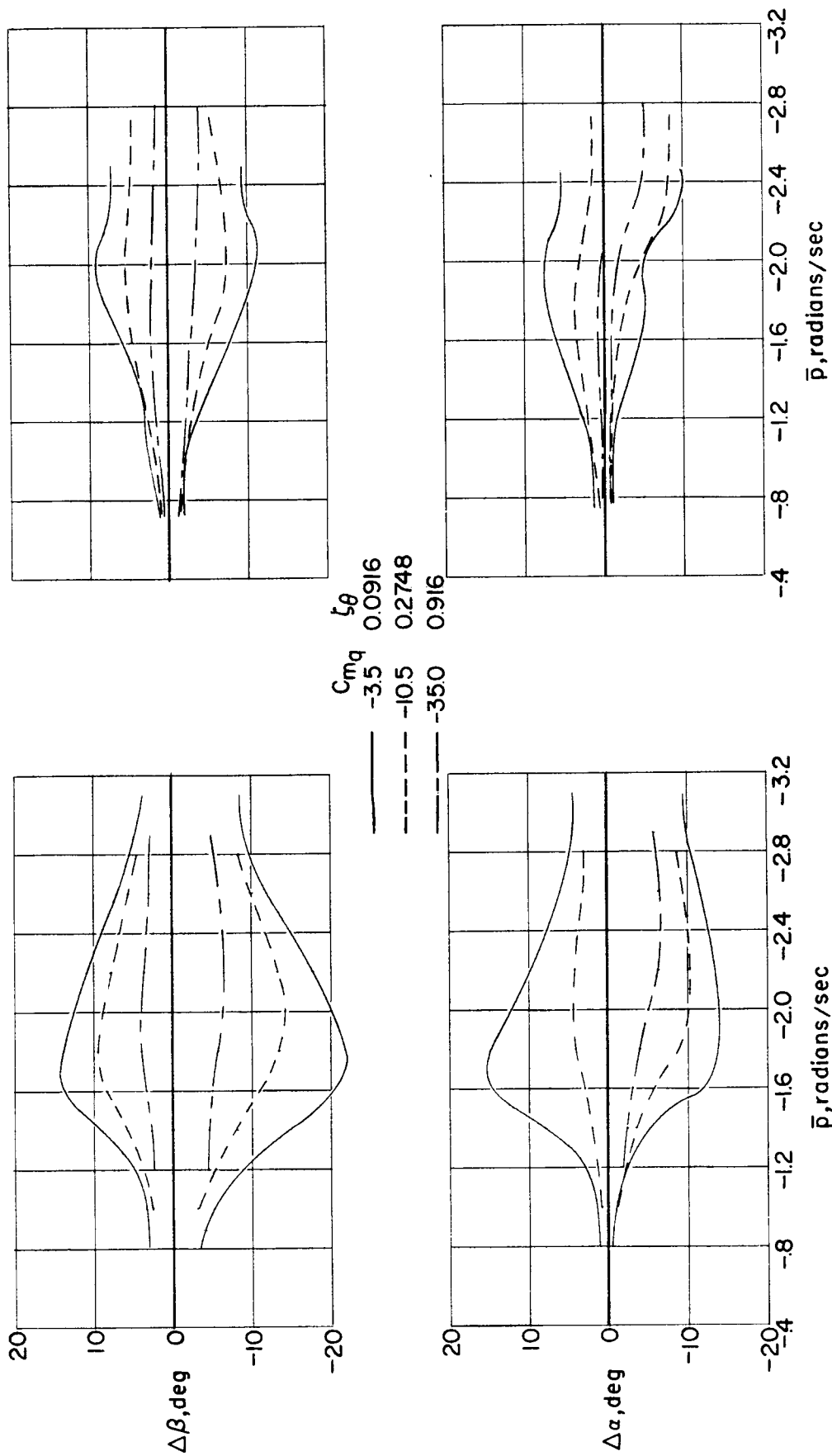


Figure 25.- Time histories showing effects of increasing  $C_{n_r}$ . Swept-wing configuration. Input B;  $C_{m_{\alpha}} = -0.18$ ;  $C_{n_{\beta}} = 0.228$ .



(a) Input B;  $C_{n\beta} = 0.057$ .

(b) Input A;  $C_{n\beta} = 0.114$ .

Figure 26.- Effects of increasing  $C_{m_q}$ . Swept-wing configuration.

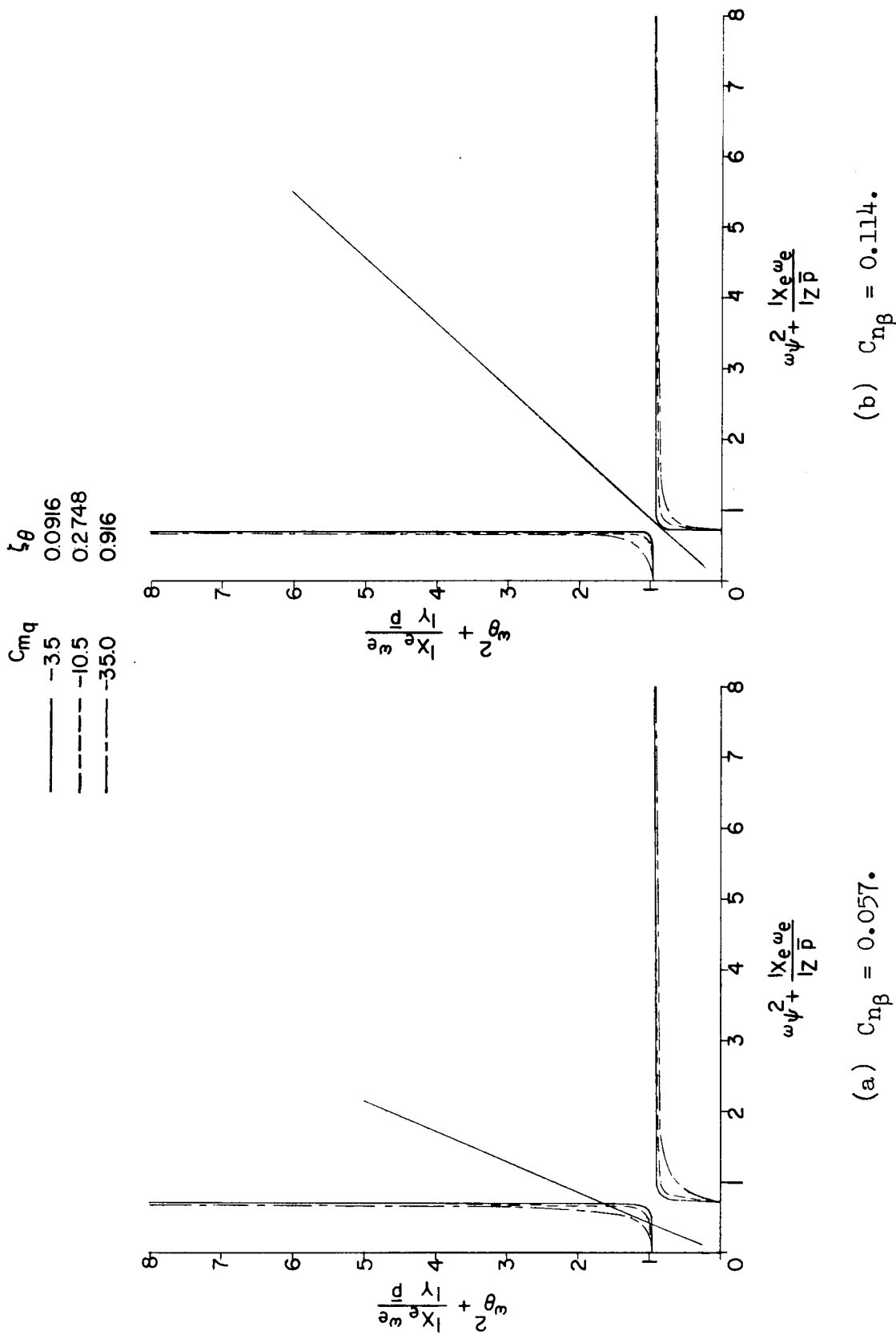


Figure 27.- Stability charts illustrating effects of increasing  $C_{mq}$ . Swept-wing configuration. Left rolls.

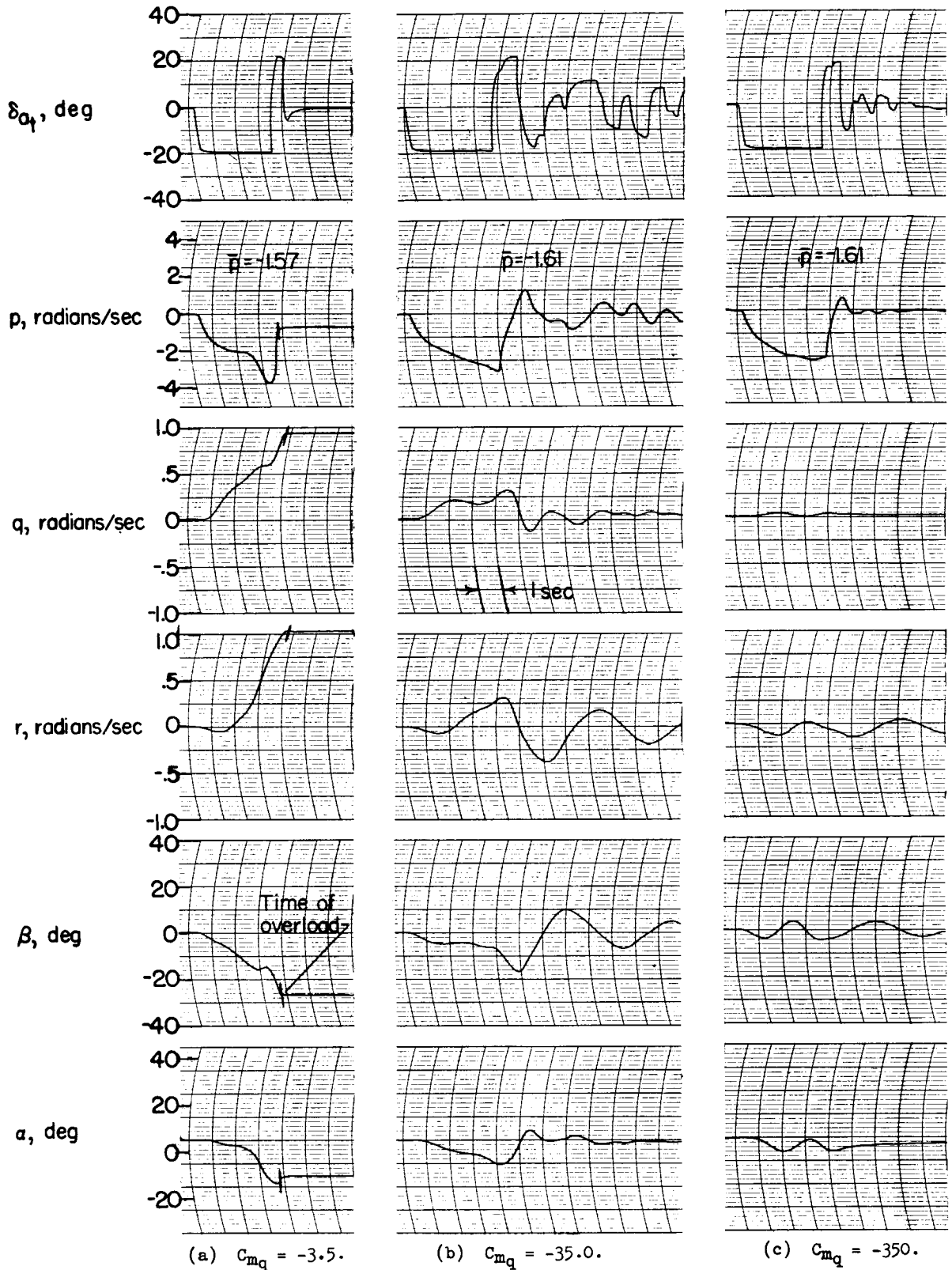


Figure 28.- Time histories showing effects of increasing  $C_{mq}$ . Swept-wing configuration. Input B;  $C_{m\alpha} = -0.72$ ;  $C_{n\beta} = 0.057$ .

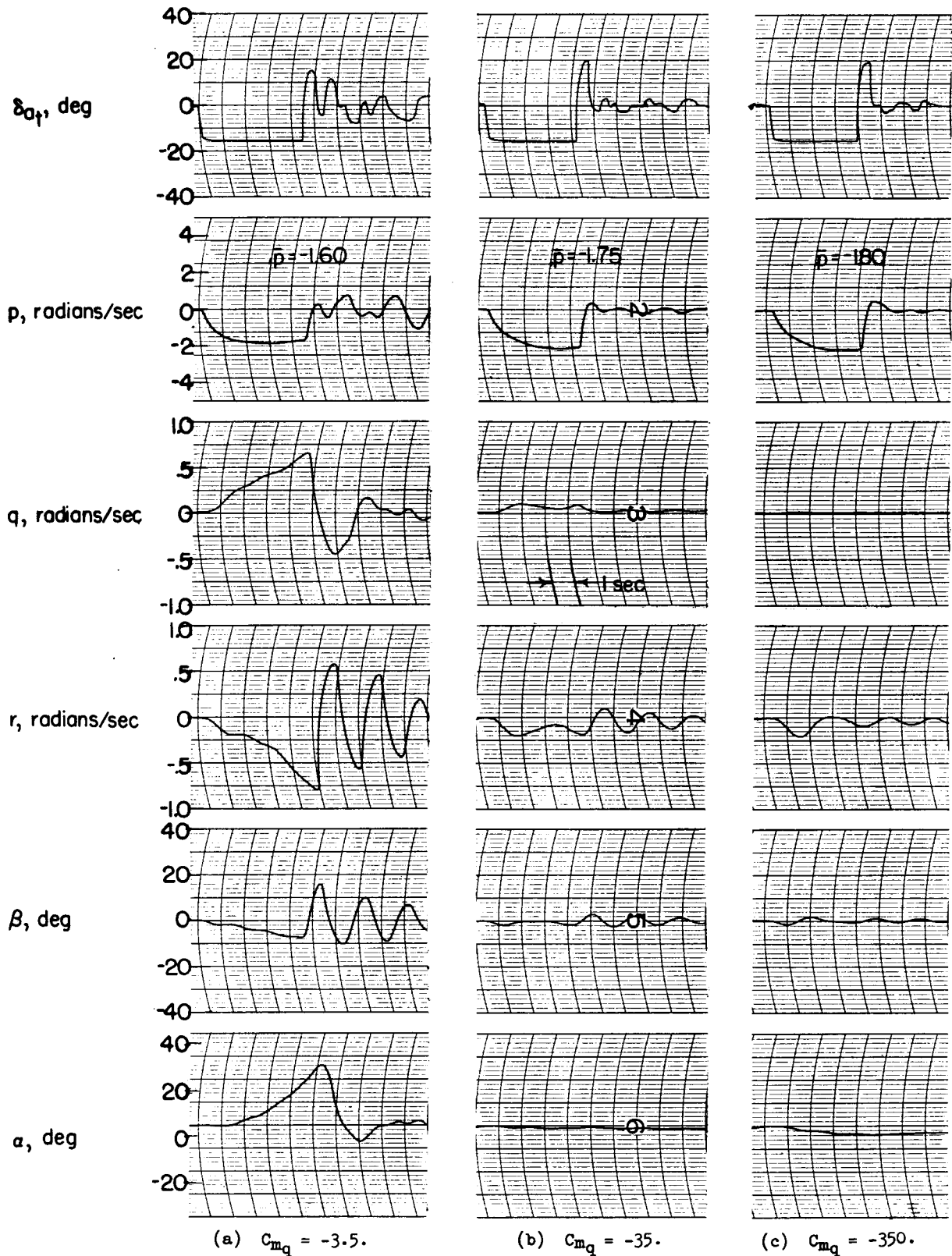


Figure 29.- Time histories showing effects of increasing  $C_{m_q}$ . Swept-wing configuration. Input B;  $C_{m_\alpha} = -0.18$ ;  $C_{n_\beta} = 0.228$ .

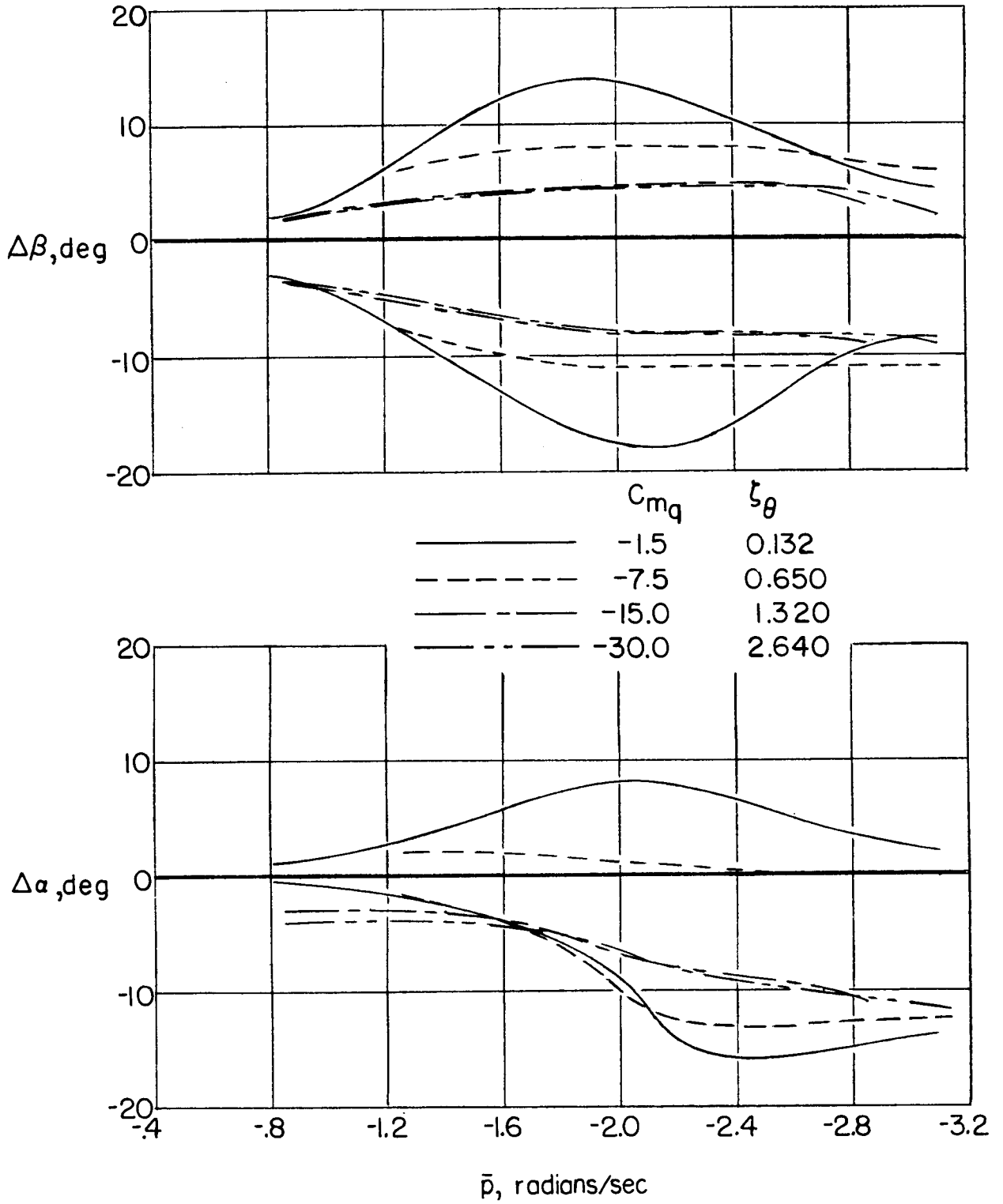


Figure 30.- Effect of increasing  $C_{mq}$ . Delta-wing configuration.  
 $M = 0.80$ ; input A.

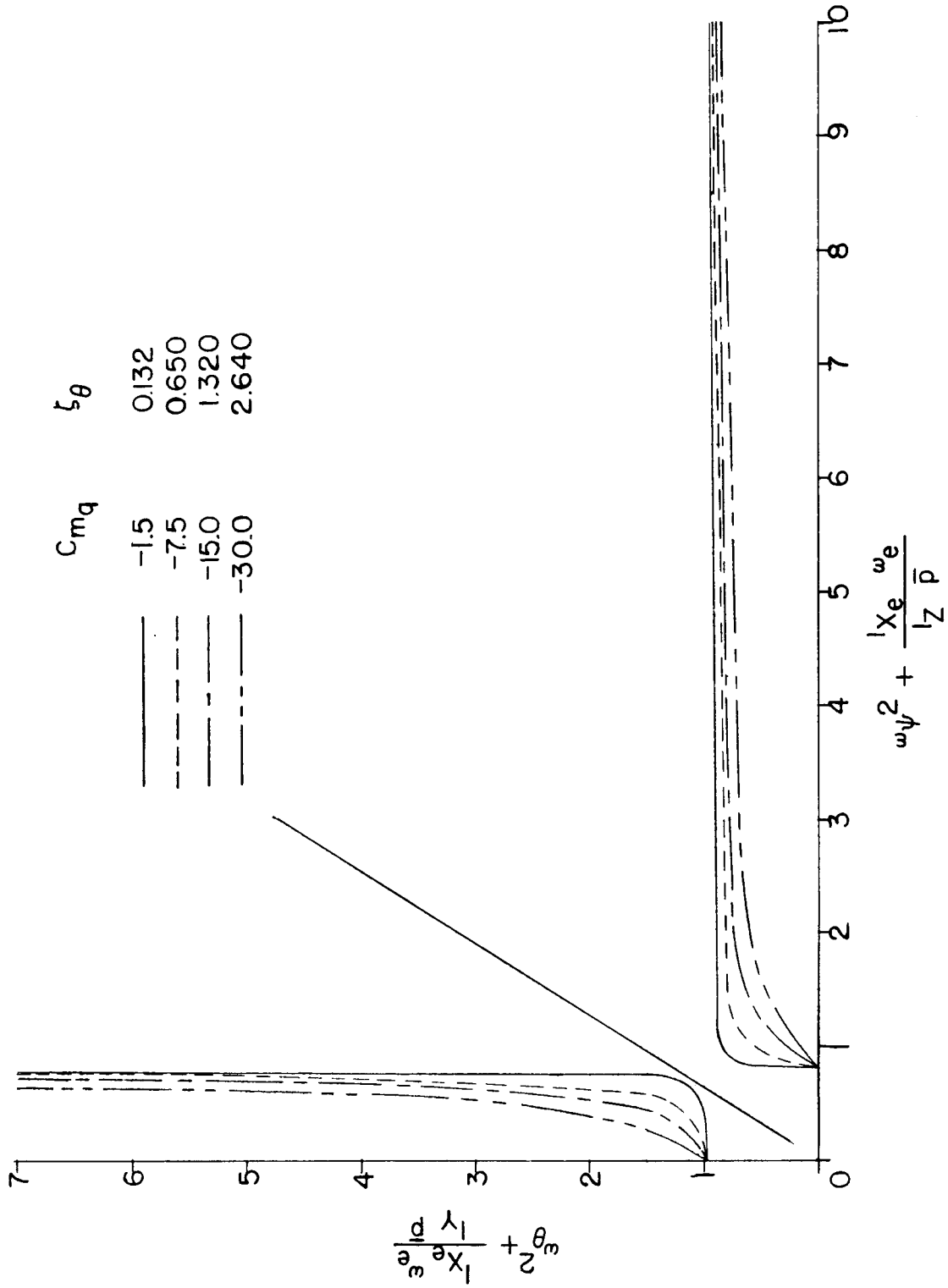


Figure 31.- Stability chart illustrating effects of increasing  $C_{mq}$ .  
Delta-wing configuration.  $M = 0.80$ . Left rolls.

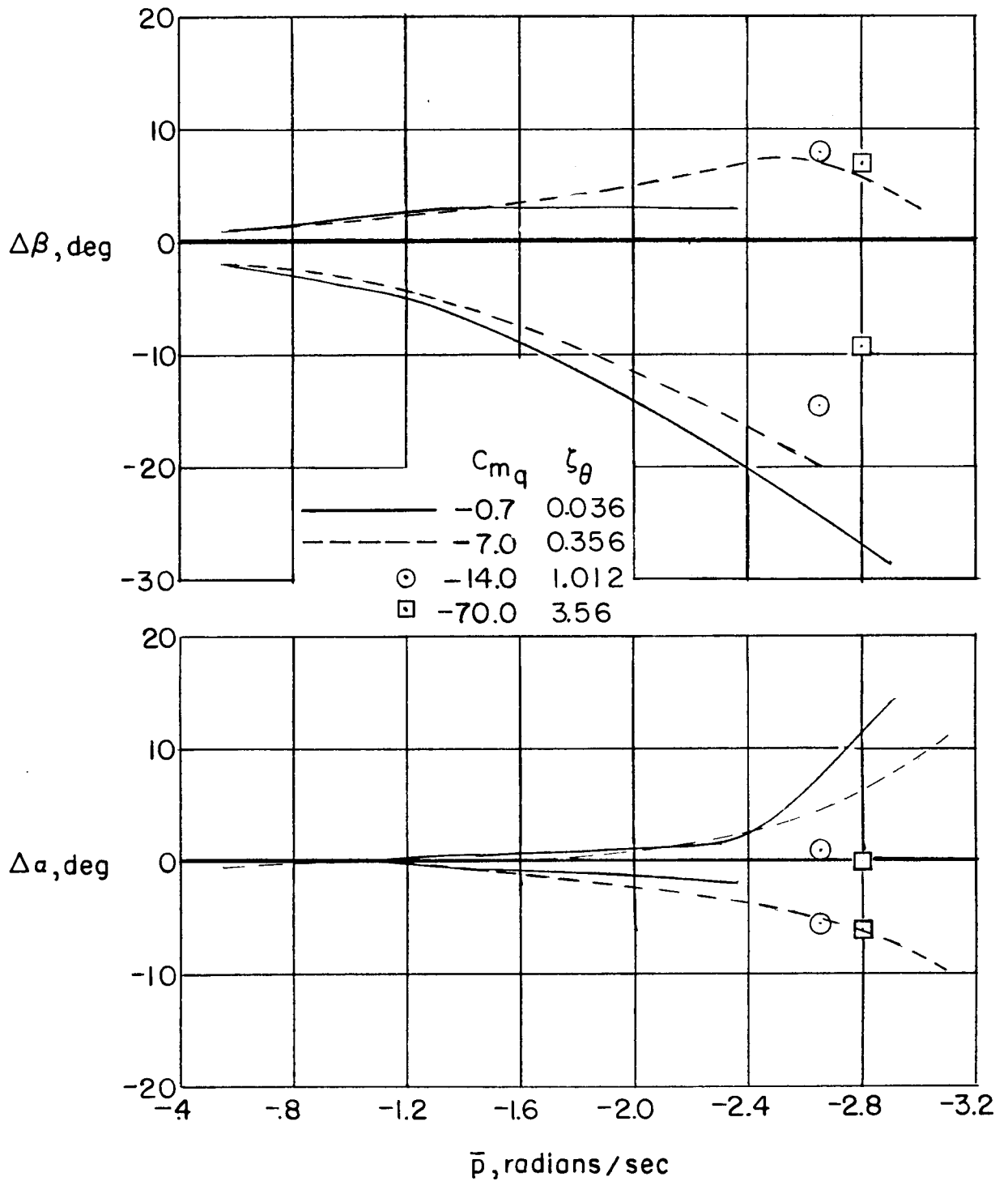


Figure 32.- Effects of increasing  $C_{m_q}$ . Delta-wing configuration.  
 M = 1.20; input A.

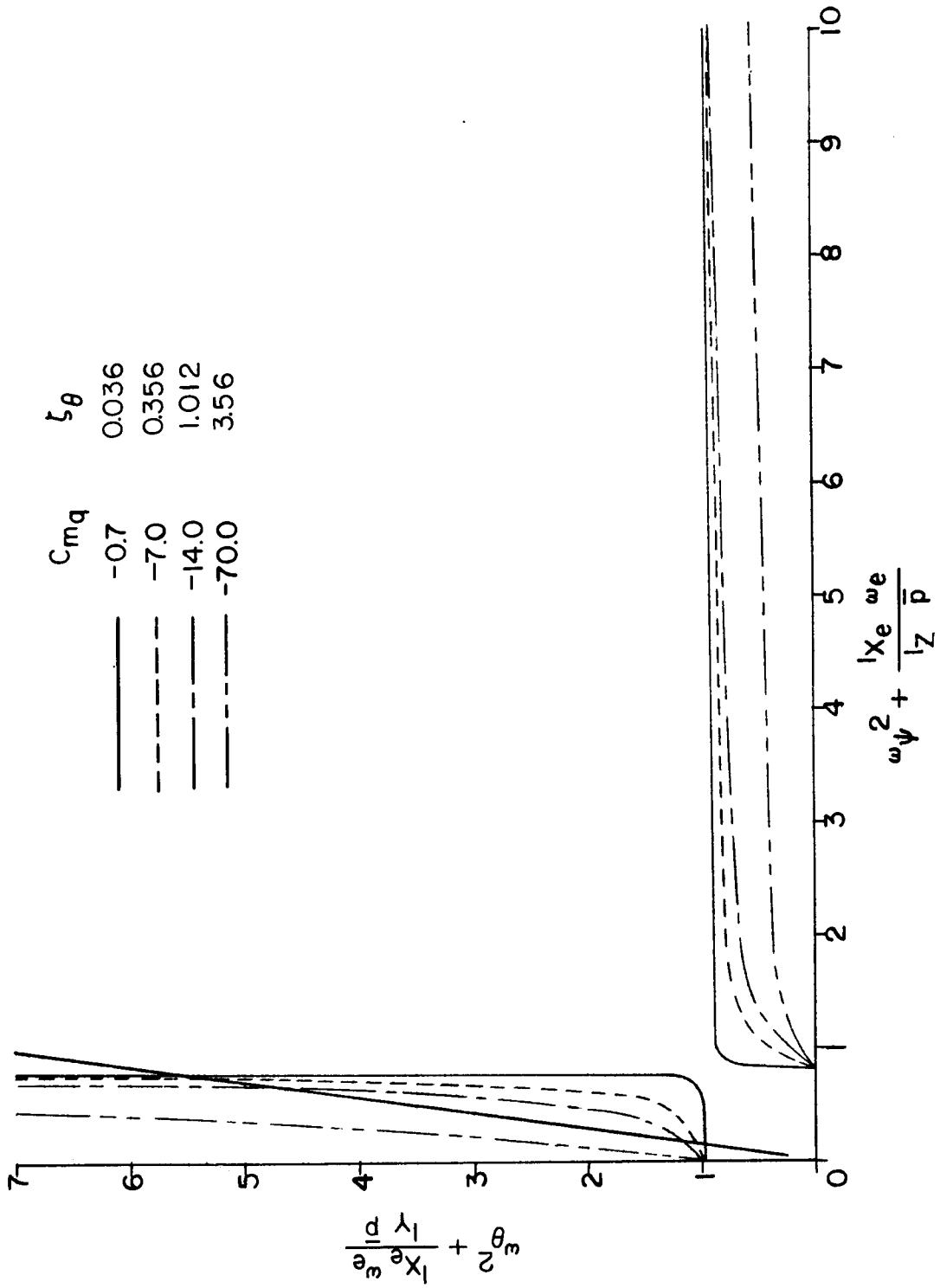


Figure 33.- Stability chart illustrating effects of increasing  $C_{m_q}$ .  
Delta-wing configuration.  $M = 1.20$ . Left rolls.

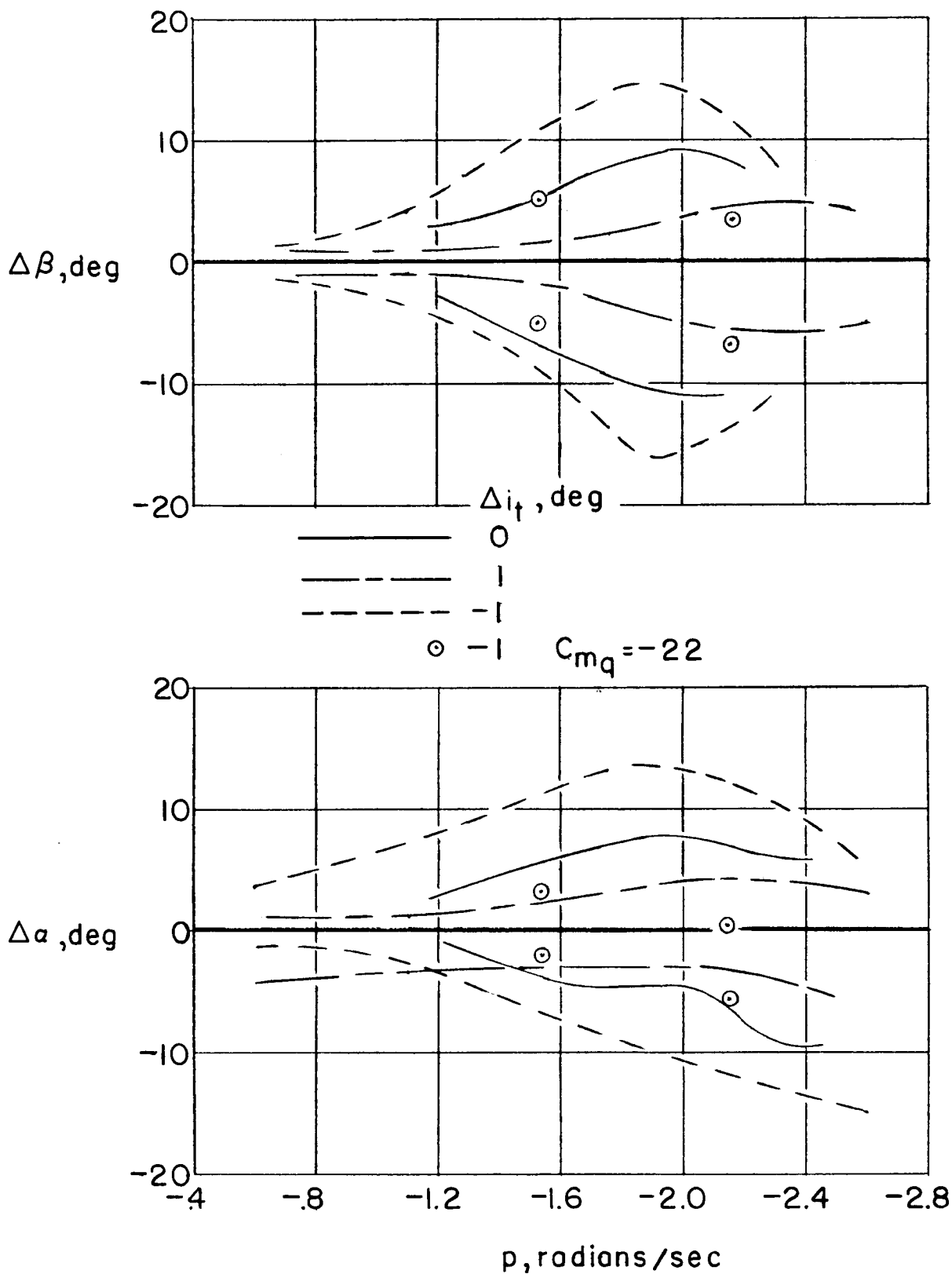


Figure 34.- Effects of simultaneous aileron and stabilizer inputs. Swept-wing configuration.  $C_{n\beta} = 0.114$ ; input A.

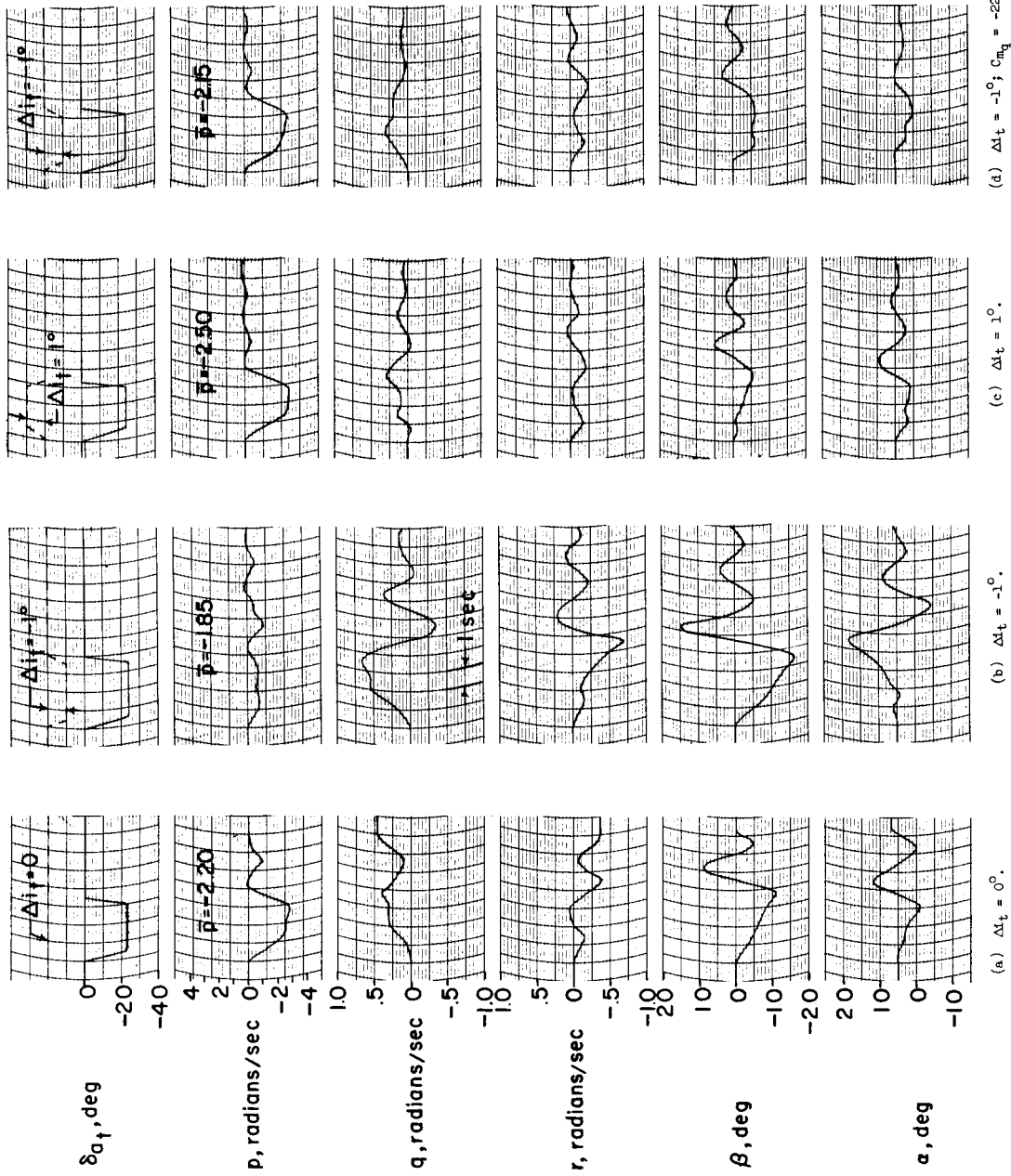
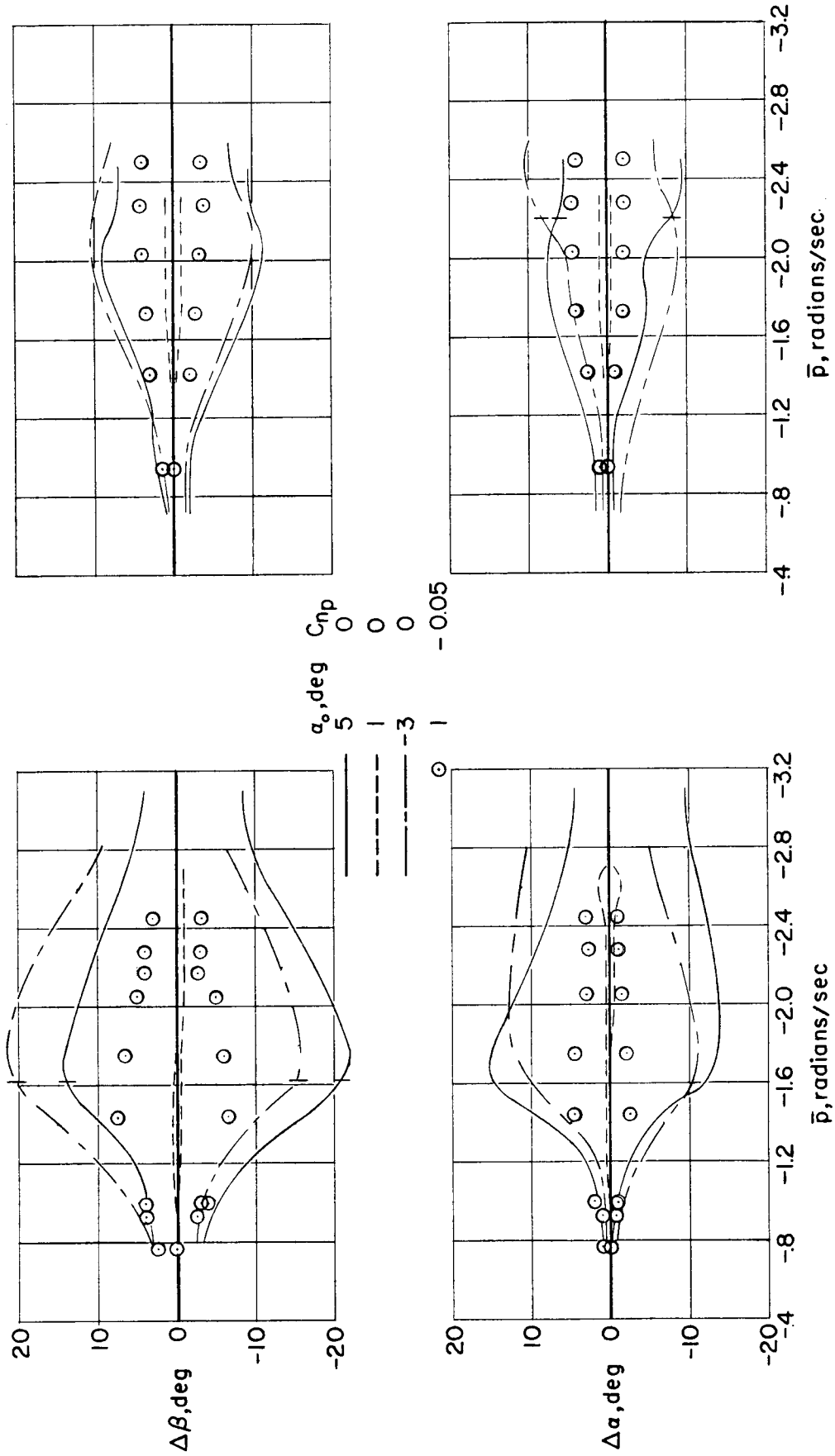


Figure 35.- Time histories illustrating effects of simultaneous aileron and stabilizer inputs. Swept-wing configuration. Input A;  $C_{N\beta} = 0.114$ .



(a) Input B;  $C_{N\beta} = 0.057$ .

(b) Input A;  $C_{N\beta} = 0.114$ .

Figure 36.- Effects of varying initial angle of attack. Swept-wing configuration.  $\epsilon = 1^\circ$ .

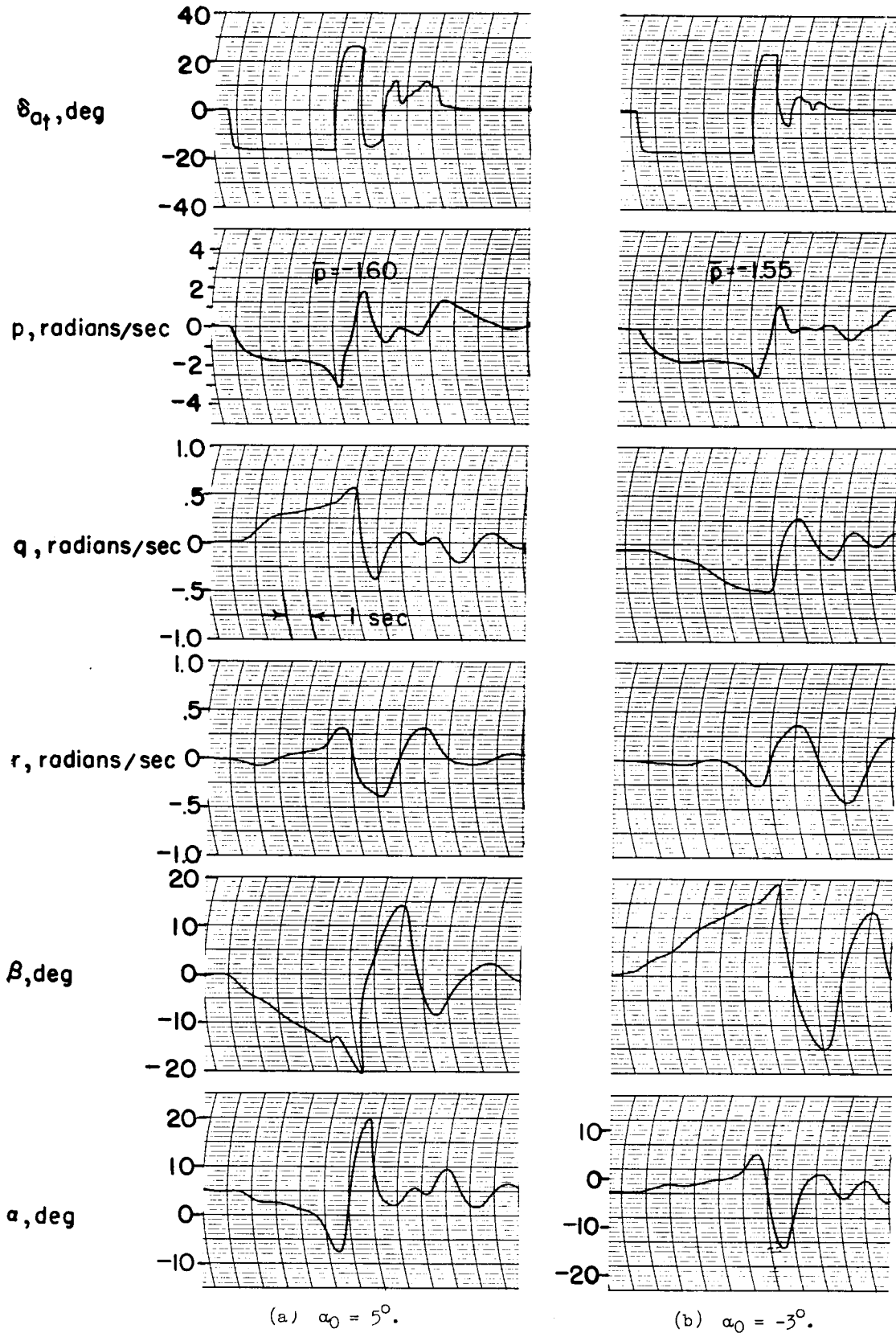
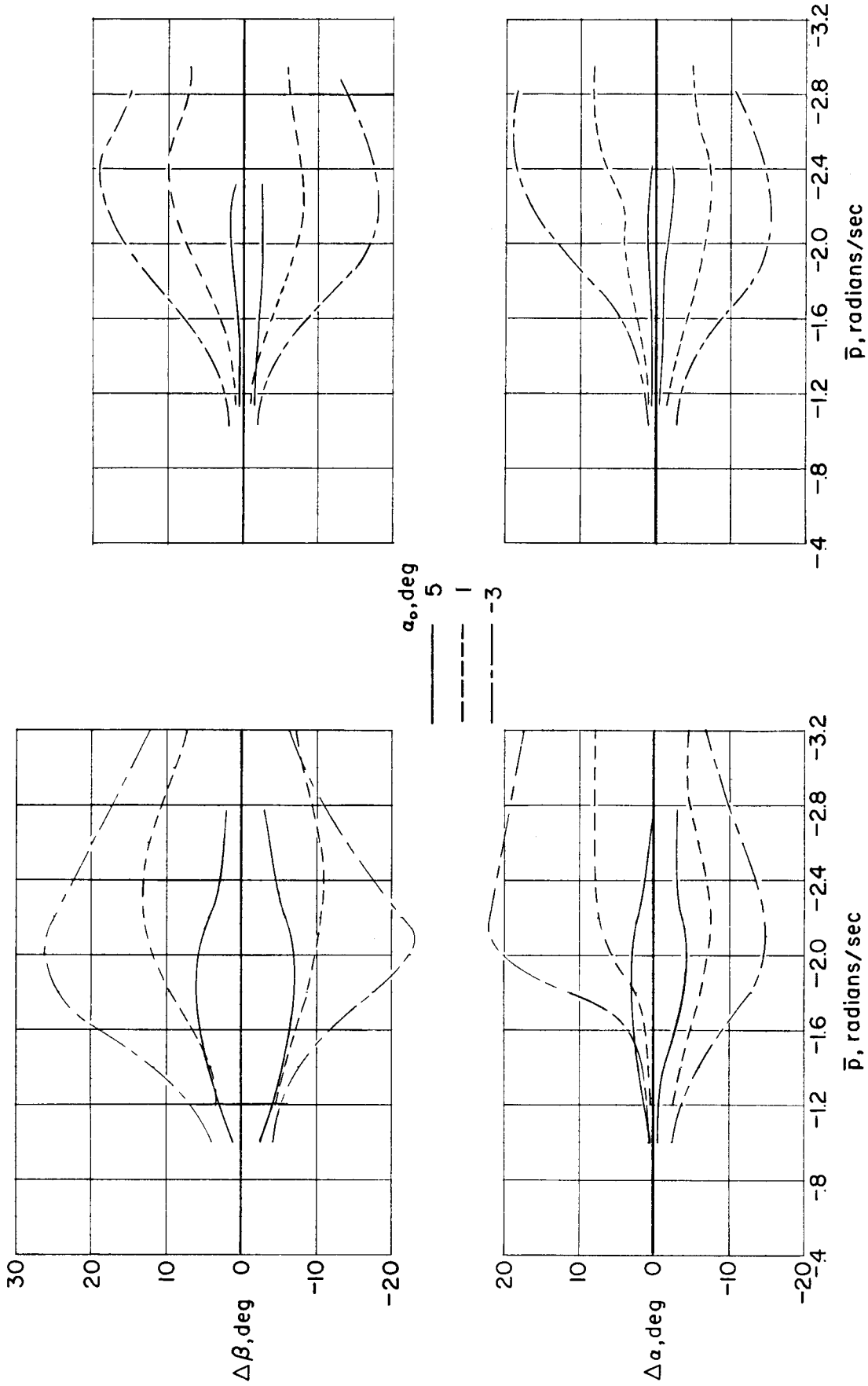


Figure 37.- Time histories showing effects of different initial angles of attack. Swept-wing configuration.  $\epsilon = 1^\circ$ .



(a) Input B;  $C_{n\beta} = 0.057$ .

(b) Input A;  $C_{n\beta} = 0.114$ .

Figure 38.- Effects of varying initial angle of attack. Swept-wing configuration.  $\epsilon = 5^\circ$ .

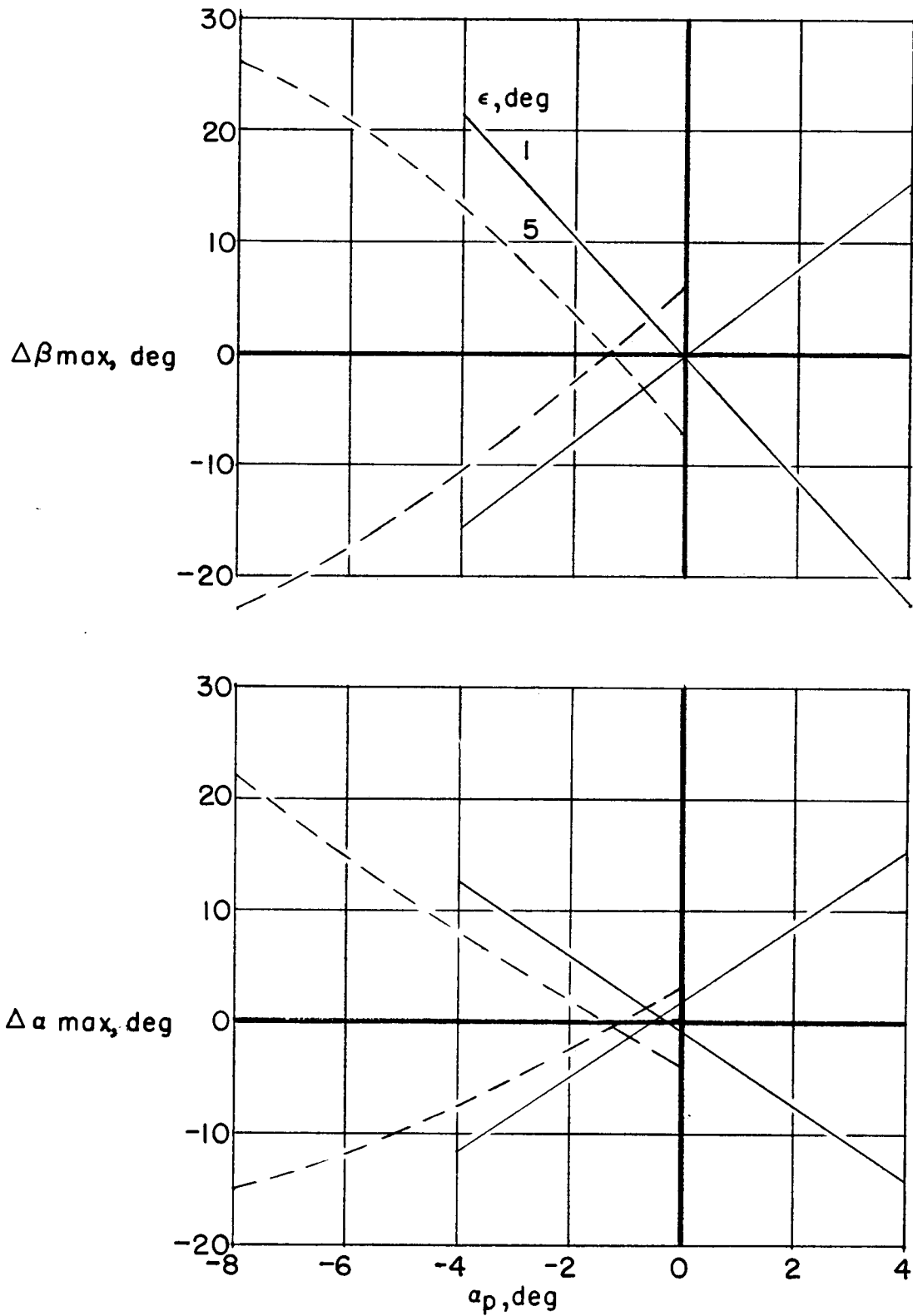


Figure 39.- Variation of peak motions with initial angle of attack of principal axis. Swept-wing configuration.

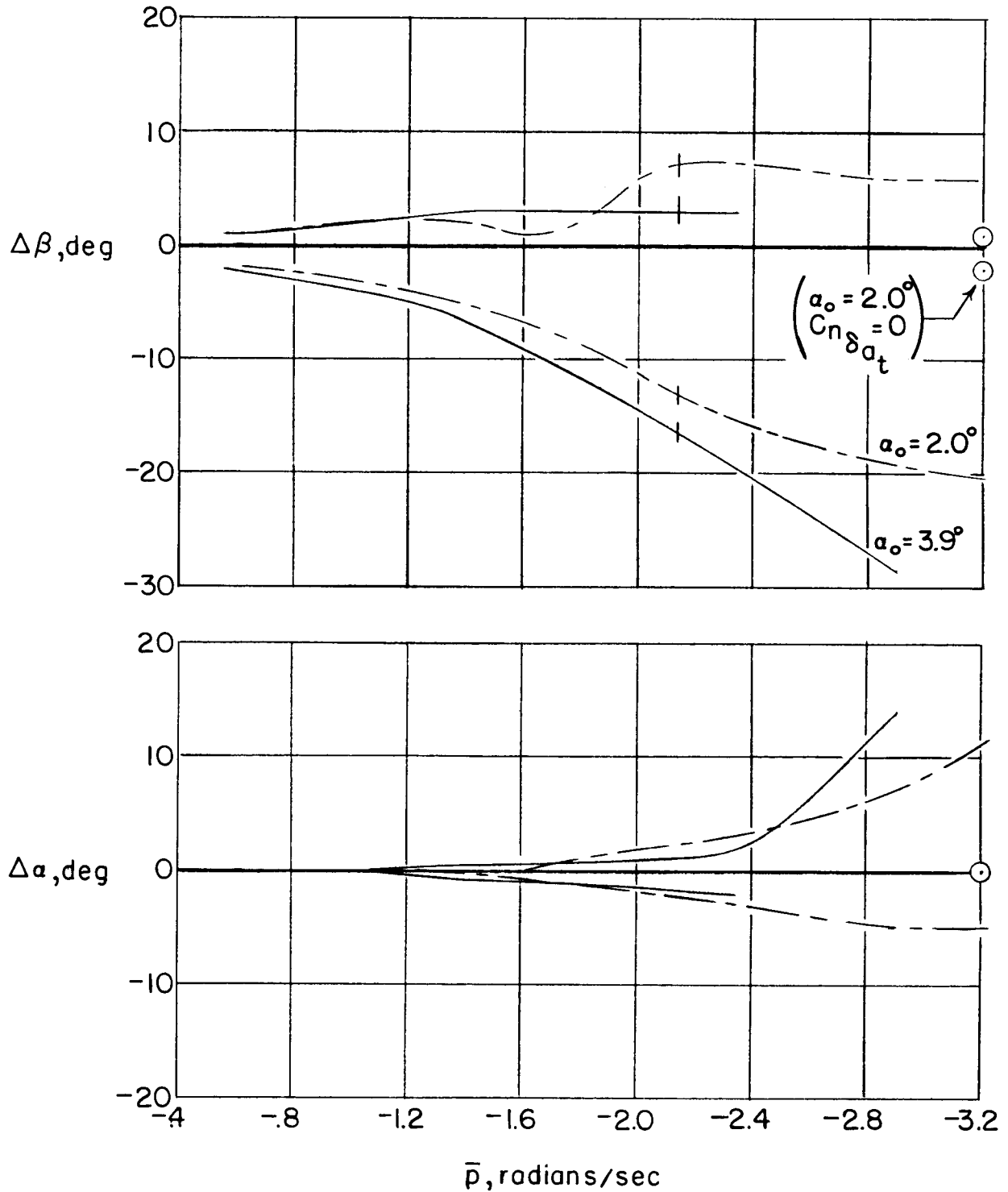


Figure 40.- Effects of initial angle of attack. Delta-wing configuration.  $M = 1.2$ .

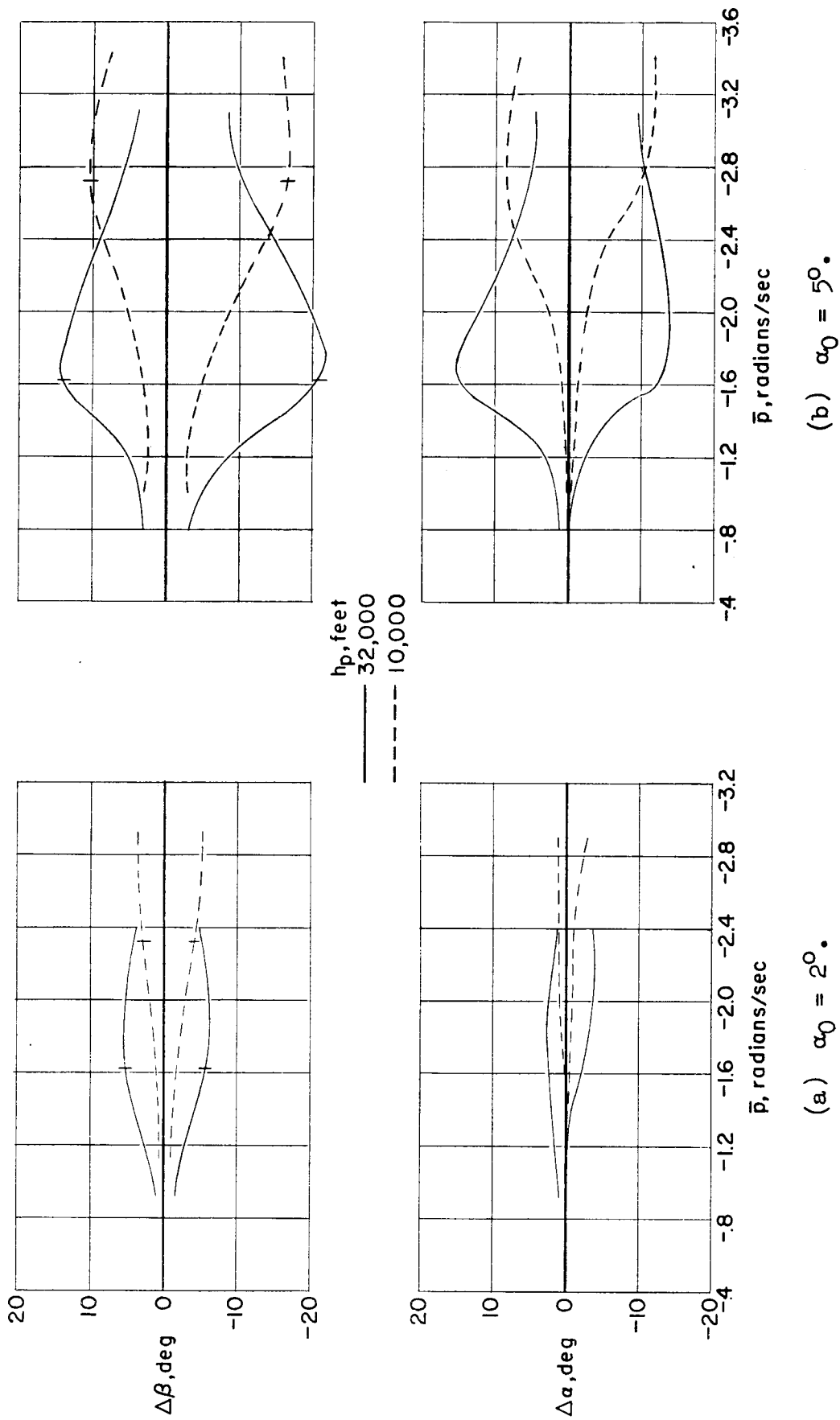
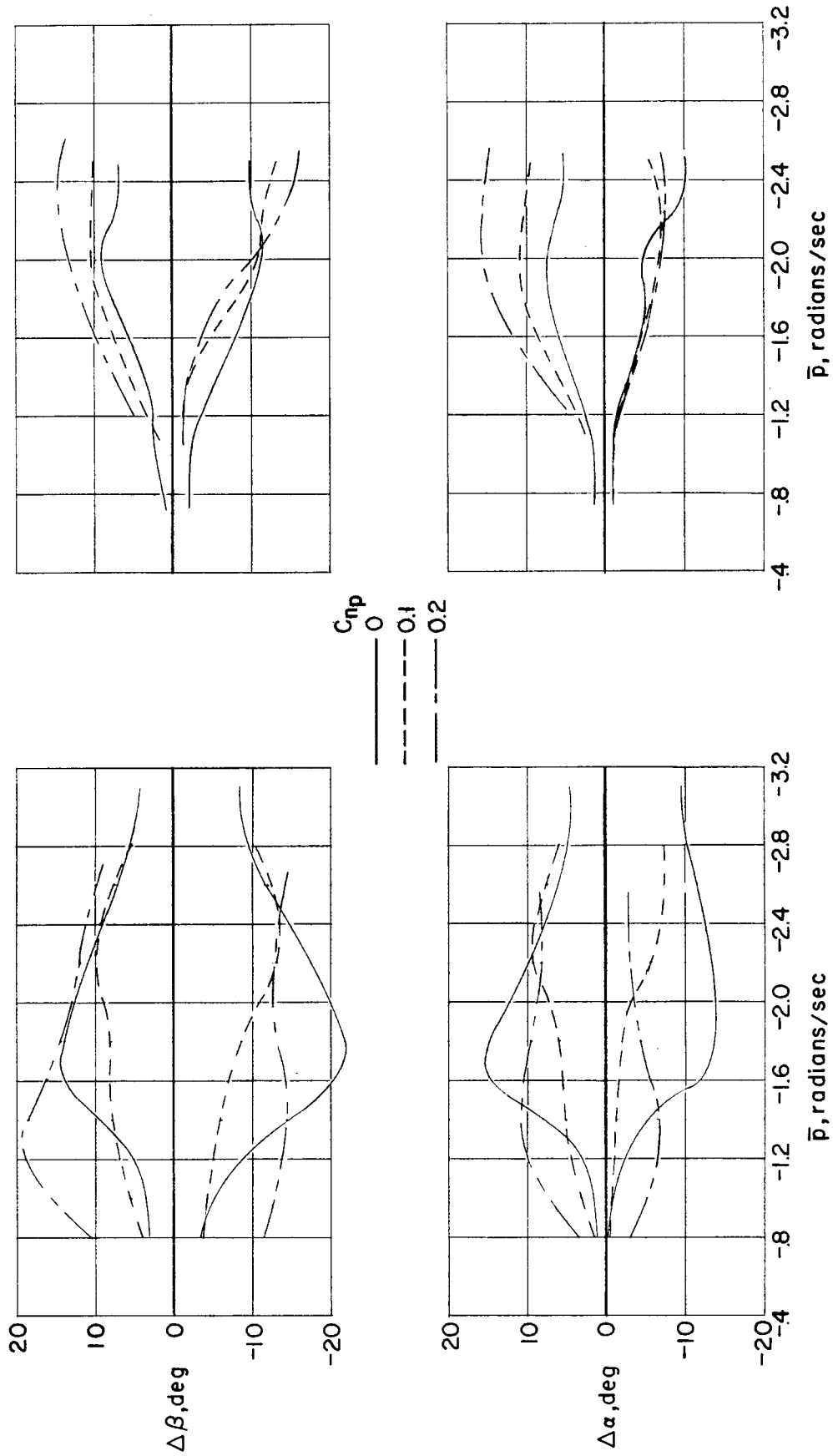


Figure 41.- Effect of altitude. Swept-wing configuration. Input B;  $C_{n\beta} = 0.057$ .



(a) Input B;  $C_{n\beta} = 0.057$ .

(b) Input A;  $C_{n\beta} = 0.114$ .

Figure 42.- Effects of increasing  $C_{np}$ . Swept-wing configuration.

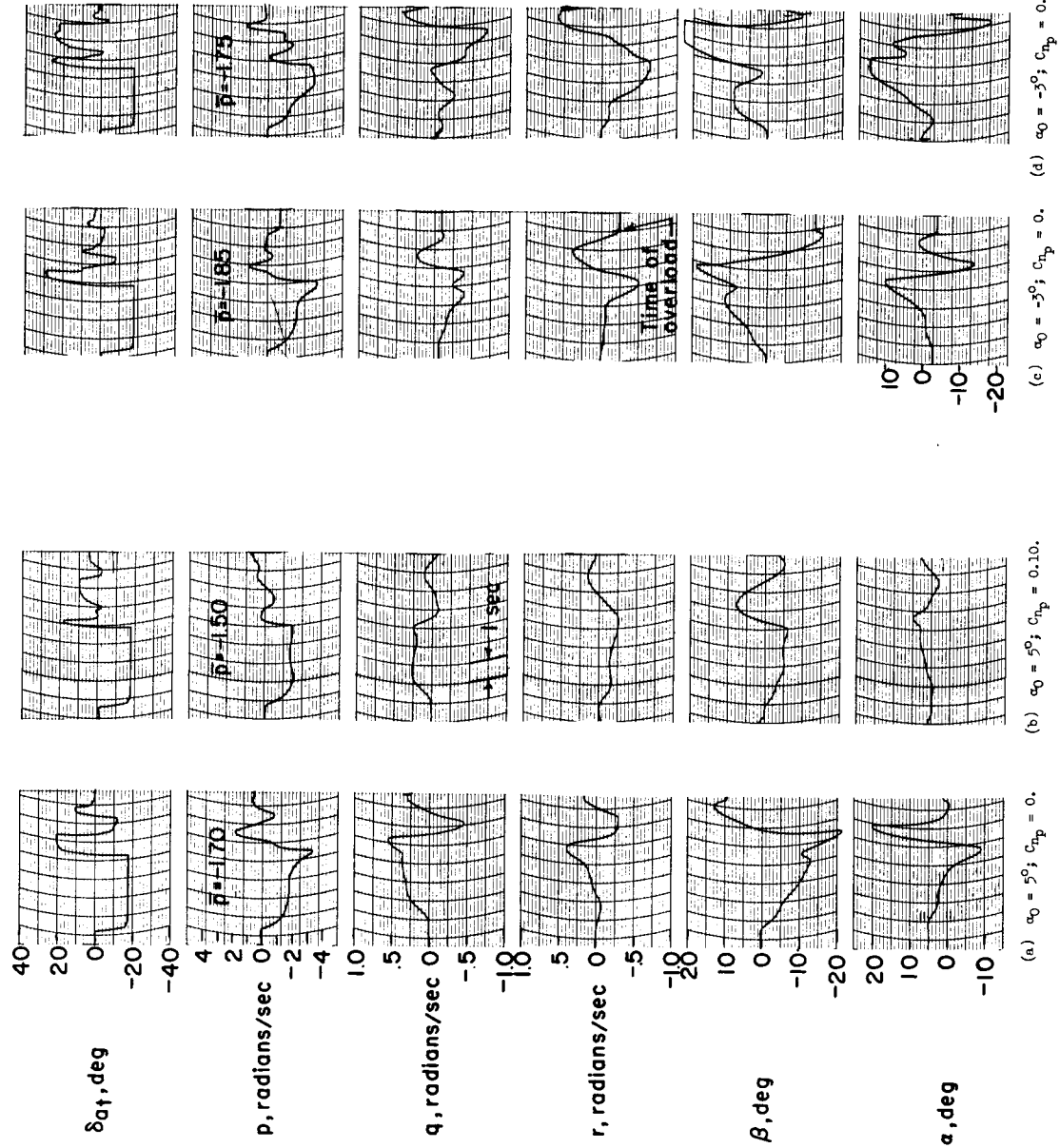


Figure 43.- Time histories showing effects of  $C_{np}$  increase at two values of initial angle of attack. Swept-wing configuration.  $C_{n\beta} = 0.057$ .

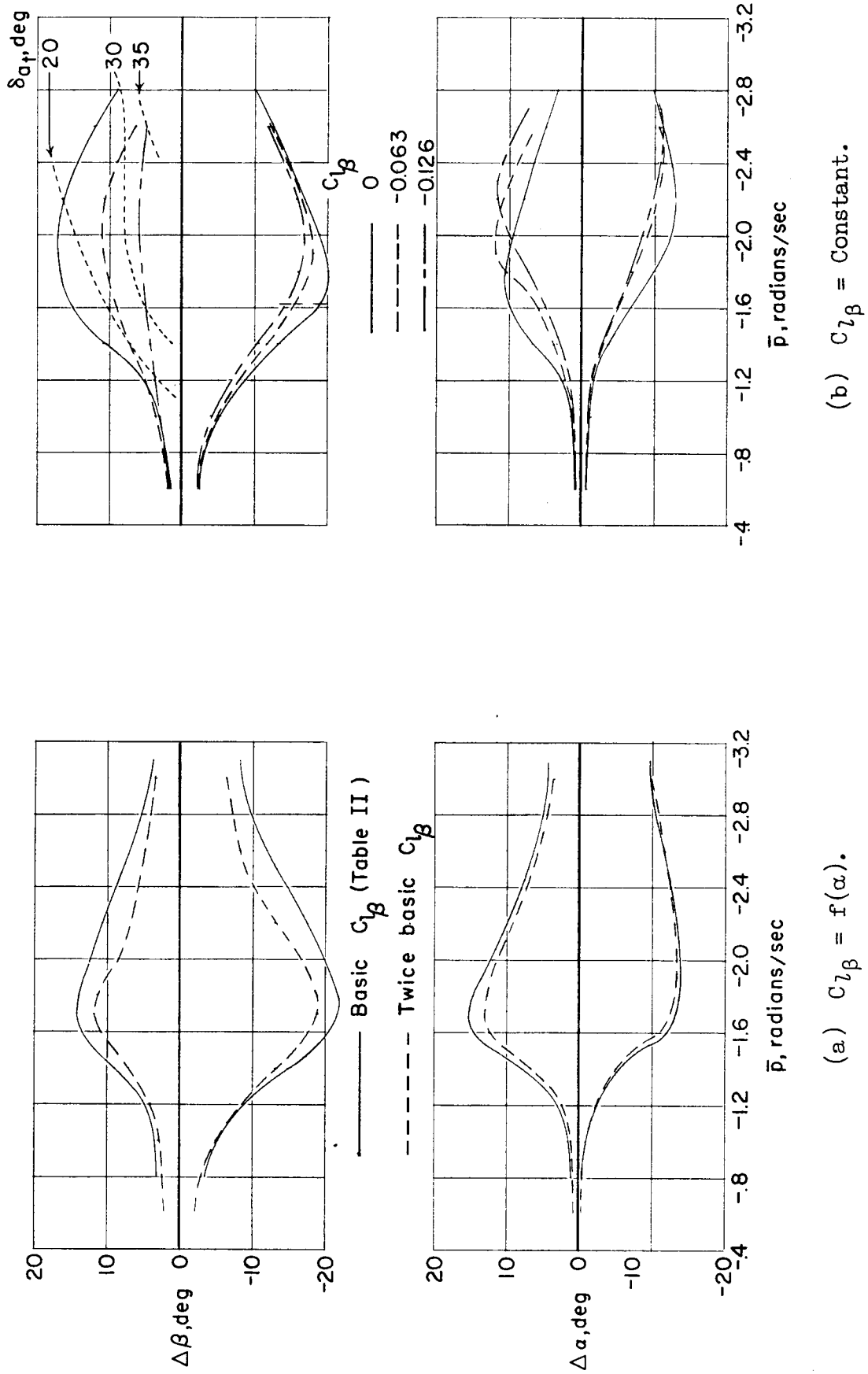
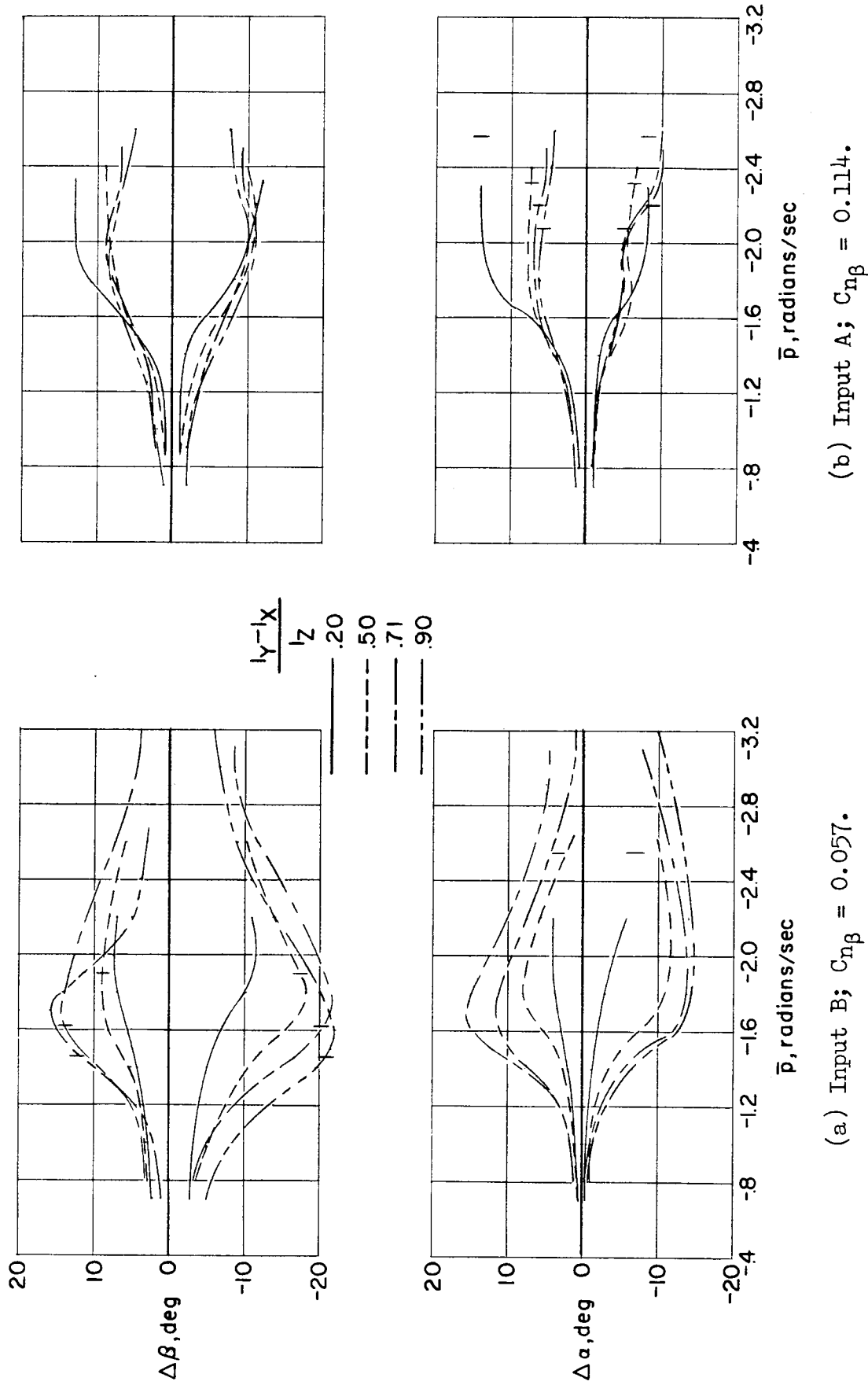


Figure 44.- Effects of variations in  $C_{l\beta}$ . Swept-wing configuration. Input B;  $C_{n\beta} = 0.057$ .



(a) Input B;  $C_{n\beta} = 0.057$ .  
 (b) Input A;  $C_{n\beta} = 0.114$ .  
 Figure 45.- Effects of variations in mass distribution. Swept-wing configuration.

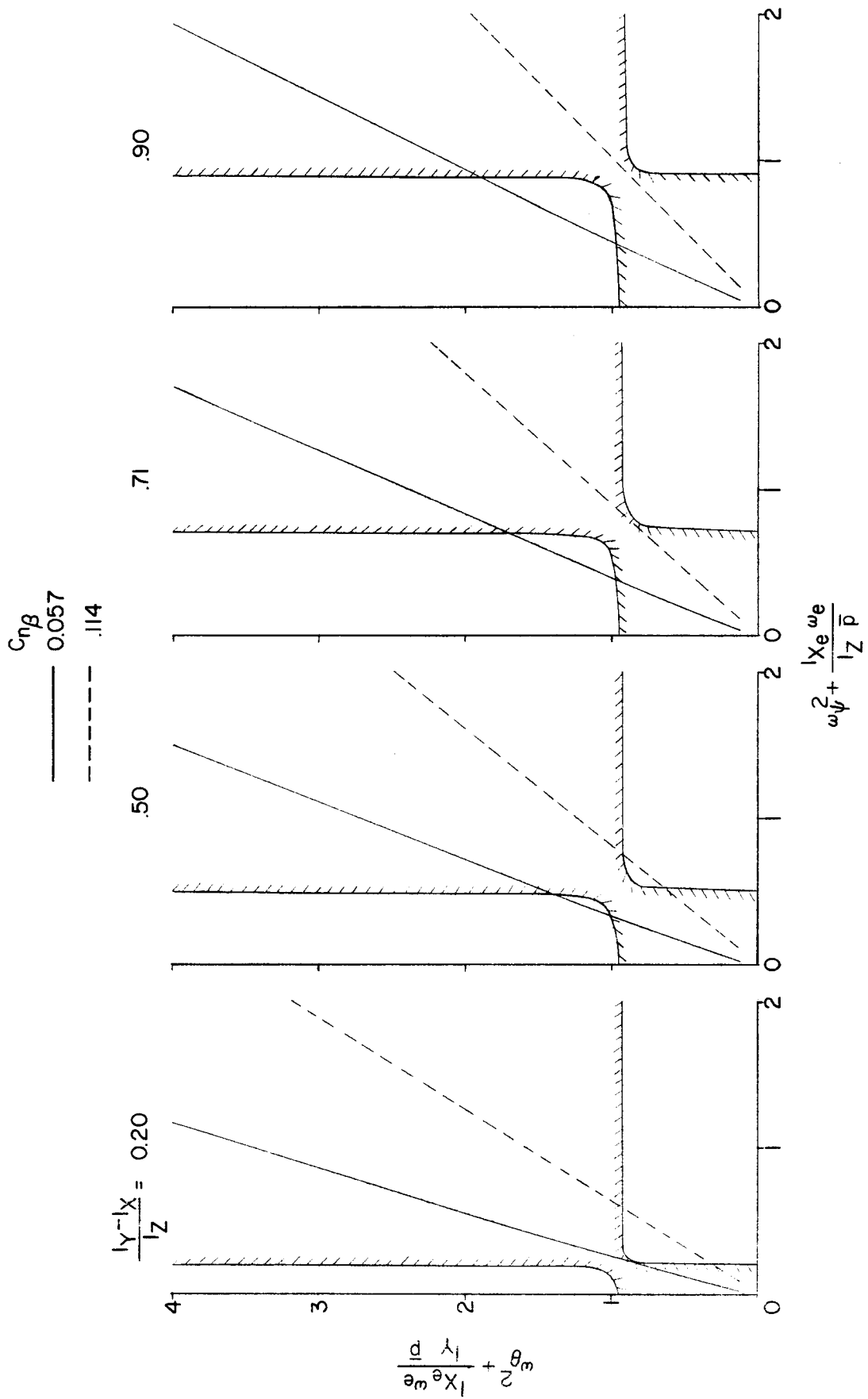


Figure 46.- Stability charts showing effects of variations in mass distribution. Swept-wing configuration. Left rolls.

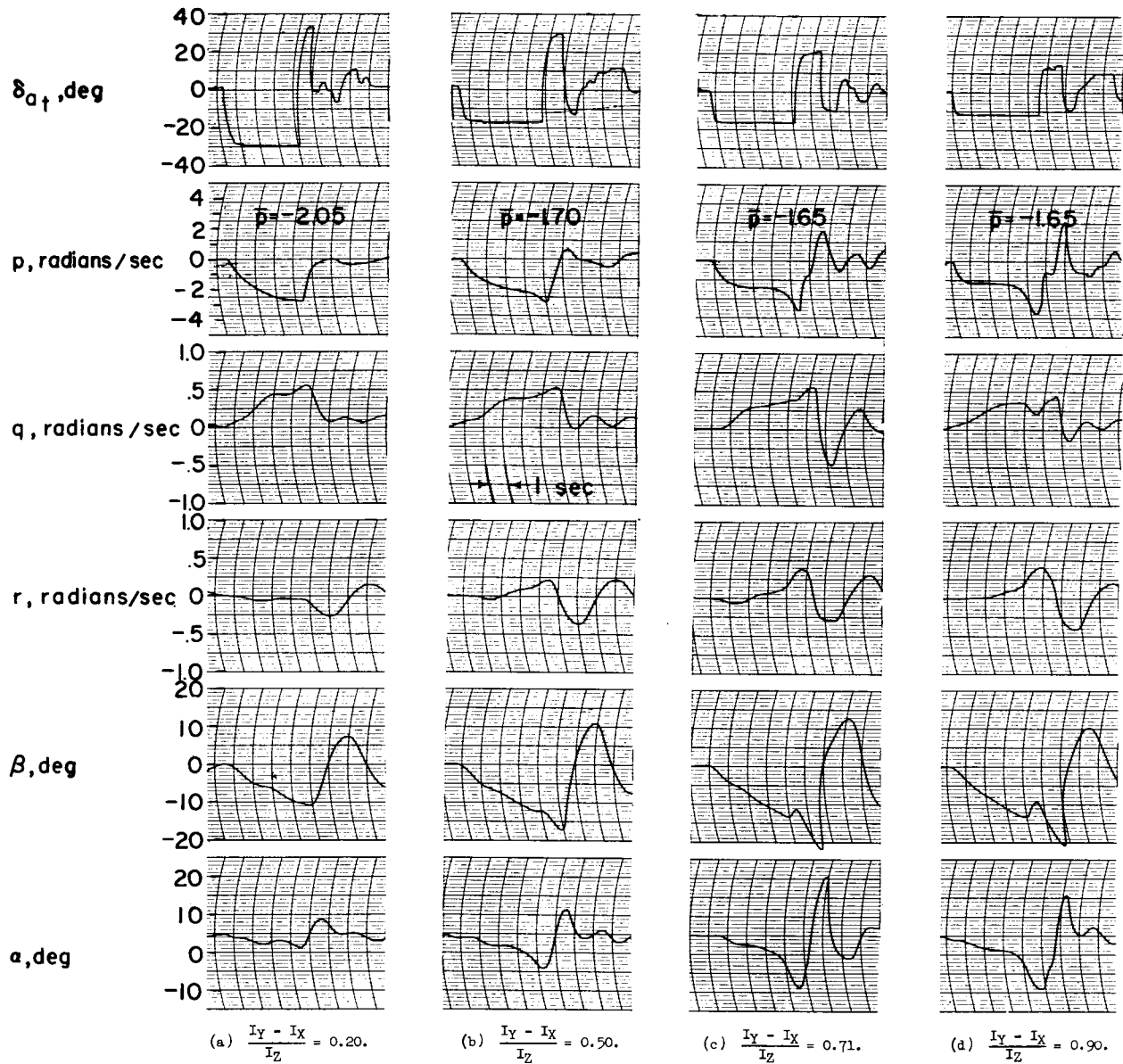
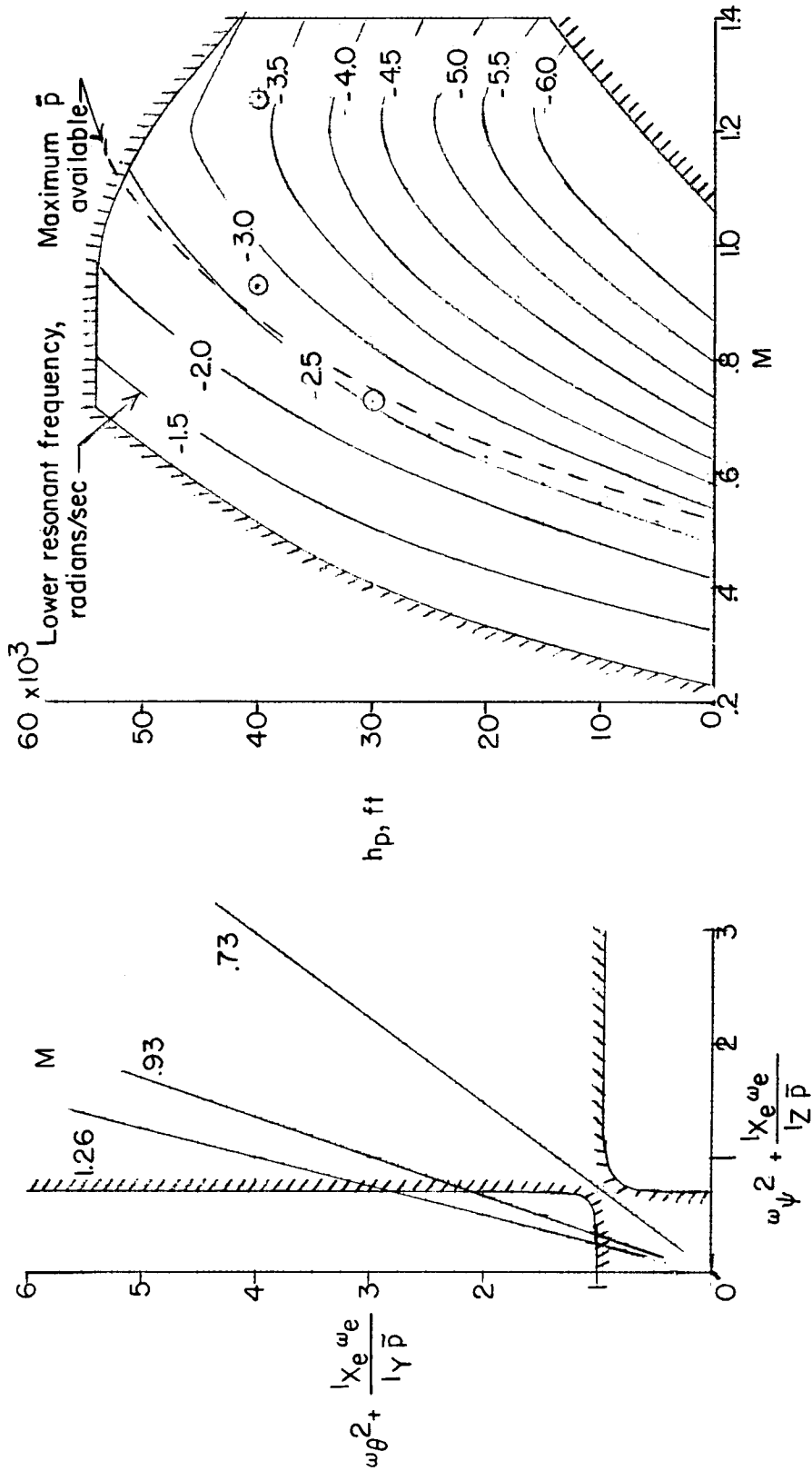


Figure 47.- Time histories showing effects of variations in mass distribution. Swept-wing configuration.  $C_{n\beta} = 0.057$ .



(a) Stability chart illustrating effects of M.

(b) Flight envelope showing lines of constant lower resonant frequency and aileron capabilities.

Figure 48.- Preliminary roll analysis. Swept-wing configuration. Initial level flight.